Description of a Test Case: Las Rives

Ariège - France

Authors: M. Dewitte[1], D. Courret[2], S. Tomanova[2], F. Lemkecher[1], L. Chatellier[1], A. Adeva Bustos[3], L. David[1]

[1] Institut Pprime – CNRS – Université de Poitiers
[2] AFB - Pole Ecohydraulique AFB-IMFT, Toulouse
[3] SINTEF Energy Research

Table of contents

List of figures

List of tables

1. Description of the Test-Case

Figure 1 and Figure 2 allow locating the HPP of Las Rives on national, regional and river scale.
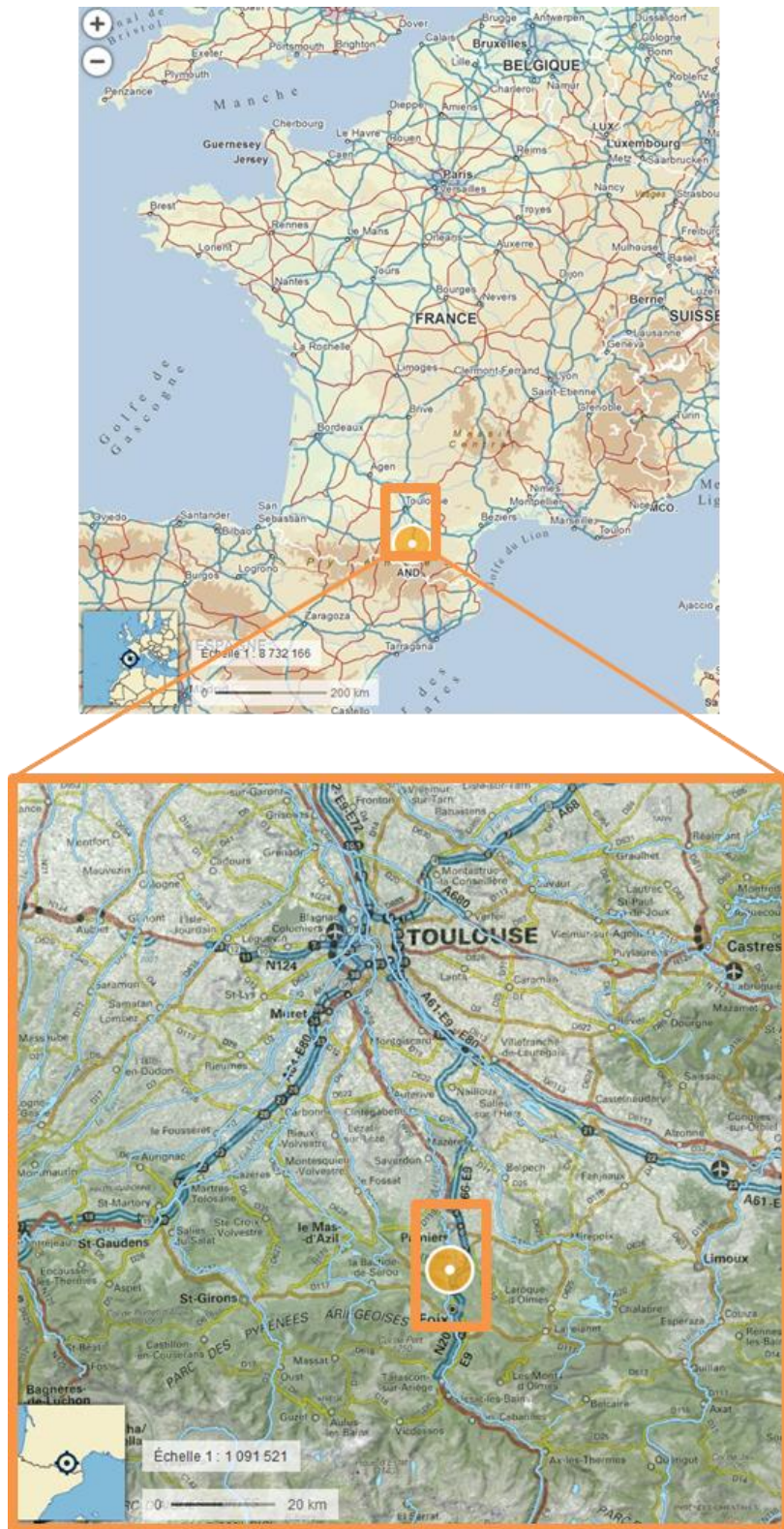
Figure 1: Location of the HPP of Las Rives at national and regional scale
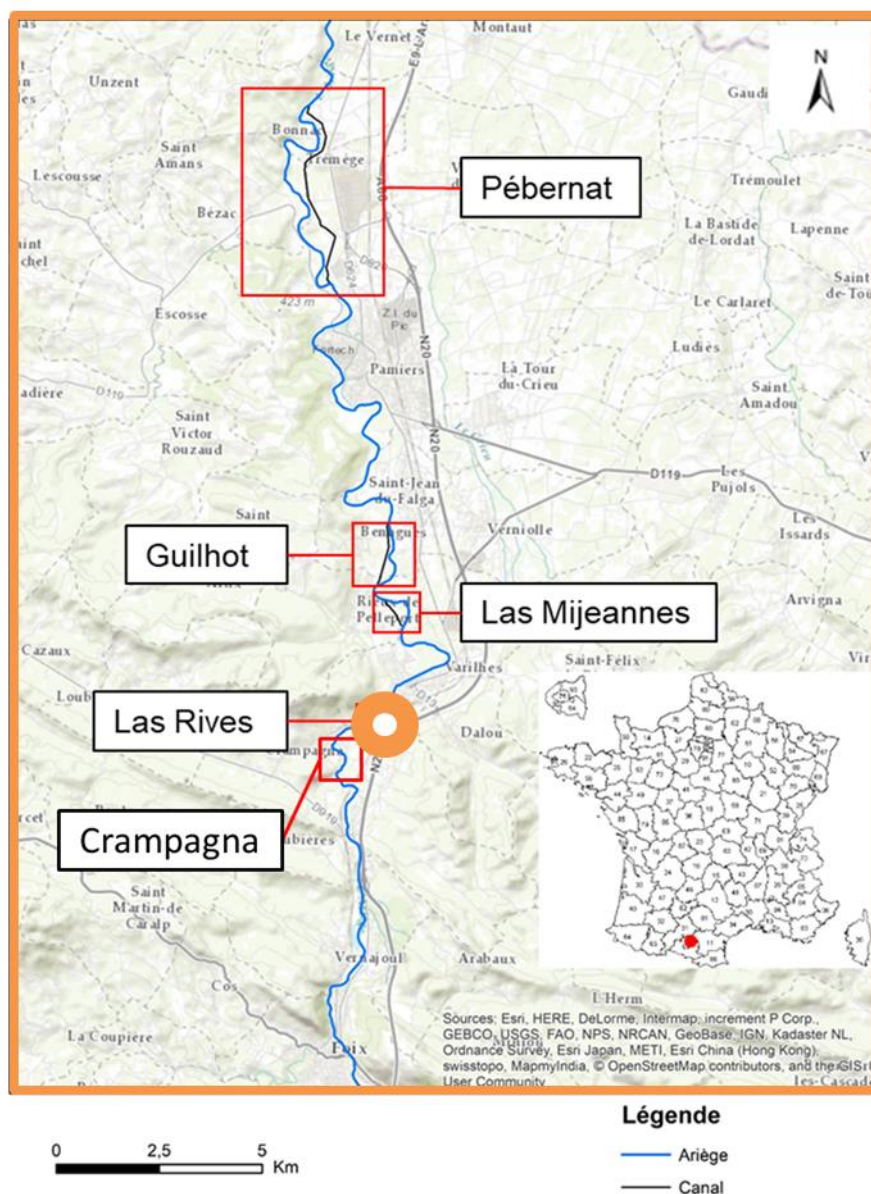
Figure 2: Location of Las Rives at the river scale

1.1. Description of the water bodies related to the HPP

The HHP of Las Rives is included in French waterbody number 170. It is related to 3 other water bodies, two upstream and one downstream. The dam of Labarre at the upstream limit of the waterbody constitutes an obstacle to upstream migration and participates to the regulation of flows with its reservoir of 400 000 m^3 (17.6 ha). The water bodies 169 and 905 are also not connected (in an ecological way) to waterbody 170.
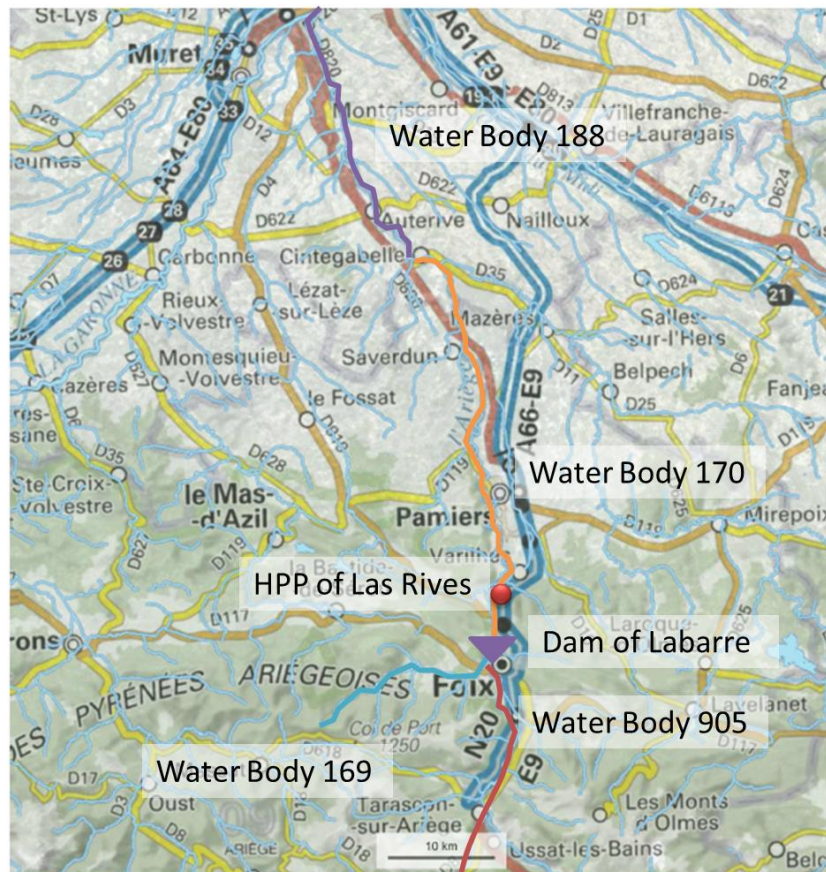
Figure 3: Water bodies related to the HPP of Las Rives

1.1.1. Hydrology of the Ariège at Foix

The hydrology of the Ariège is characterized by sustained flows in winter, high water levels in spring due to snow melting and a low water period from August to October.

During the downstream migration period of smolts (March, April, May) the mean monthly discharges are respectively 41.3 m³/s, 57 m³/s and 79.1 m³/s. The mean interannual discharge is 39 m³/s.

The HPP of Las Rives is downstream the gauging station of Foix, the mean interannual discharge is estimated at 41.8 m³/s. Indeed there are several creeks and one watercourse flowing into the Ariège between Foix and Las Rives.
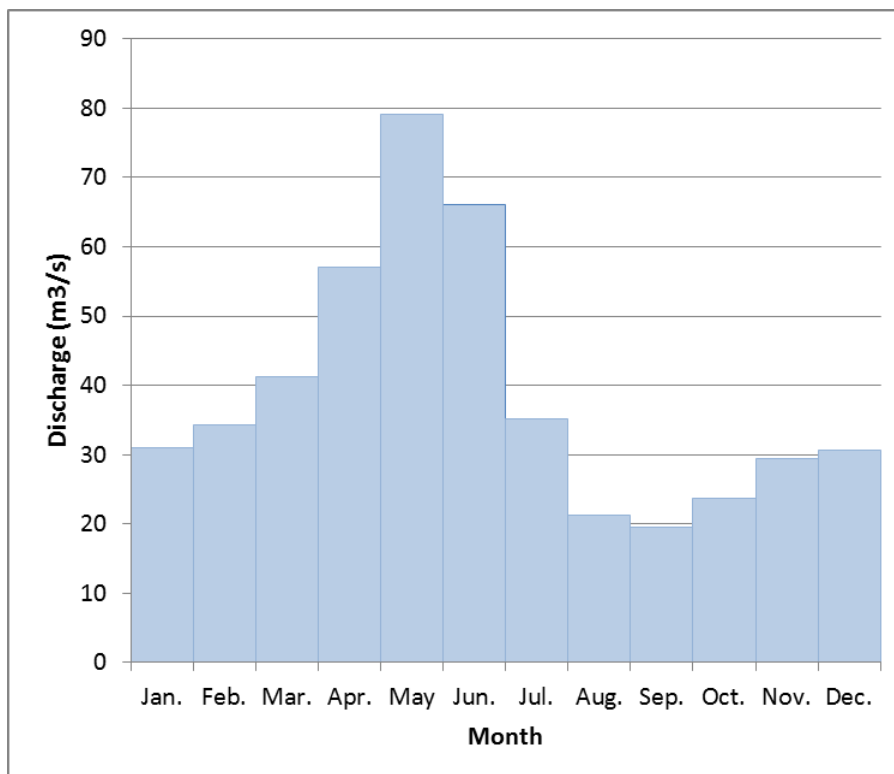
Figure 4: Mean monthly discharge of the Ariège at Foix (source: www.hydro.eaufrance.fr)

1.1.2. Main pressures

Several pressures are listed for the Ariège near Las Rives:

Table 1: Main pressures on the Ariège

Continuity (high)	Several HPP (7 on this waterbody) upstream and downstream
Hydrology (moderate) and morphology (moderate)	Presence of several large reservoirs upstream the water bodies that influence hydrology in two ways: hydropeaking management and release of water during summer to sustain low flow of Ariège and Garonne rivers.
Pollution (non-significant)	Upstream the waterbody: big city of Foix
Agriculture (significant)	agriculture with pesticides
Morphology (moderate)	former granulate extraction, blockage of the sediment transport in upstream reach due to big dams and reservoirs

A SDAGE (Schéma Directeur d'Aménagement et de Gestion des Eaux) is like a River Basin Management Plan and describes measures to be implemented. All the measures are not related to hydropower pressures.

Table 2: Measures to be implemented at the river basin scale of the Ariège

Flow change	legislation: instream flow in bypassed reach since 2014: minimum flow ≥ 1/10 of mean annual discharge
Fish migration measures	Related to HPP: Vieux Moulins: bar screen, fish ladder; Crampagna: bar screen 2cm, fish ladder; **Las Rives: trash rack with bar clearance of 2cm instead of 3cm; fish ladder (Q≥0.5m3/s)**; Las Mijeanes: Bar screen 2cm, fish ladder; Guilhot: bar screen 2cm, fish ladder ; Foulon's weir: Fish ladder; Pébernat: bar screen 2cm, downstream migration valve, fish ladder ; Saverdun: bar screen 2cm, fish ladder.
Sediment control	HPP of Crampagna, **Las Rives**, Las Mijeanes, and Guilhot equipped with **dump valves for sediment**
Pollution control	operating equipment to standards for the water treatment plant of Saverdun and Foix

Some of the measures referred below have an effect on the HPP production:

Flow changes: almost all HPP respected already the minimum flow in bypassed reach of 1/10 mean annual discharge

Continuity: For HPP Pébernat: ongoing study for the minimum biological flow;

For Las Rives and Crampagna: compliance actions for sediment continuity and downstream migration, addition of turbines.

1.1.3. Fish fauna in the Ariège
(Ecogea, 2011)

General data on fish fauna in the Ariège

The fish fauna of the Ariège is composed of amphibiotic and holobiotic species.

The **amphibiotic species** identified are:

- The Atlantic salmon (upstream migration mainly from Mai to November);
- The sea trout (upstream migration mainly from Mai to November);
- The eel (upstream migration from April to October and mainly from June to September);

The **holobiotic species** identified are:

- *Salmonidae* : brown trout (upstream migration mainly autumnal for the trout);
- *Cyprinidae*: bleak, barbell, common bream, roach, chub, dace…
- *Cobitidae*: stone loach…

Table 3: Principal migration periods of migratory species on the axis (source: (Ecogea, 2011))

Species	Winter	Spring	Summer	Autumn
Salmon		Upstream	Upstream	Upstream
	Downstream	Downstream		
Sea trout		Upstream	Upstream	Upstream
	Downstream	Downstream		
Brown trout	Upstream			Upstream
	Downstream	Downstream		Downstream
Eel		Upstream	Upstream	Upstream
	Downstream			Downstream

Legend: Downstream migration (blue), Upstream migration (yellow)

Atlantic salmon have disappeared from the Garonne and Ariège rivers during the 20th century. A reintroduction plan started in the 1990's. One of the first actions was an assessment of rearing and spawning habitat for Atlantic salmon. Until now, the dam of Labarre is not equipped with any upstream or downstream migration devices and is the upstream limit of colonization of salmon and eels. The area downstream Labarre (Foix) represents around 68 ha of habitat and 61% of the potentialities for salmonids rearing habitat within the whole basin of the Ariège river (111 ha). It has a potential production of 54 500 Atlantic salmon smolts. Figure 5 allow identifying the most productive section of the Ariège between Labarre and the confluence with river Garonne. The most productive sections are the one between Las Rives and Las Mijeannes and between Guilhot and Foulon.
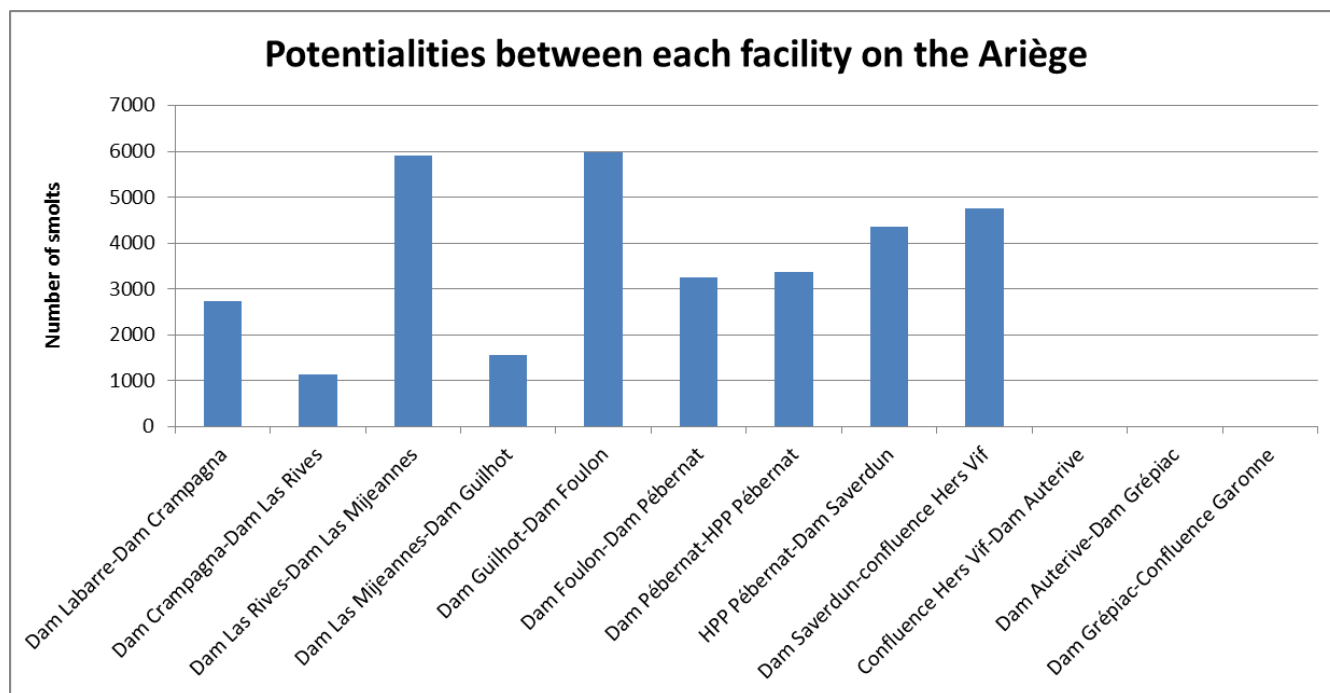
Figure 5: Potentialities of Atlantic salmon smolts on the Ariège (Ecogea, 2011)

1.2. Presentation of the HPP

1.2.1. Location of the HPP
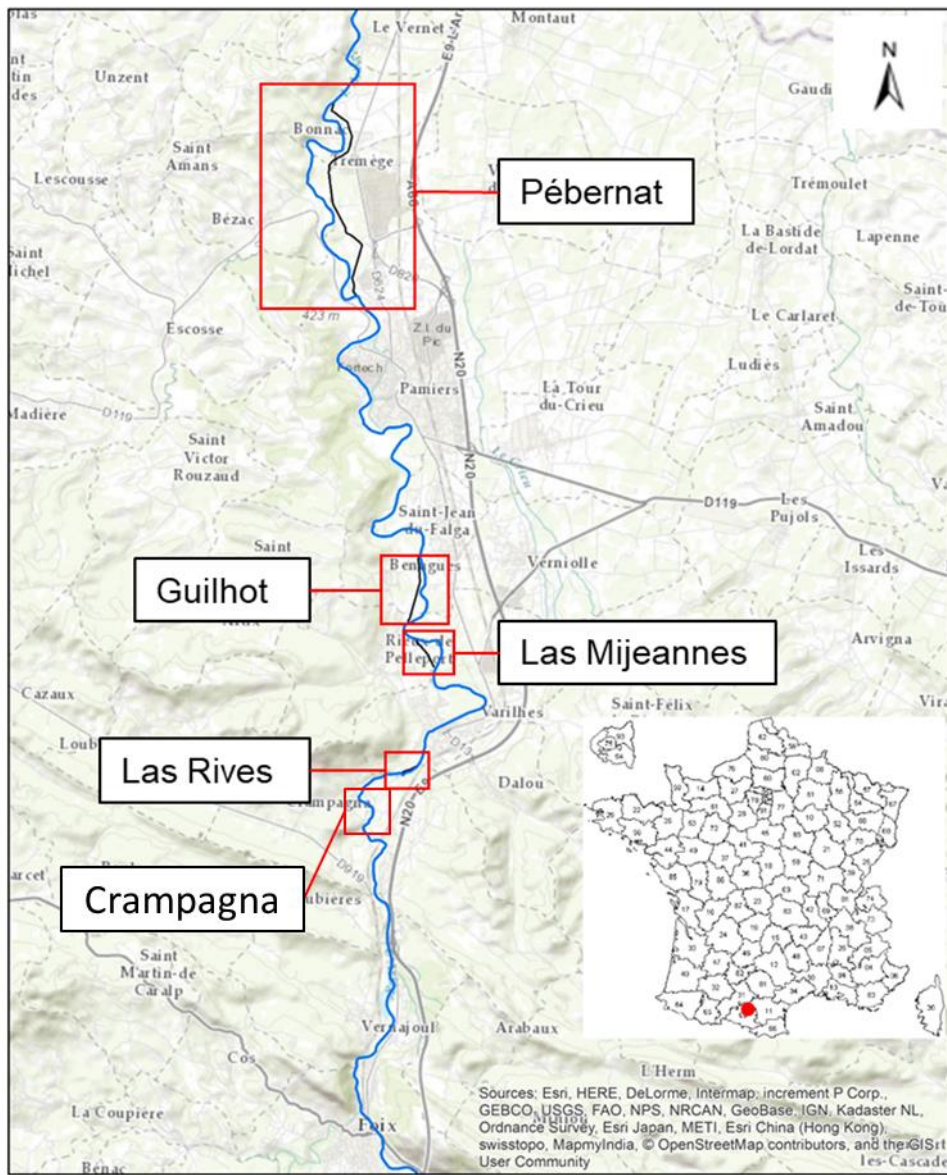
Figure 6: Location of Las Rives

Table 4: Main characteristics of the HPP of Las Rives

Watercourse	Ariège
Situation :	Commune de Varilhes
Inter-annual discharge	41.8 m³/s
Low-water flow :	12 m³/s
Instream flow in bypassed reach :	4.6 m³/s
Function of the dam :	Hydropower
Length of headrace canal :	~ 195 m
Length of bypassed reach :	~ 550 m
Maximum turbine discharge:	48 m³/s
Species concerned :	Salmon, sea trout, lamprey, eel, brown trout
Capacity of HPP	2.7 MW

The compliance of the HPP with the French law is achieved (according to L.214-17 from the French Environmental Code, the river belongs to List 2[1]) in the context of a coordinated program on the Ariège river (9 infrastructures concerned).

---
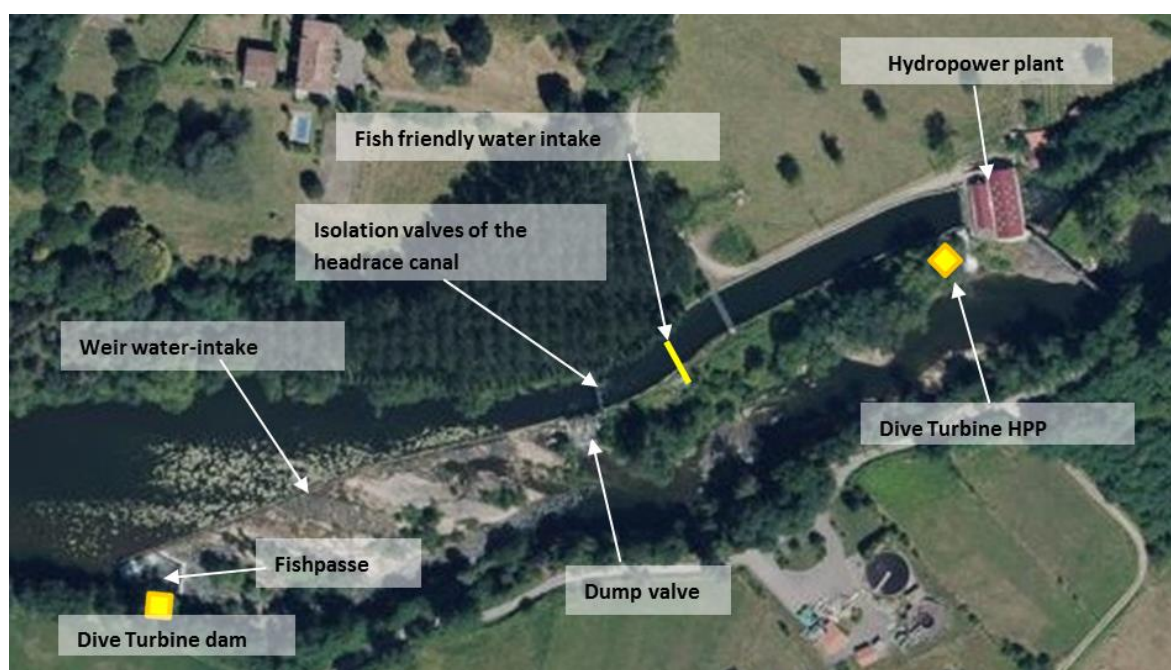
[1] River in which it's necessary to assure sediment transport and free movement of fishes. Each infrastructure has to be maintained, and equipped according to the rules settled by administrative body in concertation with the owner or at least the operator

Figure 7: Devices at Las Rives

Equipment:

3 Francis turbines (G1 to G3) at the power plant (1976)

- Maximum turbined flow: 13.3 m^3/s
- Rated head: 6.00 m
- Number of blades : 18
- Diameter of the wheel: 1.54 m
- Rotation speed: 144 rpm

Figure 8: New Dive turbine in the headrace channel (2015) (source: www.dive-turbine.de)

1 dive turbine (G4) in the headrace channel (2015):

- Maximum turbined flow: 8 m^3/s
- Rated head: ≈6.00 m
- Number of blades : 5
- Diameter of the wheel: 1,45 m
- Rotation speed: 250 rpm

1 dive turbine (G5) for the e-flow next to the fish pass (2017):

- Maximum turbined flow: 3 m^3/s
- Rated head: 4.31 m
- Number of blades : 3
- Diameter of the wheel: 1.080 m
- Rotation speed: 250 rpm

Figure 9: New Dive Turbine for the E-flow (2017) (source: www.dive-turbine.de)

1.2.2. E-flow

In France, the law of 2006 (LEMA) imposes an environmental flow that permanently guarantee the life, circulation and reproduction of the species that inhabit the waters, and also defines a minimum value of 1/10 of the mean inter-annual discharge. This should be implemented before 1rst January 2014 at the latest. The definition of the environmental flow in bypassed sections is normally based on a detailed study of hydrology (natural low flow), hydromophology and habitat. In 2014, if such study was available, its results were considered to define the environmental flow; otherwise it was mostly set to the minimum value (1/10 of the mean inter-annual discharge).

At Las Rives, a compromise was found with an environmental flow of 4.6 m^3/s slightly higher than the minimum value (4.2 m^3/s). This is linked to the discharges needed for the fish upstream migration devices: 0.5 m^3/s in the fishway + 2.75 m^3/s of attraction flow in an adjacent notch + 1.35 m^3/s in the bypass for downstream migration. It's a part of a larger compromise between the hydropower company and the authorities that include the improvement of the downstream migration conditions of fishes (replacement of the former device by a more efficient fish friendly intake) and the increase of the power plant capacity with the addition of the Dive turbine (G4) in the headrace channel in 2015. Then, in 2017, it was allowed to turbine the attraction flow with the addition of a Dive turbine (G5) at the weir, provided that it does not disturb the attractiveness of the fishway. In such way, the operator

increased its production and decreased the global mortality rate of the HPP. The replacement of the rack led to higher head losses and maintenance.

1.2.3. Downstream migration devices

Up to 2014, the former device was located just upstream of the main power plant and consisted of a unique surface bypass associated with the pre-existing trash rack and positioned laterally on the right bank. The bar spacing was 4.5 cm since the 90' and was reduced to 3 cm in 2010.

Table 5: General characteristics of the bar rack and the bypass in 2010

General characteristics of the bar rack		
Level of the bottom	329.6	mNGF
Water level	333.57	mNGF
Level of the top of the rack	334.2	mNGF
Width of the channel upstream the rack	14.05	mNGF
Longitudinal inclination of the rack b	70	°
Lateral inclination of the rack a	90	°
Water height	3.97	m
Total length of the rack	4.9	m
total immersed length of the rack	4.22	m
Total width of the rack	14.1	m
Total surface of the rack	69	m²
Total immersed surface of the rack	59	m²
Width of the bars	8	mm
Maximum turbined discharge	39	m³/s
Dimension of the bypass		
Width	1.9	m
Depth	0.5	m
Downstream migration discharge	1.2	m³/s

In 2014, the downstream migration device was completely revised. The former device was abandoned (bypass closed, increase of the bar spacing by removing some bars) and a new fish-friendly intake was built at the head of the intake channel. This project has several advantages: the flow of the downstream migration device is included in the minimum flow to maintain in the bypassed section of the river (it was not the case before), the efficiency of the downstream migration device is improved and this unique device protects the main power plant (G1 to G3) and the new Dive turbine (G4).

- Maximum turbine discharge: 45 m³/s
- Bar screen characteristics:
    - Width of the bar screen : 14 m
    - Inclination ß of 26° from the horitzontal
    - Wetted surface of the screen of 127 m² ➔ mean normal velocity of 0.35 m/s
    - Orientation of the rack : 90° (perpendicular)
    - Clearance between the bars : 20 mm
- Bypass characteristics:

- 3 entrances located at the top of the bar screen, dimensions of each entrance: 1 m wide and 0.5 m deep
- Flow for the downstream migration : 1.35 m³/s
- Downstream migration galery whose section increase when getting closer to the downstream migration channel

At the point of return of the flow into the river, the jet falls of 3.40 m into 63 cm of water when the total discharge of the river is smaller than 48.5 m³/s. The impinging velocity of the jet is about 9.4 m/s. These high velocity and low water depth pose a question about the conditions of reception of fish. The authorities have already asked the operator to increase the water depth around the impingement area of the jet (work planned in September 2019). Experiments will be conducted in spring 2019 and 2020 to assess the fish survival before and after the work.

Figure 10: Positioning of downstream migration devices

-

Figure 11: bar screen out of water

Figure 12: downstream migration duct

Figure 13: Downstream migration channel

Figure 15: outlet of the downstream migration channel

Figure 14: bar screen in water

Figure 16: Dump valve for sediments

1.2.4. Previous studies on downstream migration

1.2.4.1. Study for the efficiency of three downstream migration devices for Atlantic salmon smolts - 2001

(Croze, et al., 2001)

In 2001, the GHAAPPE (Groupe d'hydraulique appliquée aux aménagements piscicoles et à la protection de l'environnement – today the Ecohydraulic team of the AFB-IMFT) conducted a study on three HPPs on the Ariège River, including Las Rives, to assess the efficiency of three downstream migration devices for Atlantic salmon smolts.

Characteristics of power plant and downstream migration device in 2001

In 2001, the HPP had only 3 Francis turbines and a maximum turbine discharge of around 40 m³/s (3 x 13.3 m³/s). The water intake was protected by a rack perpendicular to the flow and nearly vertical, composed of 3 grids, each 4 m wide, separated by concrete pillars of 1 m width (Figure 17). The mean

space between bars was 40 mm, but there was a high variability along the rack (standard deviation: 7.5 mm, min – max 27-66 mm).

The flap gate at right bank acted as a downstream migration outlet. It was 1.9 m wide, with a depth around 0.5 m. It was protected by 8 bars of diameter 2 cm, spaced of 18 cm. The bypass entrance can be lighted by a 80W mercury vapour lamp, located around 1 m above the water surface. During the tests, the discharge of the bypass varied between 0.67 and 2.73 m³/s, with an average of 1.55 m³/s. 80% of the values were between 1.24 and 1.81 m³/s.

Figure 17: View of the former bar rack at the power plant (source: (Ecogea, 2011))

Methodology

The smolts from fish farm were marked with PIT-tag (Passive Integrated Transponder – 11 mm long, 2 mm diameter). Fish passing through the bypass were detected using two detection plates "TROVAN", located downstream a reception pool and a filtration screen that allowed reducing the discharge over the detection plates (Figure 19). It is assumed that undetected fish probably passed through the rack and the turbine. Thus, this study provided a minimum value of the bypass efficiency.

The fishes have been released in the headrace channel 5 m downstream the gates, 160 m upstream the HPP. They were alternatively released at the left and the right bank in order to exclude any effect of the release point. A total of 20 batches was release at Las Rives. Each batch is composed of 47 to 51 smolts. The release took place between 21:30 and 23:48 between the 4th of April and the 17th of May 2001.

The effect of light on the bypass efficiency was studied by comparison between periods with continuous light on and periods with light off (Figure 18).
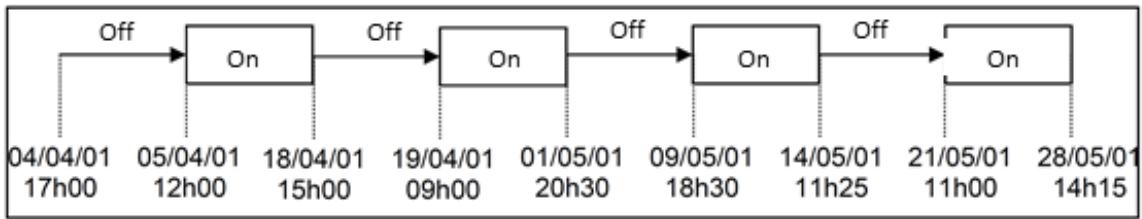
Figure 18: summary of the functioning periods of the mercury vapour lamp at Las Rives
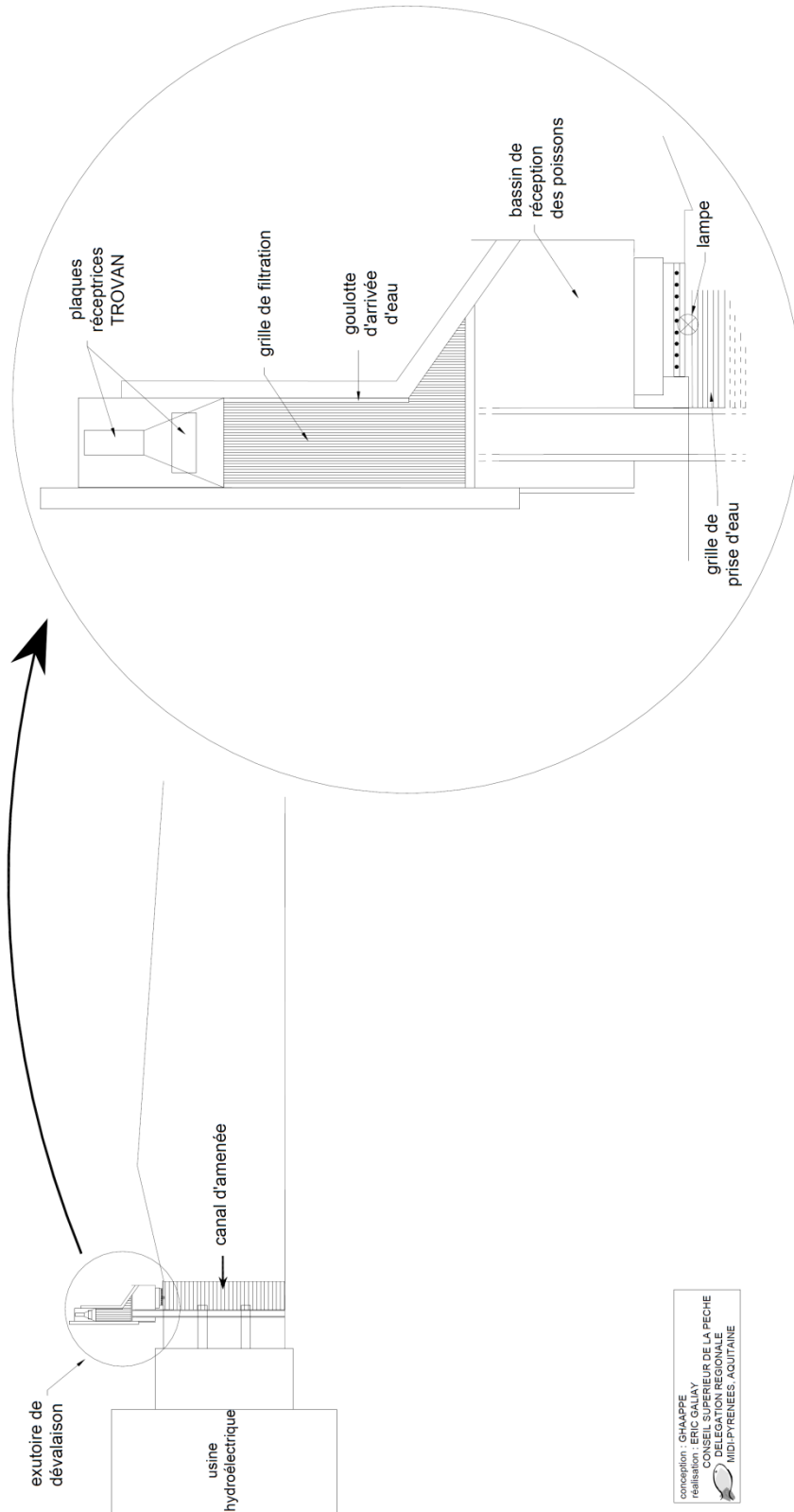
Figure 19: Diagram of Las Rives water intake (Croze, et al., 2001)

Results

Over 990 fishes released at Las Rives, 391 went through the downstream migration device. The mean efficiency was 39.5% (± 6.5%). It varied from 12.5% to 62 % depending on the batch. The efficiency of the bypass is positively correlated with its discharge (Table 6). The lightning had also a significant effect on the bypass efficiency: 49% with light on against 27.9% without.

Influence of fish size has been studied too by comparison between the size distribution of the released fish and the size distribution of the fish detected in the bypass (Table 7). Fishes smaller than 170 mm represent 42% of released fishes but also 37% of fishes taking the outlet. Smaller fishes might have more chance to pass through the rack than bigger fishes, due to a lesser repelling effect of the bar spacing.

Table 6: Summary of the efficiency of the outlet depending on several criteria

Criteria	Efficiency
Light on	49.00%
Light off	27.90%
$Q_{outlet} < 1.50\,m^3/s$	34.00%
$Q_{outlet} > 1.50\,m^3/s$	44%
Mean efficiency of outlet	**39.50%**

Table 7: Influence of fish size in downstream migration

Size	% of total released fish	% among fishes taking the outlet
< 170 mm	42.0%	37.0%
]170;180] mm	36.0%	36.5%
> 180 mm	22.0%	26.5%

These results can be explained by:

- A low repelling effect of the rack due to a bar spacing too high and very heterogeneous (40 mm and up to 66 mm) and a mean normal velocity also to high (0.67 m/s).
- An absence of effective guiding effect of fish towards the bypass by the flow field. The tangential flows to the rack are not regular from a bank to the other. They are disrupted by the pillars.
- A weak attractiveness of the bypass due to a shallow depth compared to the total depth of the intake and to a high velocity acceleration at the entrance.

Moreover, the discharge of the outlet is about 1 to 1.2 m³/s at functioning level; this represents 2.5 to 3% of the turbined flow. Larinier and Travade (1999) advocated that the discharge in the outlet represents 2 to 10 % of the turbined flow. This range should be reduced to 5-10 % when the outlet is not associated to a guidance device.

The global mortality of smolts passing the Las Rives scheme has been assessed taking into account (1) the repartition between the fish passing over the dam and those entrained in the intake canal (depending on the hydrology), (2) a bypass efficiency of 49% and (3) a mortality rate in the turbines estimated at 13 %. The global mortality rate was assessed between 1.0% and 6.6% depending on the hydrology during the downstream migration period, with an average rate of 4.5% (Figure 20).
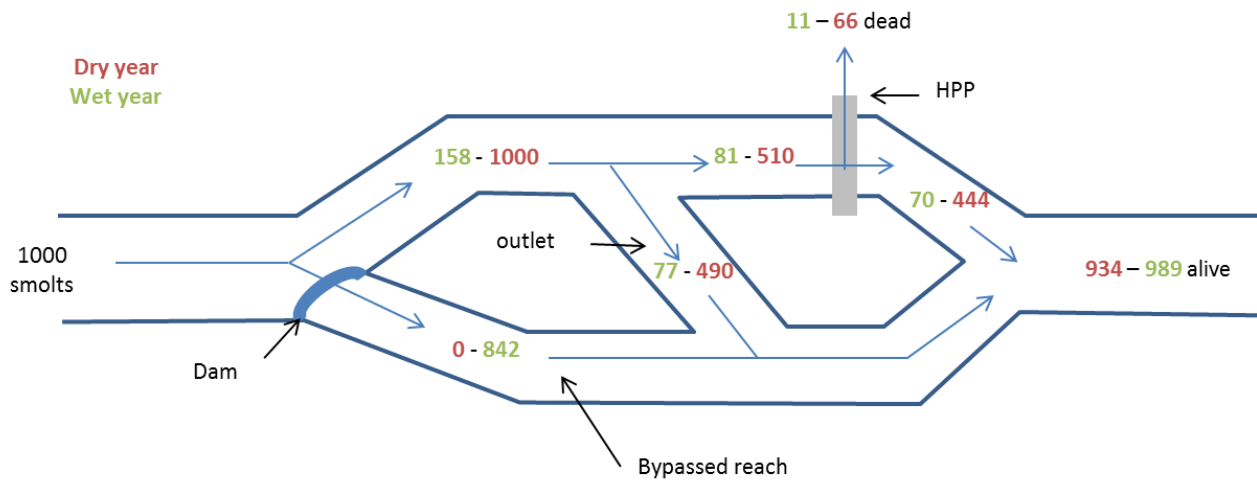
Figure 20: impact of Las Rives HPP: summary diagram of the future of 1000 smolts during a dry year and a wet year

1.2.4.2. Study for the improvement of fish crossing on the water course Ariège – 2011

(Ecogea, 2011)

In 2011, the Engineering office Ecogea led a study for the improvement of fish crossing on the water course Ariège.

Downstream migration device

In September 2010, the rack protecting the HPP has been changed. It is just in front of the HPP (as the former one), 14.05 m width, inclined of 70° to the horizontal. The bar spacing is smaller than it used to be: 3 cm. The diameter of the bars is of 8 mm. The downstream migration outlet (flap gate) is 1.90 wide and equipped with a mercury lamp, cf. Table 5.

Figure 21: Bar rack in front of the HPP from 2010 to 2014 (Ecogea, 2011)

The downstream migration discharge is around 1.2 m^3/s.

Diagnosis of downstream migration

The flow conditions upstream the HPP have been studied based on the characteristics of the bar rack, see Table 5 and Table 8.

From these characteristics, the flow conditions have been calculated; see Table 8 and Figure 22.

Table 8: Flow conditions in front of the bar rack at the HPP in 2010 (Ecogea, 2011)

Flow conditions in front of the bar rack (unclogged rack)		
Turbined discharge	40	m3/s
Mean approach velocity	0.72	m/s
Mean normal velocity	0.67	m/s
Mean tangential ascending velocity	0.25	m/s
Mean tangential lateral velocity	0.00	m/s
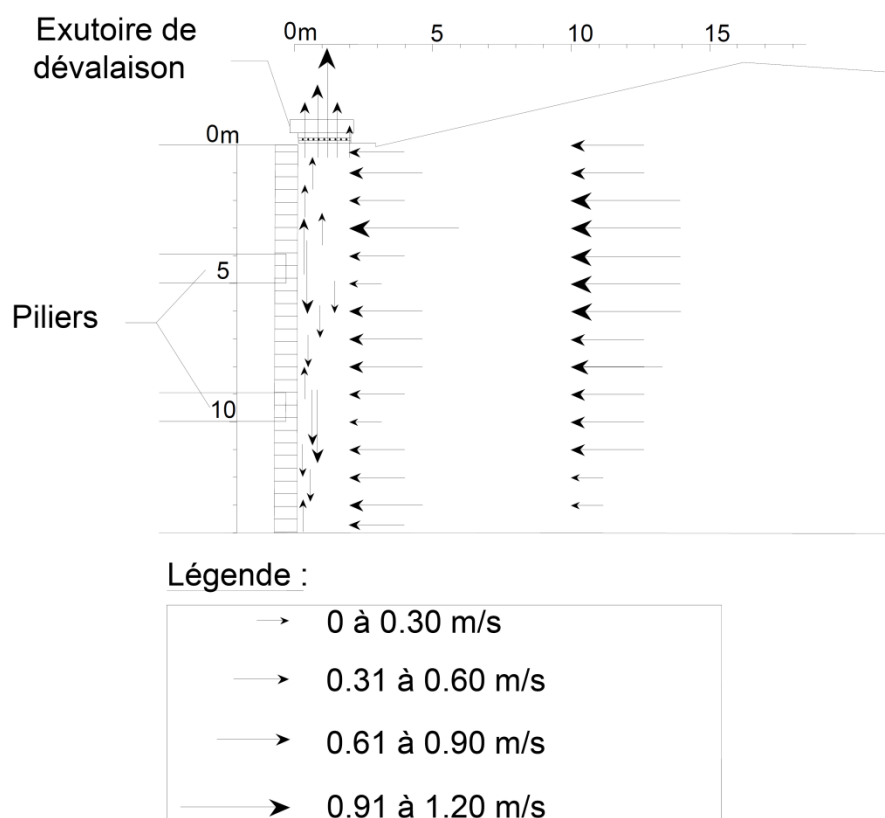
Figure 22: Mean velocity in front of the power plant and the entrance of the outlet of Las Rives (turbined flow = 39 m3/s) (source: (Croze, et al., 2001))

The mean normal velocity is greater than 0.5 m/s which is the maximum recommended value in order to prevent the fish to pass rapidly through the rack or being impinged on the grid.

Concerning the guidance efficiency, the discharge in the outlet represents only 2.5% of the turbined discharge. The bar spacing is too large to represent an efficient physical barrier for eels smaller than 70 cm, and the permeability of the grid should be around 80%. For Atlantic salmon smolts neither, the bar spacing is not small enough to constitute an efficient behavioural barrier.

The mortality in the turbines has also been estimated. For Atlantic salmon smolts it is around 13 % (Bosc, et al., 2000). For the eels, which are longer and therefore more sensitive in the turbines, the mortality should be around 33%. Taking into account the permeability of the rack, the mortality in the turbines and the hydrology during downstream migration period (distribution of downstream

migration ways between the headrace channel and over the weir depending on the hydrology), the global mortality at Las Rives should be of 4.5% for Atlantic salmon smolts and 10 % for the eels.

Despite the diminution of the bar spacing of the bar rack, the downstream migration efficiency of the device should not be greater than **50-55%**.

1.2.5. Upstream migration devices

- Pool-type fishway with alternate deep side notches, located at the upstream angle of the water intake weir (most upstream point reached by the migrating fish ont the right bank).
- Flow in the fish pass : 0.5 to 0.8 m3/s depending on the upstream level, drop between pool: 0.30 m, notch width: 0.45 m, notch depth: 0.70 m, pool dimension: 3.2 m long and 1.9 m wide, pool mean depth: 1.45 m, dissipated power: 170 to 210 W/m3.
- Built in 1987 with cost of 800 k€ (122 k€) corresponding to a discounted cost of around 200 k€ in 2018.Due to the elevation of the water intake weir in 2015, addition of pools upstream of the existing fish pass
- Attraction flow of 2.75 m^3/s formely delivered by a wide notch in the weir, located near the fishpass entrance. Since 2017, an attraction flow of 3 m^3/s is delivered by a new DIVE turbine (G5) located near the fishpass entrance which was reconfigured. The notche is now equipped with a dump valve, which is open in case of turbine shutdown. The new turbine (G5) is equiped with a fish-friendly intake for the donwstream migration.

Figure 23: upstream view of the fish pass

Figure 24: Dump valve on the new weir

Figure 25: downstream view of the new pools in the fish pass

Figure 26: former notch in the weir

Figure 27: Fish pass and the new DIVE turbine on the bypassed reach

Before installation of the DIVE Turbine (© GP Design)

After installation of the DIVE turbine (© GP Design)
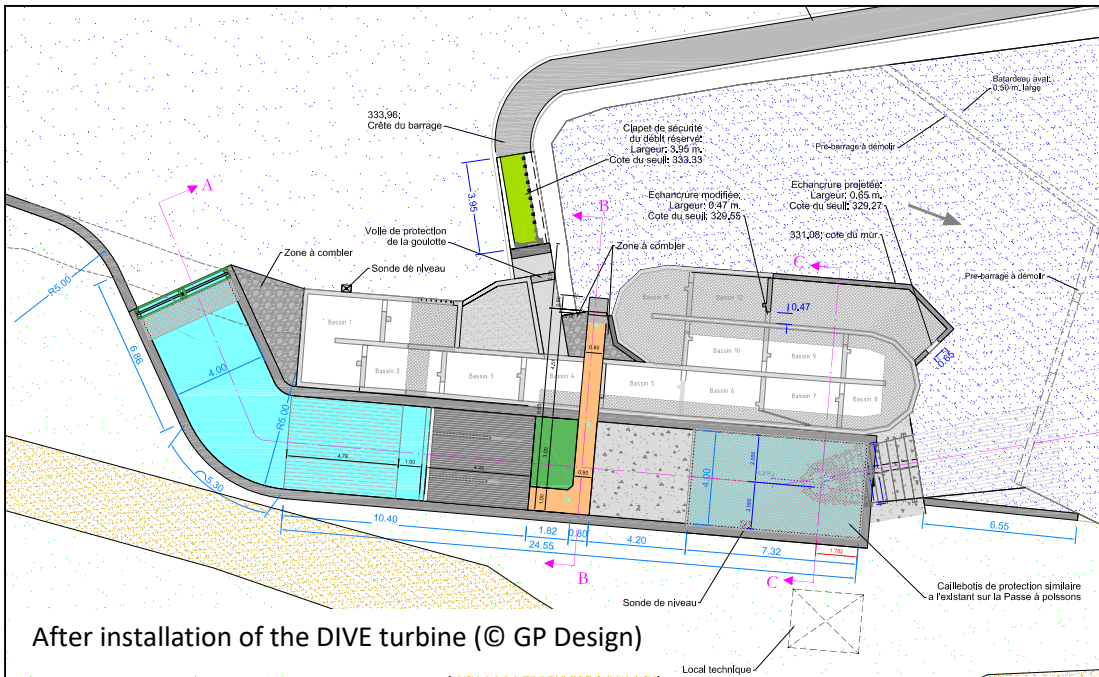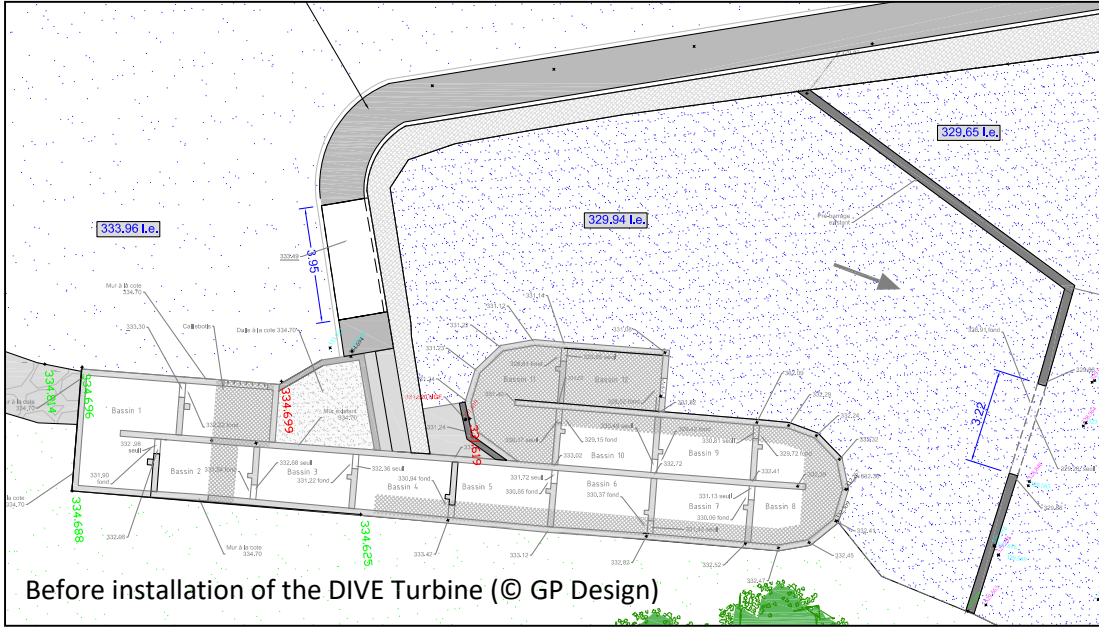
Figure 28: Configuration of the fishpass located at the upstream point of the dam (right bank)

1.2.6. Previous studies on upstream migration

1.2.6.1.   Hydraulic in the fish pass before 2017

- Attractiveness of the fishpass (Ecogea, 2011)

Upstream migration device

In 2011, the fishpass is constituted of 11 pools with alternate lateral notches, except for the downstream one which is central, and orifice. The total height of fall is also decomposed in 12 falls. A pre-barrage downstream the fishpass creates a big pool and a 13th fall. This pool also collects water from the fishpass and from the notch in the weir (appeal discharge: 4.10 m³/s). The theoretical discharge in the fishpass is 0.5 m³/s.
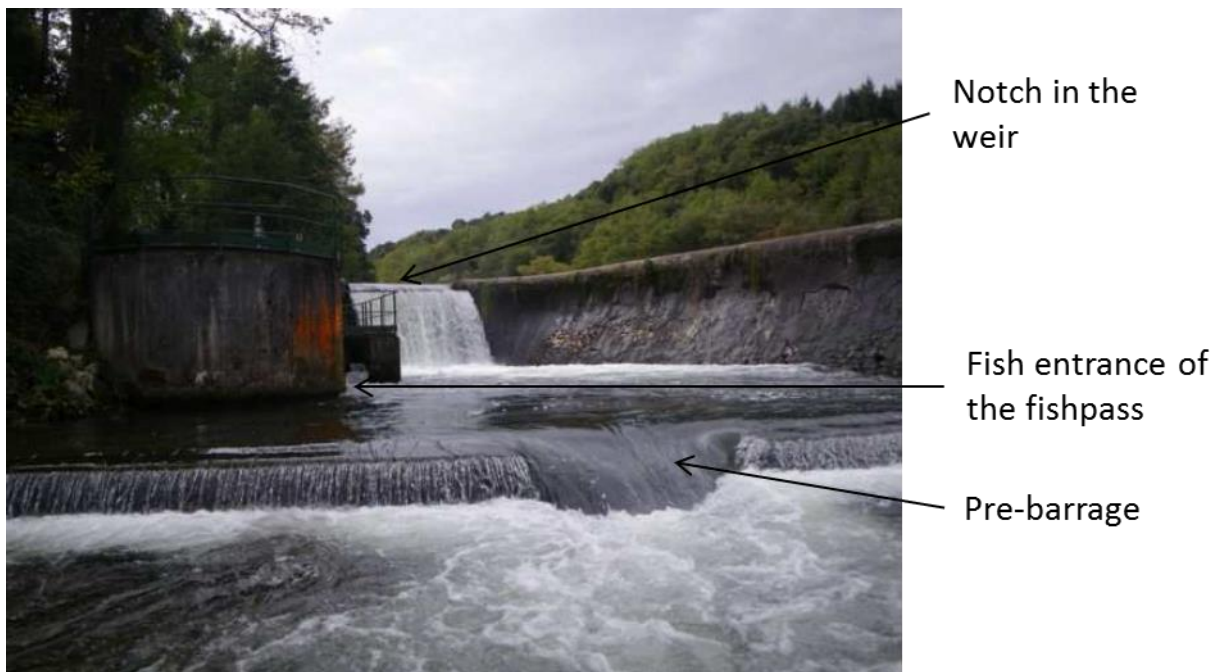
Figure 29: Downstream view of the fishpass (04/10/2010) (source: (Ecogea, 2011))

At the foot of the dam, there is pile of gravel separating the bypassed section in two parts. During low flow, the left branch is not fed; the fishes are directly guided to the fishpass through the right brank. When the dam is spilling, the left branch is fed, the fishes can get lost.
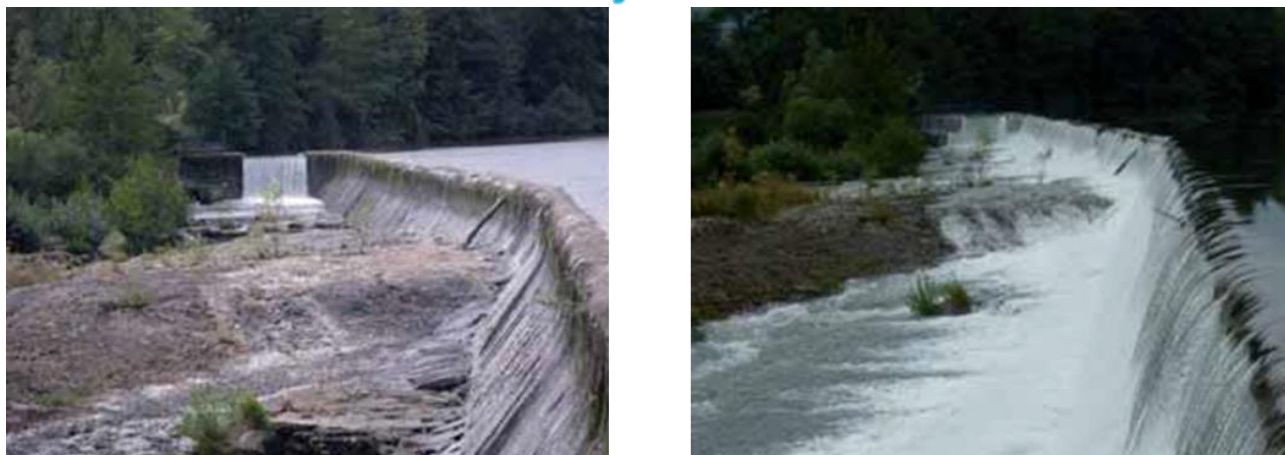
Figure 30: *left* pile of gravels blocking the passage of fish. Without spill, the fishes don't go in the left branch. *Right* picture taken when the dam is spilling (source: Rapport Ecogea, 2011)

Discharge distribution

The discharge distribution between the HPP and the bypassed reach depends on the hydrological conditions, see Table 9.

Table 9: Distribution of the discharges at Las Rives, up to 2015 (Ecogea, 2011)

Discharge of the Ariège at Las Rives	Turbined discharge Qt (m^3/s)	Downstream migration discharge Qe (m^3/s)	Discharge in the fishpass Qp (m^3/s)	Appeal discharge in the notch Qa (m^3/s)	Discharge over the weir Qs (m^3/s)
Low-water (13.6 m^3/s)	8.0	1.0	0.5	4.1	0.0
Mean interannual discharge (MID) (41.8 m^3/s)	36.2	1.0	0.5	4.1	0.0
1.5xMID (62.7 m^3/s)	40.0	1.0	0.6	5.5	15.6
2xMID (83.6 m^3/s)	40.0	1.0	0.7	6.7	35.2

Today's distribution is quite different due to the 2 new turbines and the new downstream migration device, see Table 10.

Table 10: Distribution of the discharges with the actual configuration (since 2017)

Discharge of the Ariège at Las Rives	Turbined discharge at the HPP (G1+G2+G3) Qt (m^3/s)	Turbine discharge by the Dive (G4) (m^3/s)	Downstream migration discharge Qe (m^3/s)	Discharge in the fishpass Qp (m^3/s)	Attraction flow turbined at the dam (G5) (m^3/s)	Discharge over the weir Qs (m^3/s)
Low-water (13.6 m^3/s)	4.0	5	1.35	0.5	2.75	0.0
Mean interannual discharge (MID) (41.8 m^3/s)	32.2	5	1.35	0.5	2.75	0.0
1.5xMID (62.7 m^3/s)	40.0	5	1.35	0.6	3.00	12.75
2xMID (83.6 m^3/s)	40.0	5	1.35	0.7	3.00	33.55

Diagnosis of upstream migration

In order to assess the hydraulic attractiveness of the fishpass some simulations were made. And the proportion of the total discharge of the Ariège in each reach has been studied, see Table 11.

Table 11: Proportion of discharge in the reaches (source: (Ecogea, 2011))

Discharge of the Ariège at Las Rives	Proportion of the discharge in the bypassed reach dedicated to upstream migration $((Qp+Qa)/(Qe+Qp+Qs))$	Proportion of the total discharge of the Ariège transiting in the bypassed reach $(Qbr*/Qariège)$
Low-water (13.6 m^3/s)	100%	41%
Mean interannual discharge (MID) (41.8 m^3/s)	100%	13%
1.5xMID (62.7 m^3/s)	28%	36%
2xMID (83.6 m^3/s)	17%	52%

* Qbr: for the computing of the proportion of the total discharge of the Ariège transiting in the bypassed reach, the discharge allowed to downstream migration is included, which is not the case in the first column of the table

The proportion of discharge dedicated to upstream migration compared to the discharge in the bypassed reach is one of the parameters influencing the attractiveness of the fishpass. The proportion of discharge in the bypassed reach dedicated for upstream migration is very high for a discharge of the Ariège below the mean interannual discharge because there is not water overflowing the spillway. When the discharge is higher, water spills over the weir and the water from the upstream migration device represents only 28% to 17% of the discharge in the bypassed reach (for 1.5xMID and 2xMID), but this represents an acceptable proportion of the discharge to attract fishes in the fishpass.

Furthermore, the attractiveness of the bypassed reach, which depends on the proportion of discharge in the bypassed reach compared to the global discharge of the Ariège, also varies. For the mean interannual discharge only 13% of the discharge of the Ariège flows through the bypassed reach, so the attractiveness of the bypassed reach is probably lower. Due to the distribution of the discharges between the HPP and the bypassed reach, a significant part of fishes migrating upstream may enters the tailrace channel instead of the bypassed reach. Those fishes may accumulate a certain delay to migration.
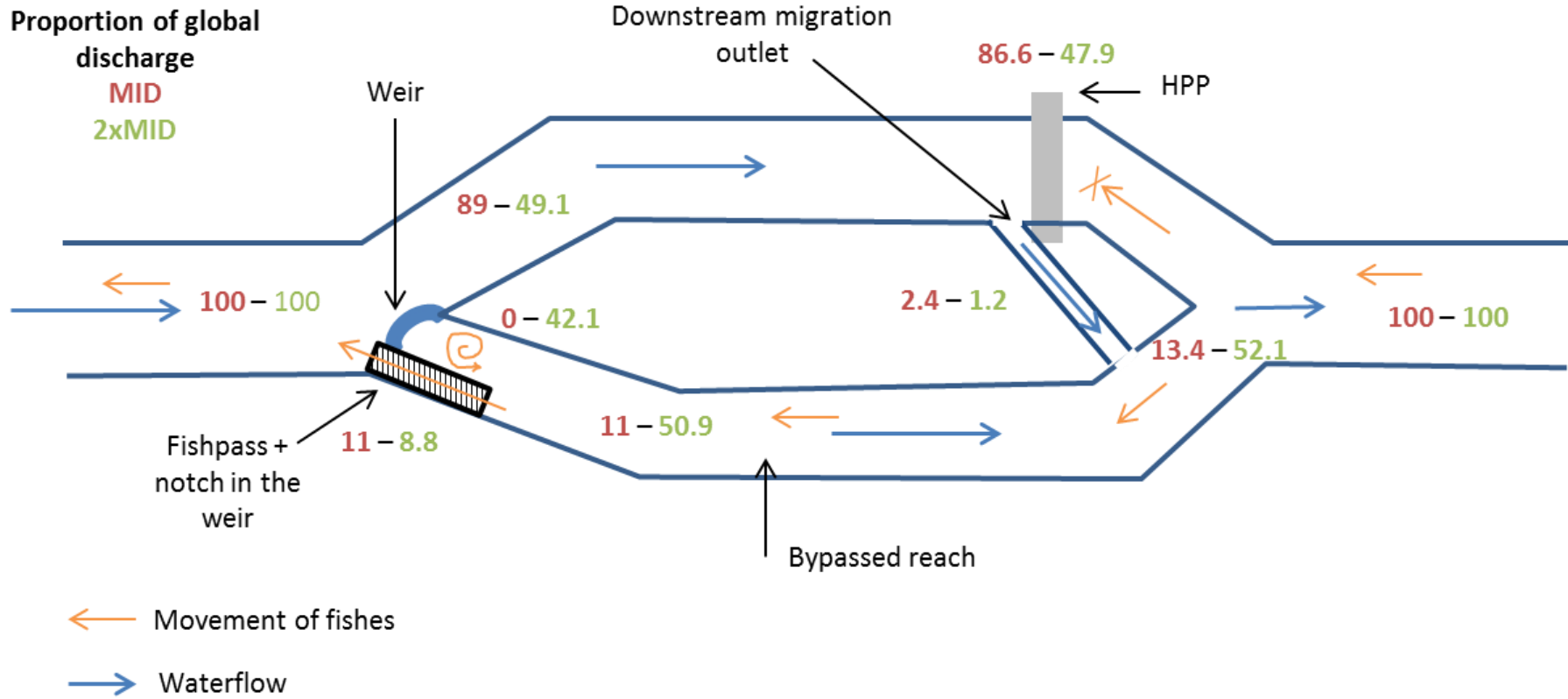
Figure 31: Proportion of global discharge in each reach influencing the attractiveness of upstream migrating devices with the former configuration (up to 2015)
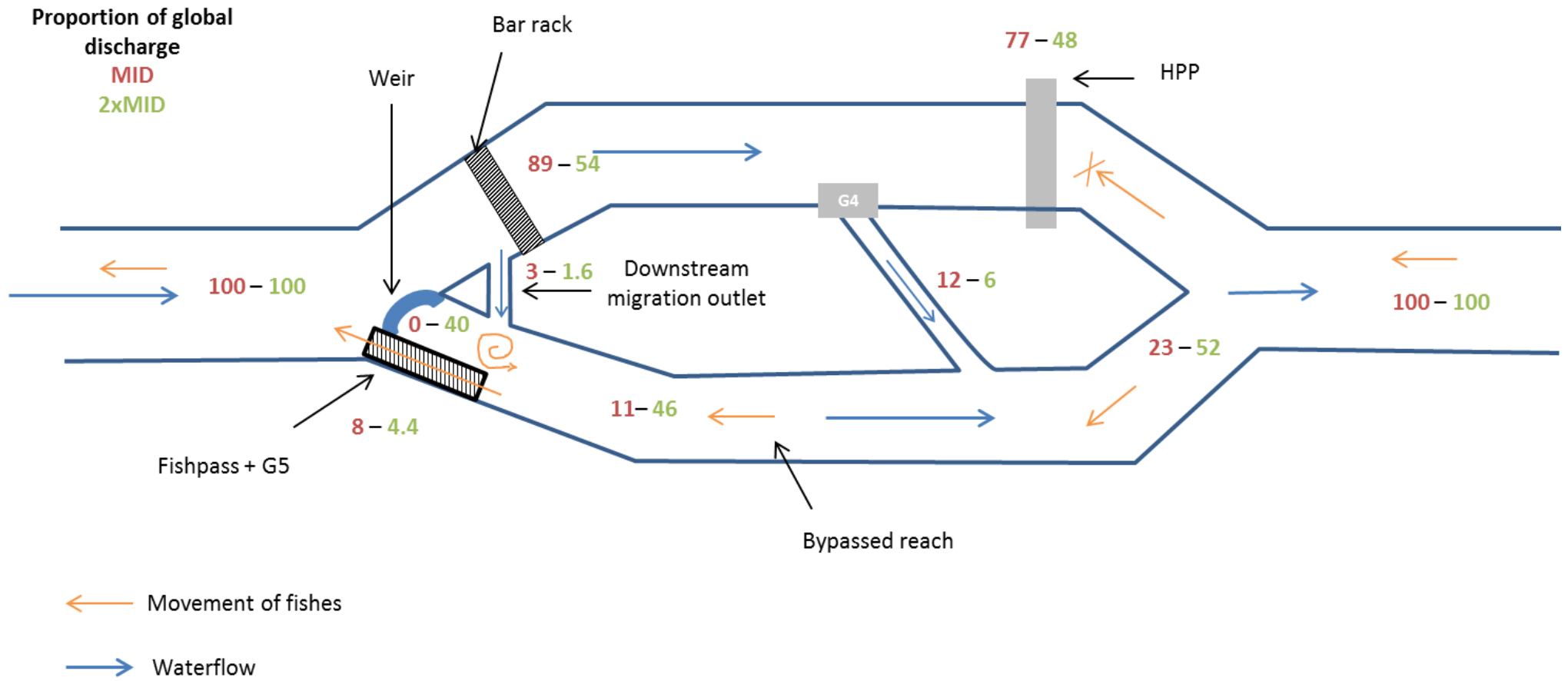
Figure 32: Proportion of global discharge in each reach with the site configuration today (since 2017)

The new configuration of Las Rives in 2017 changed the distribution of discharges. The proportion of discharge in the bypassed reach is greater than it used to be for the MID, it should be more attractive. But then the fishes can be confused in the bypassed reach because of the refund of G4 which represents 50% of the discharge in the bypassed reach for the MID.

Thanks to the tool CASSIOPEE developed by the AFB, the hydraulic conditions in the former fishpass were modelled. The falls are quit regular (30 cm) except the upstream one (38 cm). The dissipated powers are between 260 and 280 W/m^3. Salmonids and brow trouts can cross the device without big difficulties. Plunging jets are limiting the passability of the device by lampreys and eels. However, since there are bottom opening, the impact is considered limited.

The new fishpass (with the added pools in 2017) was not modelled.

2. Objectives on this Test Case

What we are planning?

In Las Rives different activities are planned:

- test of the efficiency of the fish friendly water intake for the smolts of Atlantic salmon and silver eels;
- assessment of the survival rate at the HPP;
- hydraulic measurement and modelling of the flow field of the fish friendly water intake in order to characterize the attractiveness of the bypasses;
- test of different shapes of outlet;
- Tests of survival of fish passing by the downstream migration device.

Why are we planning this on this Test case?

The test case site of Las Rives is very practical due to its location near Toulouse, where the Ecohydraulic team of the AFB-IMFT is working. The hydropower plant of Las Rives is part of a section of 20 km with 5 hydropower plants. We have data before and after the modernization of the devices. The fish friendly water intake is designed with the latest recommendations.

What are we expecting?

We expect from this test case to consolidate the design recommendation for fish friendly water intake, to precise the criteria to design the reception pool.

Relevance in FIThydro?

We will respond to some objectives of the project and WP2 like applying the existing SMTDs on a test case, have feedback on their use and application range.

3. Presentation and results of activities in FIThydro

3.1. Efficiency of downstream migration devices

3.1.1. Introduction

In 2017, the French Agency for Biodiversity, EDF (Electricité de France) and the engineering office Ecogea launched the EFIGRI project (Etude de l'efficacité des prises d'eau ichtyocompatibles pour les smolts de saumon atlantique et les anguilles argentées – Study on the effectiveness of fish-friendly water intake for Atlantic salmon smolts and silver eels). The FIThydro project concerns only a part of this global project.

This study aims to assess the effectiveness of fish-friendly water intake for Atlantic salmon smolts and silver eels during two downstream migration periods, at hydropower plants with a maximum turbined flow between 30 and 50 m^3/s. Atlantic salmon smolts were monitored during spring 2017 and spring 2018. The silver eels were monitored during autumn-winter 2017-2018 and autumn-winter 2018-2019 (monitoring still on-going). These periods correspond to the natural downstream migration periods of these species.

The fishes are monitored along 5 hydropower plants: Crampagna – Las Rives – Las Mijeannes – Guilhot – Pébernat (only 4 for the smolts, without Crampagna).

Only the results at Las Rives are presented.
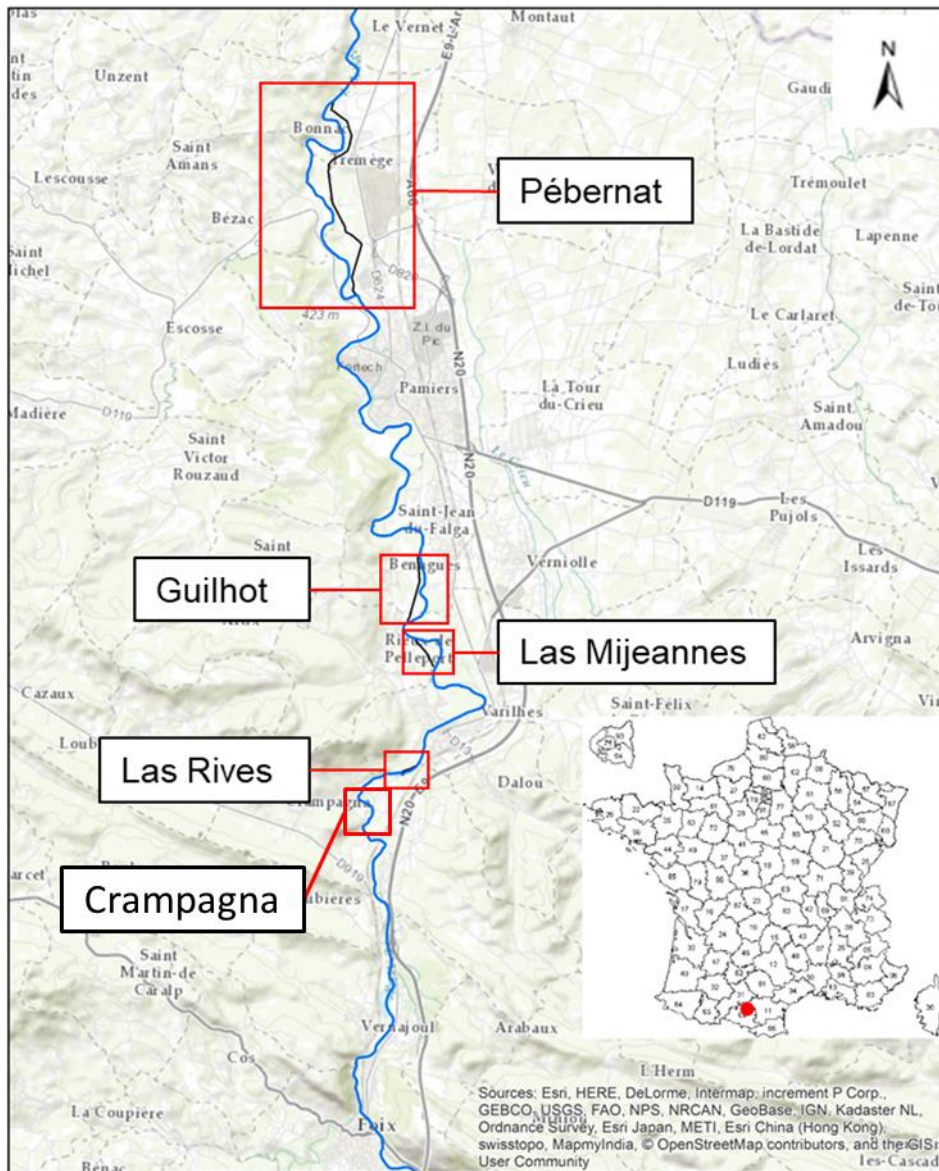
AFB, 2017

3.1.2. Methodology

3.1.2.1. Technology

The fishes are monitored by Radio-telemetry in order to identify their downstream migration paths at hydroelectric schemes (over the weir, using the bypass or passing through the rack and the turbine). This technology has been chosen because it allows assessing precisely the efficiency of the downstream migration devices at each site and to monitor the progression of fish from upstream to downstream. This technology has already been used in previous studies and allows a reliable identification of fish and of their migration path.
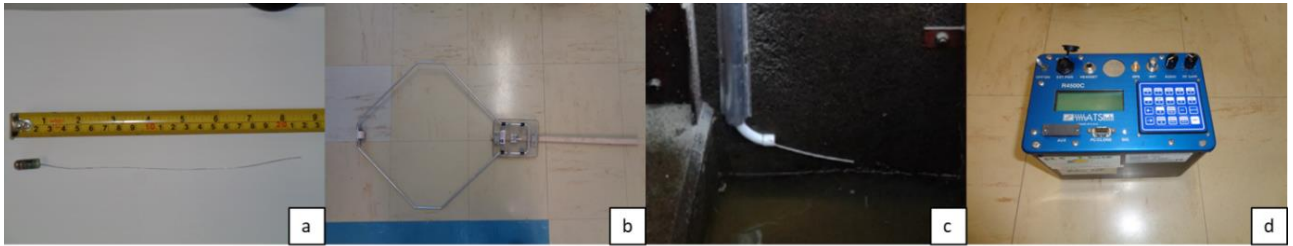
Figure 33: Radio telemetry material used: a) mark F1720 for Atlantic salmon smolts, b) aerial loop antenna, c) immersed strand antenna, d) receiving station RC4500 from ATS.

3.1.2.2. Set of detection antennas

To identify the path of downstream migrating fish among the 3 possibilities (over the weir, using the bypass or passing through the rack and the turbine), 5 zones are equipped with antennas (Figure 34):

➔ Entry zone (E) upstream the trash rack, detecting the fishes coming in front the downstream migration device;
➔ Upstream zone of the downstream migration device (A) indicating the approach and the entry through the device;
➔ Zone in the downstream migration device settled in the downstream migration channel (P) confirming that the fish is using it;
➔ Zone in the headrace channel (C) indicating the passage through the trash rack towards the turbines;
➔ Zone in the bypassed reach of the Ariège (T) indicating passage through the weir (fishpass or spillway) or through the downstream migration device.

The efficiency of device for downstream migration is defined as the ratio between the number of smolts using the device (detected at P) and the number of smolts that enter the intake (detected at E).
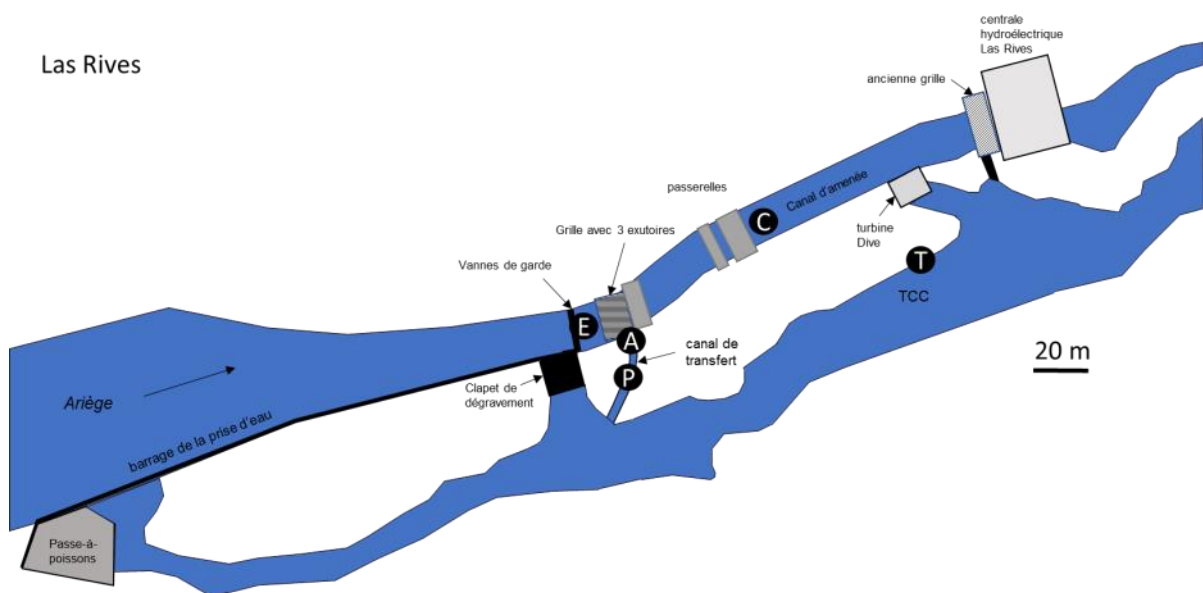
Figure 34: Set of detection antennas installed at Las Rives

3.1.2.3. Tagging and release

Atlantic salmon smolts are marked with type mark F1720 (Advanced Telemetry Systems, 45 ppm, guaranteed lifetime 1 day, observed lifetime 8-10 days, size of transmitter 20*7mm, 2g).

Eels are marked with type mark F1215C (Advanced Telemetry System, 45.80 ppm, guaranteed lifetime 25 days, observed lifetime 3 months, size of transmitter 55 or 65*10mm, 13g).

Smolts Spring 2017 and 2018

In spring 2017, 2 batches of 25 smolts were released upstream Las Rives.

In spring 2018, 4 batches of 25 smolts were released upstream Las Rives.

Silver eels winter 2017-2018 and 2018-2019

In January 2018, 2 batches of eels for a total of 96 were released upstream Las Rives.

In December 2018, 1 batch of 98 eels was released upstream Las Rives.

Table 12: Size of tagged fishes

Size (mm)	Smolts 2017	Eels 2018	Smolts 2018	Eels 2019
min	161	549	161	585
average	175	651	175	694
max	187	930	190	927

3.1.3. Results

Smolts in spring 2017 and 2018

Overall in spring 2017 and 2018, 137 smolts were monitored at Las Rives. 35 passed directly over the weir during overflow events, 88 used the downstream device and 14 passed through the rack and via the turbines. The efficiency of the fish-friendly intake is 86.3% (88 /[14+88]) (Tetard S, 2019).

Eels in winter 2017-2018 and 2018-2019

In winter 2017-2018, 74 silver eels were monitored at Las Rives: 73% passed directly over the weir during overflow events and 27% used the downstream device. In winter 2017-2018, 60 silver eels were monitored: 20% passed directly over the weir during overflow events and 80% used the downstream device. No eel passed through the rack and via the turbines. The efficiency of the fish-friendly intake is 100% (Tomanova S, 2019).
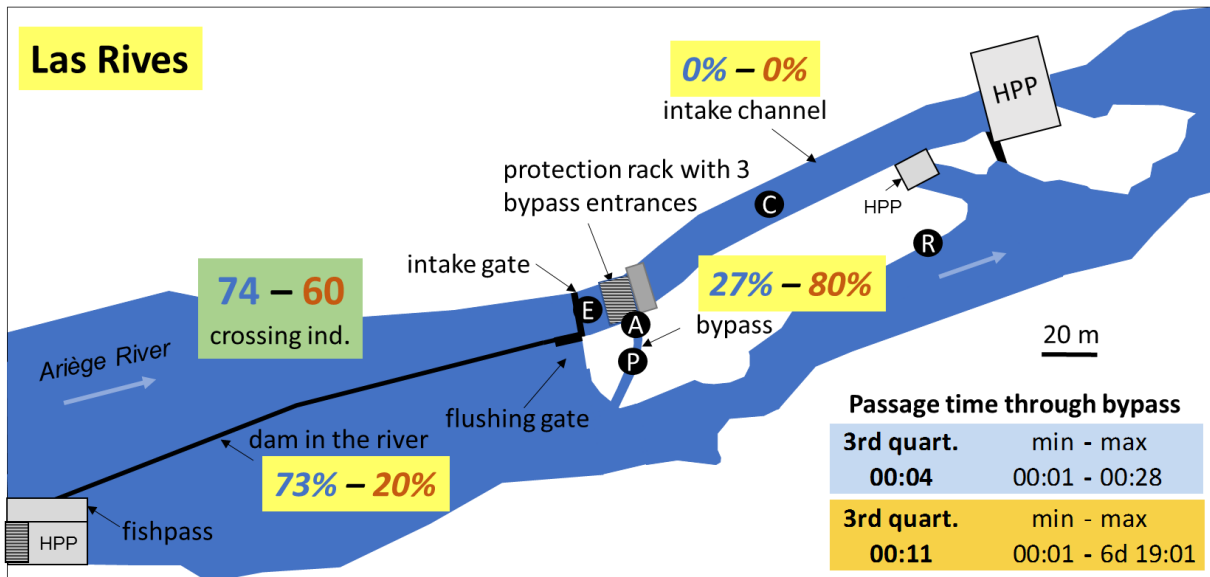
Figure 36: Passage routes of downstream migrating silver eels at Las Rives, overall in spring 2017 and 2018 (Tomanova S, 2019).

3.2. Harmlessness of downstream migration device

3.2.1. Objectives of the study

At Las Rives hydropower plant, a new downstream migration device was built in 2015 in order to protect downstream migrating fishes (atlantic salmon smolts and silver eels) and avoid them to pass through turbines. This device is located at the head of the headrace channel. It is a inclined bar rack (barspacing 20 mm, inclination 26° to the horizontal) combined with 3 outlets at the top of the bar rack. The downstream migration discharge (1.35 m^3/s) is collected in the downstream migration duct and is controlled by a weir. Then the discharge is evacuated to the bypassed reach through a channel.

Following the implementation of the downstream migration device, some issues were addressed:

- About the landing conditions of fishes at the foot of the control weir at the end of the downstream migration duct : fishes fall of 0.9 m without any water cushion at the beginning of the downstream migration channel ;
- About the landing conditions in the bypassed reach of downstream migrating fishes passing through the device : low water level in the jet landing area;

The landing conditions of fishes at the foot of the control weir have been improved during Fall 2017 thanks to the implementation of an inclined ramp over 2.6 m long downstream the control weir, see Figure 37.
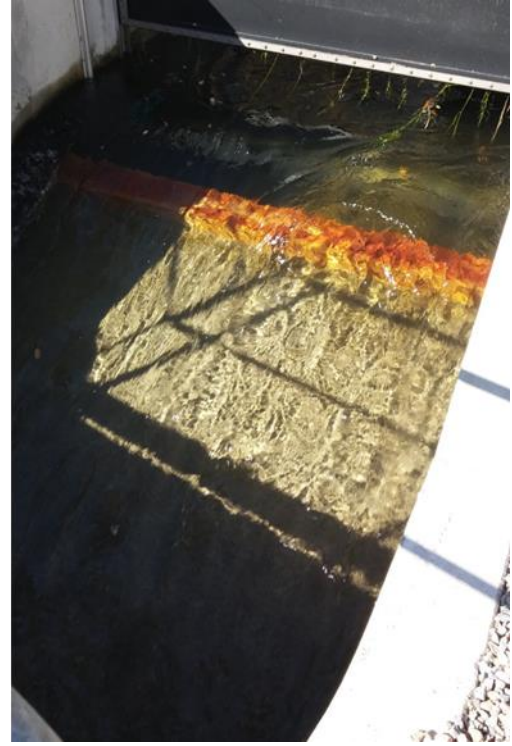
Figure 37: left drop after the control weir until 2017; right: inclined ramp after the control weir today

The objectives of the study are:

- Characterize the actual hydraulic landing conditions of the downstream migration discharge in the bypassed reach (output velocity from the downstream migration channel; impact velocity in the bypassed reach; water level in the bypassed reach) in order to rely it to the damage rate of fishes;
- Study different solutions to improve landing conditions (extension of the downstream migration channel in order to reach a deeper zone; better dispersion of the jet).

3.2.2. Characterization of actual hydraulic conditions

In order to determine the flow conditions in the downstream migration channel, the velocity and the water level are computed from the Manning-Strickler formula. We make the hypothesis that the flow is in uniform regime (water surface parallel to the floor of the channel):

$$Q = KSR^{2/3}\sqrt{i}$$

With :

- **Q** discharge in the channel (m³/s)
- **K** roughness coefficient (m$^{1/3}$/s)

- **S** flow section (m²),
- **R** hydraulic radius (m) obtained par ratio between flow section and wet perimeter (**S** / **P**).
- **i** slope of channel (m/m)

From the slope of channel and flow velocity at the output of the channel, it is possible to calculate the jet trajectory in the channel axis until the impact with the landing water surface and its velocity.

For this purpose, a trajectory equation of a projectile in free-fall is used, the air friction is neglicted (Chow 1959 ; Duarte et al. 2016). This approach already shows results congruent is calculations and reality, for example at the downstream migration duct at Mauléon on the Saison river (France).

$$x(t) = x_0 + V_{x0} * t$$

$$z(t) = z_0 - \frac{1}{2} * g * t^2 + V_{z0} * t$$

$$V_x(t) = constante = V_{x0}$$

$$V_z(t) = V_{z0} - g * t$$

With :

- x_0 and z_0 coordinates of the starting point of the jet, according the axis of the jet (x) and in altitude (z).
- V_{x0} and V_{z0} the component of flow velocity along the axis of the jet and vertical, at the starting point of the jet (output of downstream migration channel), calculated regarding the flow velocity at the end of the downstream migration channel and the final orientation of the channel (V_{z0} positive if it is oriented upward and negative if oriented downward).
- **t** time in seconds.
- **g** acceleration of gravity (9.81 m/s²).
- $V_x(t)$ and $V_z(t)$ the components of flow velocity along jet axis and the vertical at moment **t**.

Considering a downstream migration discharge of 1.35 m³/s, **the water depth in the channel is about 0.28-0.29 m and the flow velocity is about 5.2-5.3 m/s**. Considering a height of fall of the jet in the landing pool between 3.36 and 3.65 m, the impact velocity and the horizontal distance travelled before entering the landing pool are about:

- V_{impact}= **9.6-10.0 m/s**
- $D_{horizontal}$= **4.20-4.45 m**

Time of fall is about 0.80-0.84 s and the distance travelled along the jet axis is 5.5-6.0 m.
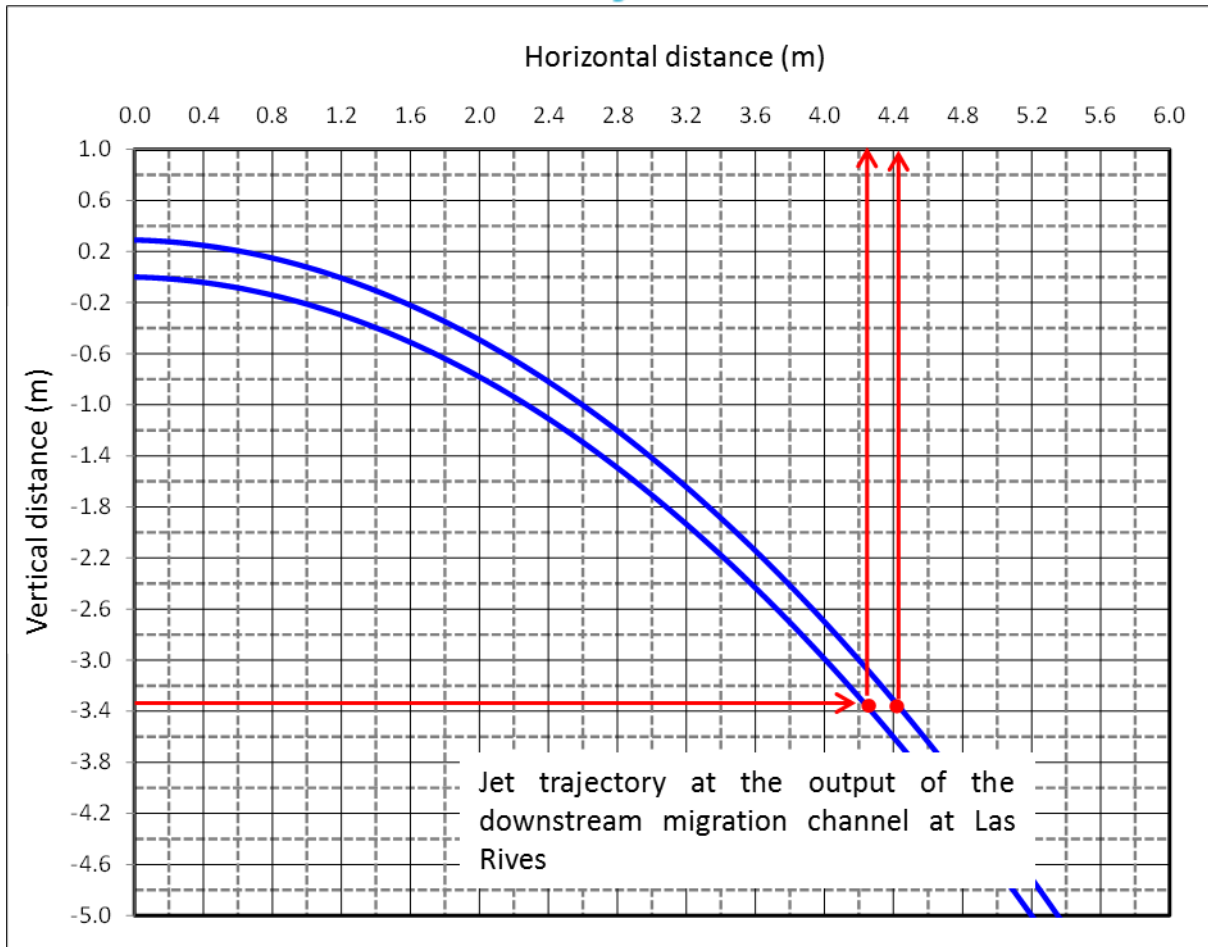
Figure 38: Jet trajectory at the output of the downstream migration channel at Las Rives in actual setting (with V_{x0} and V_{z0} equal to +5.25 m/s and -0.18 m/s respectively).

The impact area of the jet on the floor constitute of bedrock is clearly identifiable (Figure 39). This area has a surface of about 3 m², its width is 2.15 m. This is over the 1.27 m of final width of the downstream migration channel, the jet spread out laterally during the fall.

For recall, the downstream migration channel of 0.9 m wide widens symmetrically at its terminal part on a length of 1.47 m to attain 1.27 m. This corresponds to a gain of 0.24 m width/m of length and an opening angle of the walls of 7.2°.

The discharge goes through the part where the channel widened in 0.276s (1.27 m/5.25 m/s). Hence a « widening velocity » of the jet of 1.34 m/s. Taken into account the time of fall of the jet (0.80-0.84 s), we can deduce a widening of 1.07-1.12 m during the fall, and so a total width of the jet at the impact about 2.34-2.39 m.

The two jet widths (width of the impact mark on the floor of the landing pool and calculated width) correspond. The jet takes benefit of the widening.
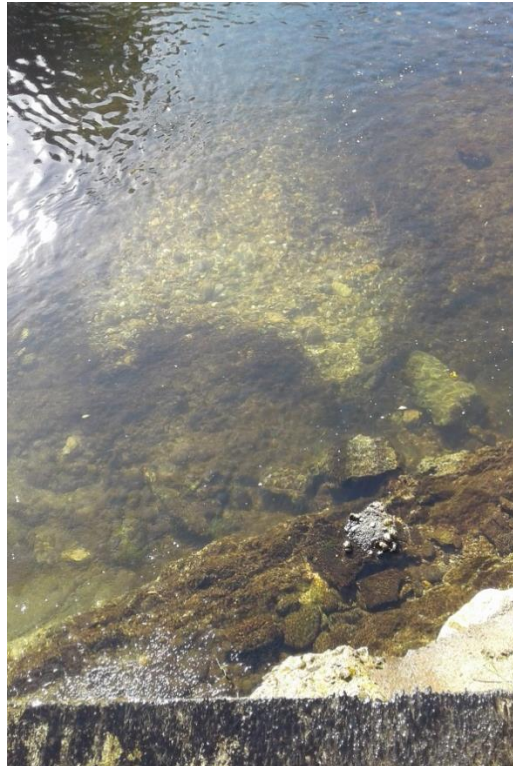
Figure 39: Impact area of the jet – view from the downstream end of the downstream migration channel

Figure 40 allows to represent the jet trajectory calculated and to compare the deduced impact point in the landing pool with the impact zone observed on the floor.

On this profile establish in the axis of the downstream migration channel, we can note a deeper zone (> 2 m) but this one is 11 m away from the downstream end of the channel and at 7.3 m of the actual impact zone of the jet.
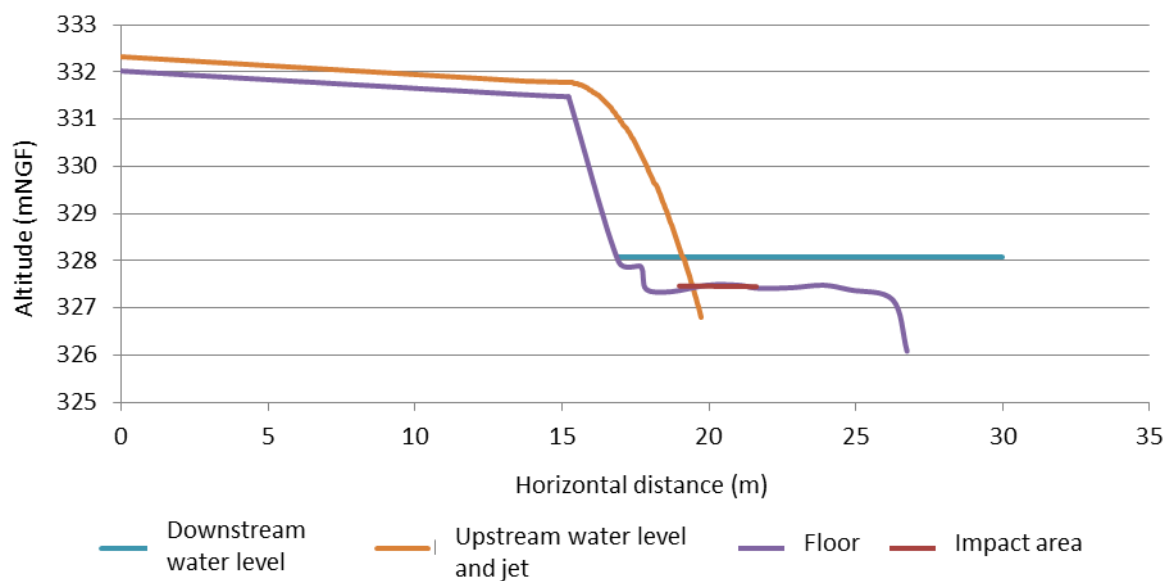
Figure 40: Calculated trajectory of the jet in actual setting

3.3. Hydraulic modelling

3.3.1. Characterization of currentology upstream the bar rack

3.3.1.1. Deployment of the ADCP probe

The currentology measures upstream the bar rack have been made with an Acoustic Doppler Current Profiler (ADCP) StreamPro Teledyne RDI (Figure 41). The probe is equipped with 4 sensors which issuance-reception beams are inclined of 20° to the axis of the probe. The width of a beam is 3°. The probe is vertically settled and slightly immersed (a few cm). The device measures the water depth, and the 3 components of flow velocity within 20 measurements cells uniformly distributed along the water column. The division of the cells is continuous during the measures and defined according maximal depth provided by the operator. The frequency of measure acquisition is 1 Hz.

Figure 41: Pictures of the ADCP StreamPro assembled on its trimaran and the probe with a closer view of the 4 sensors

The flow conditions in Las Rives turned out to be to restless to deploy correctly the ADCP the common way, i.e. assembled on a trimaran and manoeuvred with a system of ropes. Furthermore, it is not certain that the "Bottom Tracking" system allows the device to measure its own movement to the bottom in the case where the ADCP stands above the inclined bar rack. Finally, the presence of metal pieces in the water intake could disturb the functioning of the compass and therefore the computing of its own path.

That is why a support and movement cart system was developed to deploy the ADCP in a good way (Figure 42). The support is constituted of aluminium beams of square section (289*289 mm²) with different pieces of 2 or 3m long clipped with each other's. These structures are usually used to set stages up for shows or stands. With a length 1 m higher than the water intake length, the weight was about 94 kg. Setting up such a support demands 6 persons. The movement cart has been made with NORCAN elements and handled with a rope system. This system allows a stationary and precise positioning of the ADCP probe, controlled by the operator and thus not using the "Bottom tracking" of the device.

In order to control the positioning of the probe, in particular it altitude to the bending of the support, the exact positioning of the top of the probe was measured thanks to a tacheometer LEICA TS02-Ultra-7 (directly aimed in "laser beam" mode).

Figure 42 : Support and movement carts system allowing the deployment of the ADCP

The measures were made by positioning the probe at stationary points within time to get at least 30 valid measurements. Each transversal transect is described by several measurements points spaced with 1.0 m in general and 0.5 m for the transect at the top of the bar rack where a higher precision of measure was desired. Along the vertical banks of the water intake, the first and the last measurements points were placed between 1 m and 0.5 m from the bank to avoid that the measurements beams impact the wall.

At Las Rives, measures were made at 4 transversal transects located 2, 4, 6 and 10 m upstream the top of the bar rack (Figure 43). The immersion point of the bar rack is located about 0.65-0.7 m upstream the top of the bar rack. The entrance of the outlets stands about 1.85 m from the top. The transect at 10 m stands about the foot of the bar rack and the 2 m transect stand just upstream the entrance of the outlets (about 0.15 m).
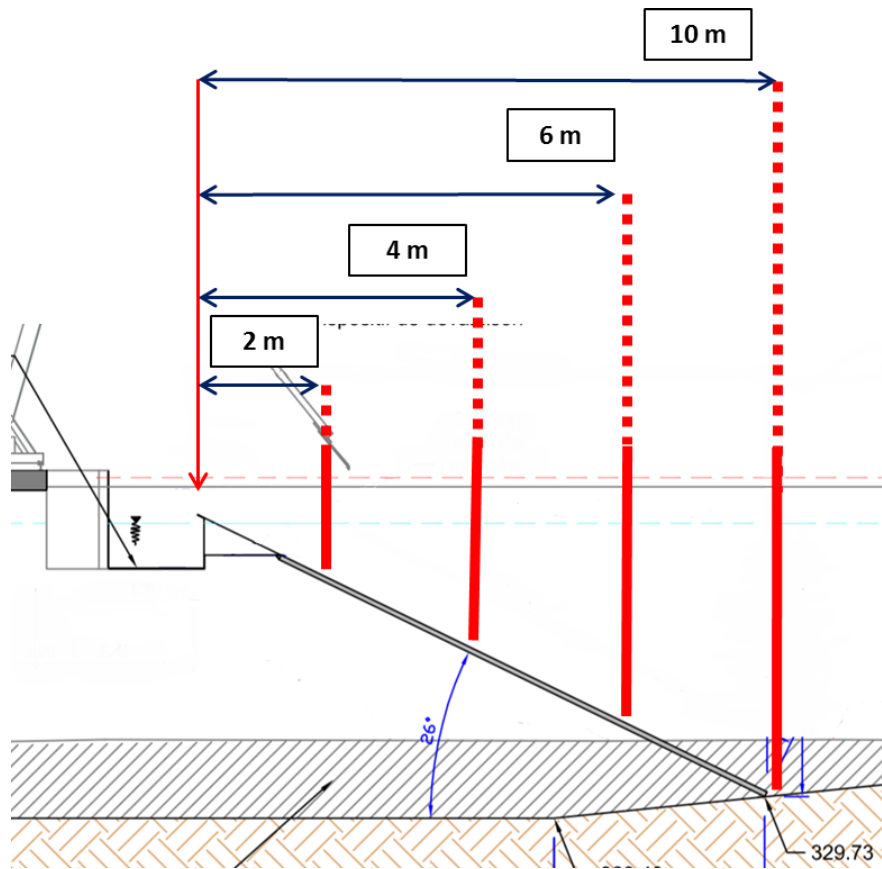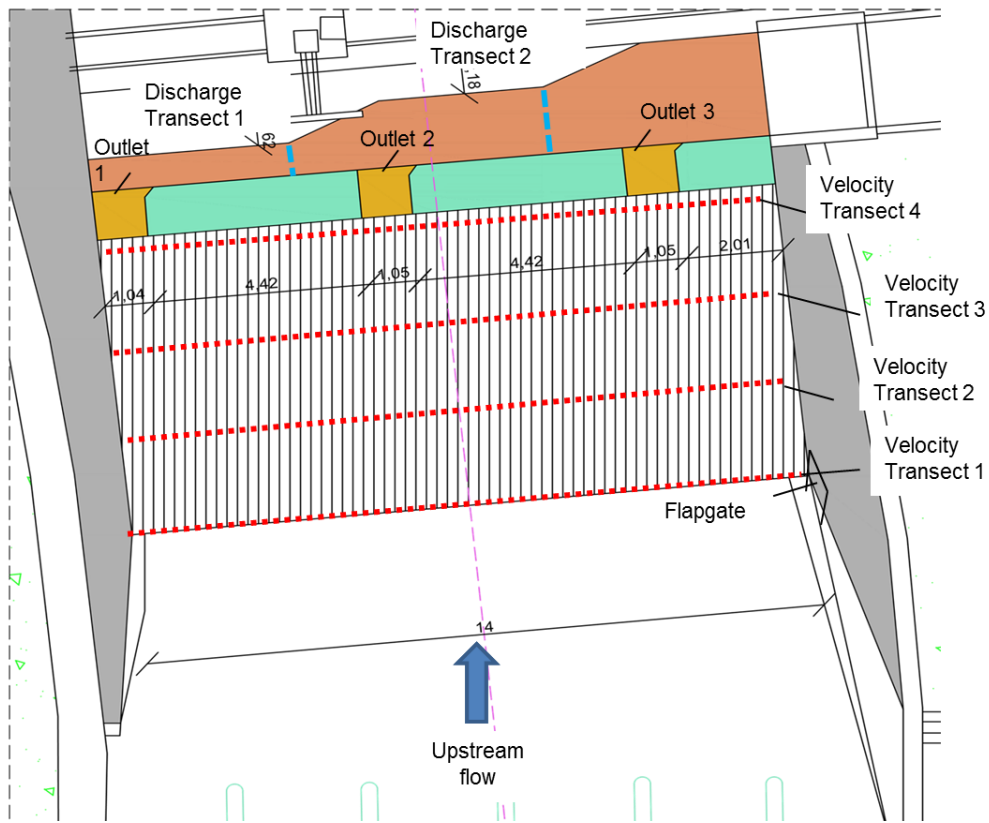
Figure 43: Positioning of the ADCP measurements transects at Las Rives

3.3.1.2. Acquisition, processing and representation of the data

The measure acquisition was made with Teledyn Winriver II software. The data were then export with ASCII format.

The results allow characterizing the different components of flow velocity (Figure 44):

- The component in the axis of the water intake V_X

- The component transversal to the axis of the water intake V_Y (positive from the right bank to the left bank)

- The vertical component V_Z (positive bottom-up)

- The component normal to the bar rack V_N

- The component tangential to the bar rack V_T
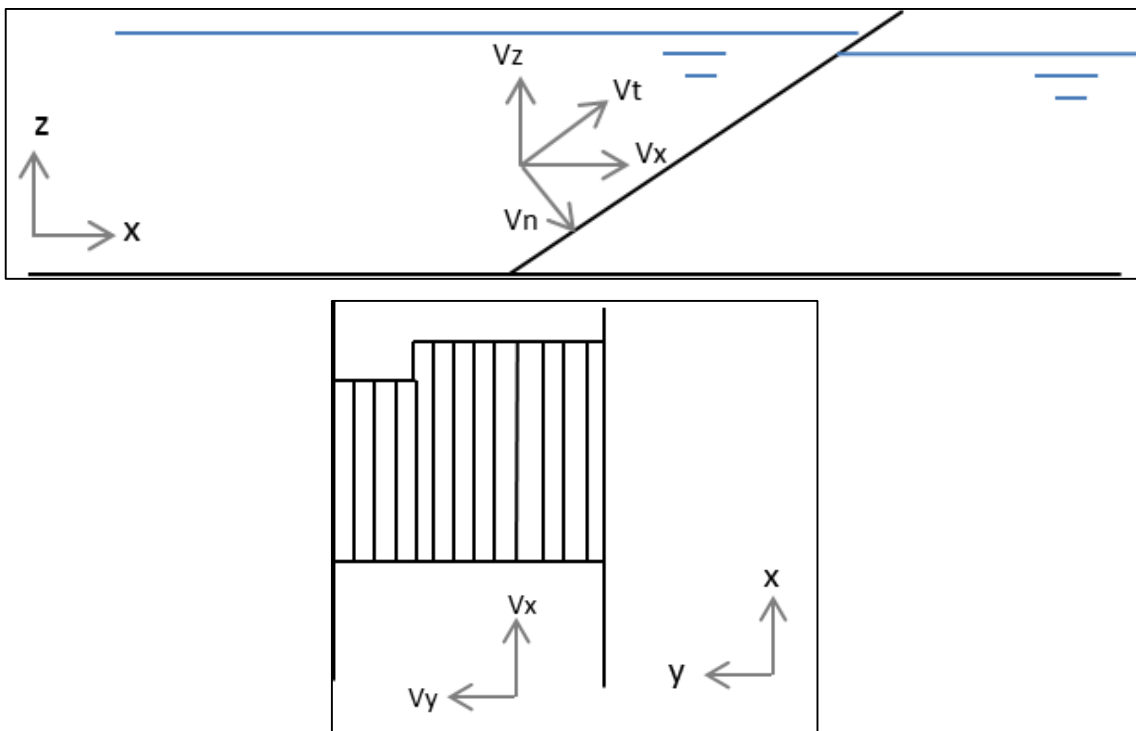
Figure 44: Diagram of the components of analysed velocity; longitudinal view (top) and plan view (down)

The results are presented either under dimensional form, or under dimensionless form in being divided by the output velocity at the water intake V_0; determined from the mean turbined discharge during the measurements and the flow section at the foot of the bar rack (also called approach velocity).

3.3.2. Distribution of discharge between the 3 outlets

3.3.2.1. Methodology

The distribution between the 3 downstream migration outlets was characterized carrying out:

- 2 gaugings with a flowmeter in the downstream migration duct

- o The first gauging in the portion between the first outlet at the left bank and the central outlet, just upstream the first enlargement

- o And the second gauging in the portion between the central and the third outlet at the right bank, just upstream the second enlargement (section 1 and 2, see Figure 45)

- And an assessment of the total discharge transiting by the downstream migration duct thanks to a « weir law »

The discharges of the outlet in central and right bank position are obtained by subtraction of these different measurements.

Figure 45: Positioning of the gaugings in the downstream migration duct at Las Rives

3.3.2.2. *Gaugings with the flow meter in the downstream migration duct*

The gaugings in the downstream migration duct were made with an electro-magnetic flow meter Marsh McBirney, FLO-MATE 2000. The measurements on each section were made the following way:

- Measure if the width of the section and cutting in verticals 10 cm from each bank then in equal parts from ± 20 cm ;

- For each vertical:

- o Measure of water height;

- o Measure of the velocity in 6 points in the water column since the hypothesis of a logarithmical velocity profile cannot be made: bottom, 20%, 40%, 60% and 80% of water height and finally to the surface. Each measure consists in an average of the velocity in 30 seconds

Near lateral walls, the device had sometimes some measurements issues with certain values missing periodically. This had for consequence to avoid the computing of the average value by the device. To limit the waste of time due to this issue, 2 measurements of velocity over 15 seconds were made at each point.

The operator in the downstream migration duct was equipped with waders with felt soles to reduce risk of skidding on the metal bottom of the duct, a helmet, a life jacket and a harness to be secure via a rope by a second operator. A special care was brought to stand as downstream as possible from the measurement section in order not to skew the measure.

Figure 46: Example of an electro-magnetic flow meter and an operator in position in the downstream migration duct
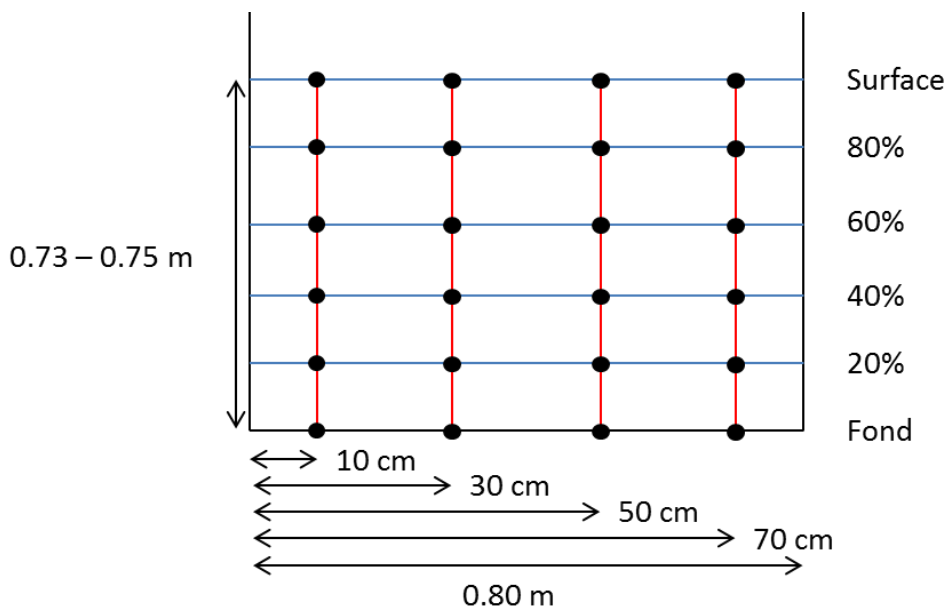
Figure 47: Cutting of a section during the measure by a flow meter, in red the verticals, the black dots correspond to the measurement points

The discharge is calculated according norm EN ISO 748:2007, by the method of mean section, by calculating the mean velocity between the banks and the closer verticals. The mean velocity on each vertical is calculated that way:

$$V_{moy} = 0.1(V_s + 2V_{0.8} + 2V_{0.6} + 2V_{0.4} + 2V_{0.2} + V_{pf})$$

Then a mean velocity is calculated for each flow section between the verticals and the closer bank; by making an average for the sections without including the banks, and by applying following formula:

$$V_{moy\ section} = \frac{m}{m+1} * V_{moy\ closer\ vertical}$$

Here, $m = 10$ due to the smooth nature of the duct.

The discharge by flow section is then calculated:

$$Q_{section} = V_{moy\ section} * H_{eau\ moy} * L_{\text{écoulement}}$$

In order to have the total discharge, just summon all discharge per section.

3.3.3. Assessment of the total discharge transiting through the downstream migration duct thanks to a « weir law »

The total discharge transiting through the downstream migration duct could be evaluated by gauging in the duct downstream the third outlet. However, the gauging is quite complicated at this place. Indeed, the velocities are high and it is more complicated for the operator to stand in the duct.

That's why, it was preferred to assess the total discharge transiting through the migration duct at the control weir, from a transcript of the characteristics of the weir (width, level of overflow), of the duct when approaching the weir (width, bottom) and water level upstream.

The different levels have been measured thanks to a tacheometer LEICA TS02-Ultra-7 (aimed at a prism settled on a stick). The levels were readjusted in altitude referring to reference points.

To compute the total discharge, the tool Devers from Cassiopée® software was used, taking into account the correction linked to the high flow velocities in the duct when approaching the control weir (Bos correction (1989)). The calculation need to determine the value of the flow coefficient, which depends on:

- The ration between the width of the weir and the width of the duct, which rules the intensity of lateral detachments. In this situation, the weir is as wide as the duct upstream, there is no lateral detachment. This leads to a high value of flow coefficient.
- The ratio between the head on the weir and the water level upstream (the difference being the height of the weir against the floor) which rules the intensity of vertical detachment.
- The type and the shape of the weir.

The resolution of the flow coefficient relied on elements from the « hydrometry » guide from the ONEMA (Le Coz et al. 2011).

3.3.4. Data of functioning during the measures

The data of functioning of the HPP during the measures were provided by the operator ONDULIA. These data included:

- At the HPP: water levels upstream and downstream, and power output produced, which allow calculating the turbined discharge according an assessment of the global performance of the turbines.
- At the bar rack: the water level at the dam, upstream and downstream the bar rack.

These data were provided with a time slot of 10 minutes. This allows assessing the functioning conditions of the HPP during the measures.

3.3.4.1. Measurements of July 2017

The 11th and 12th July 2017, ADCP and current meter measurements were done at Las Rives. Figure 48 and Figure 49 correspond to the conditions during the measurements. The ADCP measurements happened on July 11th 2017 between 10:50 and 17:00. The current meter measurements were made on July 12th 2017 between 15:20 and 17:20. During these measures the Ariège discharge at Foix varied between 17 and 24 m^3/s, and was in average equal to 19.5 m^3/s. The HPP didn't operated at its maximum during the measurements (45 m^3/s). The mean turbined discharge during the ADCP measurements was 14.7 m^3/s and was 12.7 m^3/s during the current meter measurements.

The variation of the water level upstream the bar rack were weak, between -0.7 and -2.2 cm to the line of the dam on July 11th, and between 0 and -2.6 cm on July 12th.

Please note that during the measurements, at the upstream corner of the dam, some infrastructures works were in progress in order to install a new turbine (G5 turbing the E-flow). Hence, the bottom gate dealing with draining the fine sediments from the foot of the grid was open. The measurements conditions were impacted by these flow changes.

The standard discharge used for the study of the measures in front of the bar rack corresponds to the sum of the turbined discharge and the downstream migration discharge: the discharge upstream the bar rack.

The discharge upstream the bar rack used to have dimensionless values is Q=16.87 m^3/s and give a output velocity V_0=0.29 m/s for a surface of the water intake S=58.52 m².
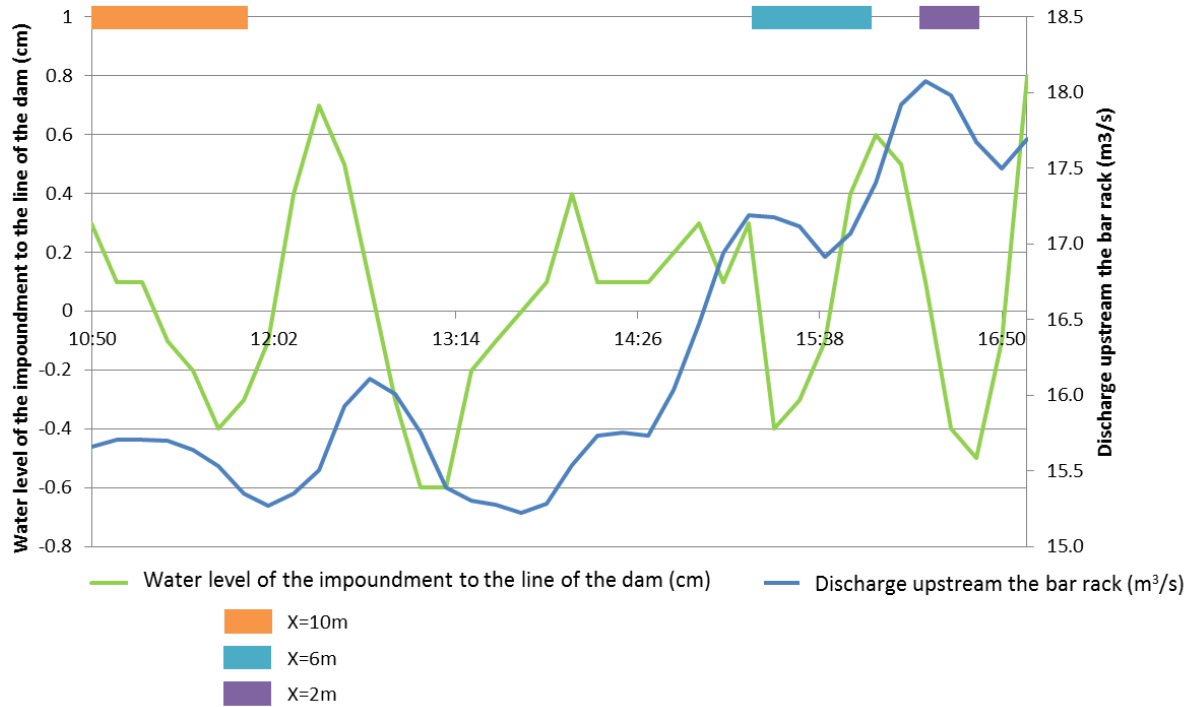
Figure 48: Evolution of the impoundment water level and the discharge upstream the bar rack during the ADCP measurements on July 11th 2017
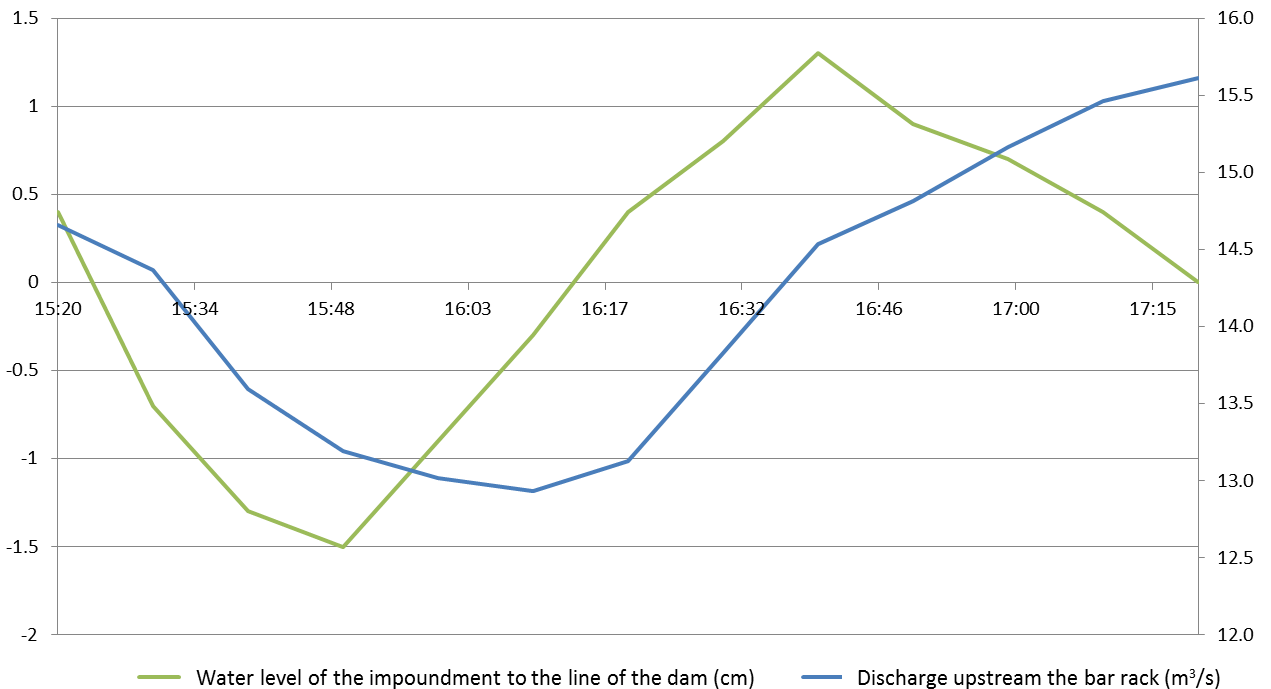
Figure 49: Evolution of the impoundment water level and the discharge upstream the bar rack during the current meter measurements on July 12th, 2017

3.3.4.2. Measurements of July 2018

The 3rd July 2018, the discharge of the Ariège varied between 54.20 and 55.25 m^3/s at the hydrometric station of Foix located upstream.

The measures at Las Rives happened between 11:30 and 16:30. The turbined discharge at the HPP (G1 to G4) was quite steady and between 43.4 and 46.6 m^3/s. The HPP worked full power during the measures (design discharge of 45 m^3/s). The total discharge of the Ariège was recalculated at the site of Las Rives and varied between 48.7 and 59.7 m^3/s. The water level at the dam varied between -2.2 cm and 8.5 cm (to the crest of the dam), cf.Figure 50.
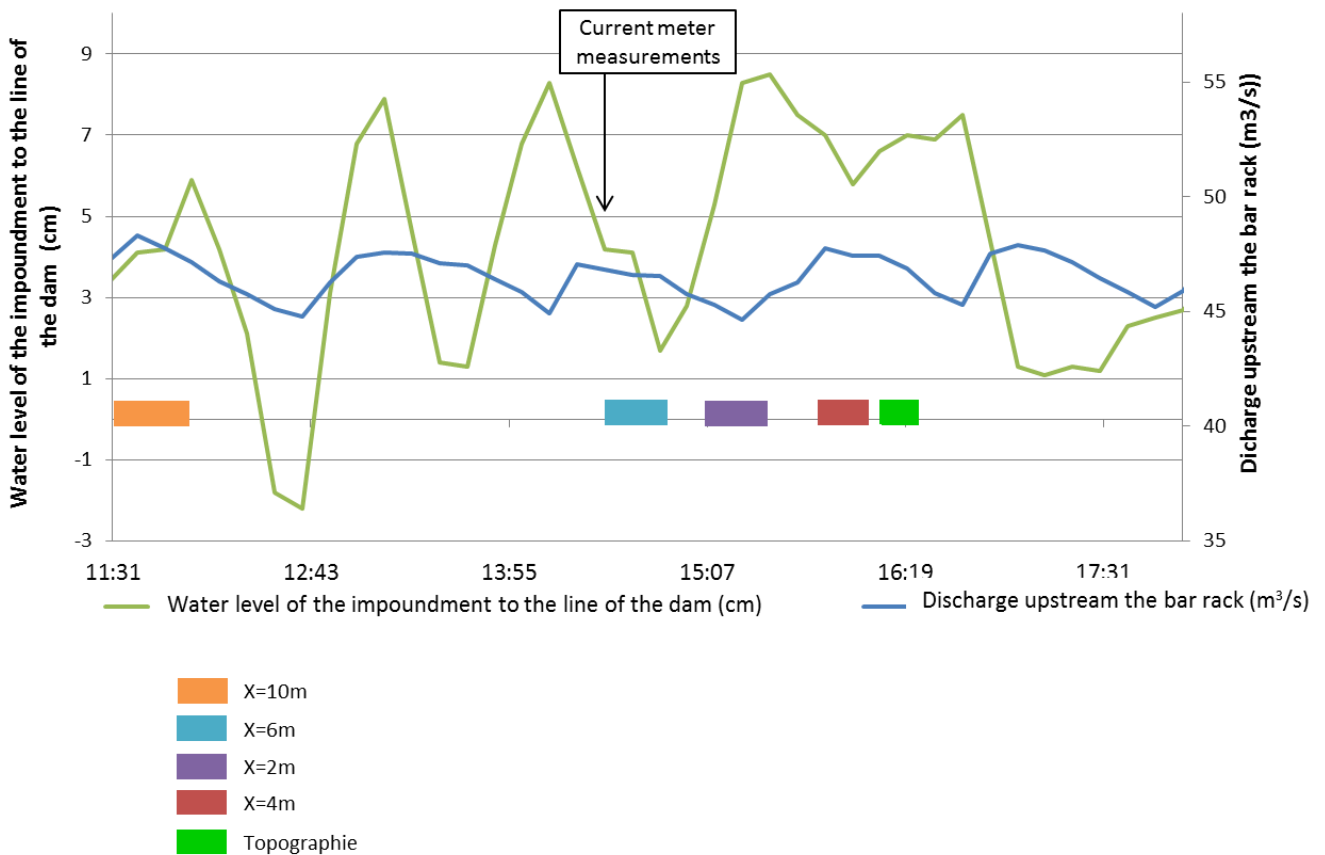
Figure 50: Variation of water level and total discharge of the Ariège during the measures at Las Rives

The discharge upstream the bar rack used to have dimensionless values is Q=46.78 m^3/s and give a output velocity V$_0$=0.8 m/s for a surface of the water intake S=58.52 m².

3.3.5. Discharge transiting through the downstream migration duct and distribution between the outlets

3.3.5.1. Measurements of July 2017

Table 13 presents the assessment of total discharge going through the downstream migration duct and the distribution of the discharges between the outlets (the detailed calculations are presented in annex).

The total discharge is assessed to 1.312 m³/s, that means 97%of the theoretical value (1.35 m³/s). The discharges of outlet 1 (left bank), 2 (middle) and 3 (right bank) are respectively 0.271 m³/s, 0.360 m³/s and 0.682 m³/s. The discharge feeding of the two first outlets seems disfavoured compared to the third, at the right bank. This is a usual phenomenon linked to the head losses along the downstream migration duct, but here it seems quite exacerbated for outlets 1 and 2.

The entrance velocity of outlet 1 (0.52 m/s) is below the targeted theoretical value (0.90 m/s). The entrance velocity of outlet 2 is also below this value. However, the entrance velocity of outlet 3 is greater than this value.

Table 13 : Total discharge going through the downstream migration duct and the distribution of discharges between the outlets at Las Rives in July 2017

		Value (m³/s)	Proportion of total discharge	Mean velocity in the outlet (considering H = 0.5 m and L = 1.05 m)
Discharge outlet 1	Gauging	**0.271**	**20.6%**	0.52
Discharge outlet 2	Difference	**0.360**	**27.4%**	0.69
Discharge outlets 1+2	Gauging	0.630	48.0%	
Discharge outlet 3	Difference	**0.682**	**52.0%**	1.30
Total Discharge	Discharge formula	1.312	100.0%	

3.3.5.2. *Measurements of July 2018*

Table 14 presents the assessment of the total discharge transiting through the downstream migration duct, and the distribution of the discharge between the outlets (the detailed calculation are presented in Annex 1).

The total discharge for allocated to downstream migration is assessed to 1.13 m³/s, i.e. 84% of the theoretical value. The discharges of outlet 1 (left bank), 2 (central) and 3 (right bank) are respectively of 0.184 m³/s, 0.488 m³/s and 0.463 m³/s. The discharge supply of the first outlet seems to be disadvantaged regarding the two others. It is a common phenomenon due to the head losses along the duct, but it seems here quite exacerbated for outlet 1.

The velocity at the entrance of outlet 1 (0.36 m/s) is therefor quite below the targeted theoretical value (0.90 m/s). The velocities at the entrance of outlets 2 and 3 are close to this value.

Table 14: Total discharge transiting through the downstream migration duct, and distribution of the discharges between the outlets at Las Rives

	Value of discharge (m³/s)	Proportion of total discharge	Velocity at the entrance

				of the outlet (m/s)
Discharge outlet 1	Gauging	**0.184**	**16.2%**	**0.36**
Discharge outlet 2	Difference	**0.488**	**43.0%**	**0.98**
Discharge outlets 1+2	Gauging	0.671	59.2%	-
Discharge outlet 3	Difference	**0.463**	**40.8%**	**0.93**
Total Discharge	Discharge formula	1.134	100.0%	-

3.3.6. Currentology upstream the bar rack

3.3.6.1. Measurement of July 2017

Figure 51 presents the cartography of components V_X and V_Z of the dimensionless velocity at the 3 transects. The bar rack is viewed from upstream.

At the 2 transects located at 10 m and 6 m upstream the top of the bar rack the components V_X vary between $0.6V_0$ and $1.2V_0$, with higher values on the middle part reaching up to $1.8V_0$.

At the transect located 2 m upstream to top of the bar rack (about 0.15 m upstream the entrance of the outlets), the components V_X decrease significantly, it is linked to the obturation of the top of the grid on the same depth of the outlets with values between 0.6 to $1V_0$ and stay high in front of the outlets with values between 1.2 and $1.8V_0$ (that means 0.35 to 0.52 m/s). The outlet at the right bank is widely favoured (52% of the total downstream migration discharge). The components V_X at the entrance of the outlet are lower than the calculated velocity thanks to the assessment of the discharges in the outlets (between 0.52 and 1.30 m/s), however the transect is not located at the direct entrance of the outlets, but 15 cm upstream, a part of the discharge going through the outlet arrives laterally downstream the transect.

The vertical components of V_Z are very different on the 3 transects. For the transect located at 10 m, we note the effect of the opening of the bottom gate located at the right bank, it generates vertical velocities up to $-0.2V_0$ on over 4 m wide. For the transect located at 6 m, the V_Z values stay low (values between, -0.05 and +0.1 times V_0) with positive values at the left bank and lightly negative at the right bank. At the transect located at 2 m upstream the top of the grid, the V_Z components are noticeably negative (oriented to the bottom), with valued about -0.2 times V_0 between the outlets and about -0.1 times V_0 near the outlets. This evolution is linked to the fact that the flow has to "plunge" under the top of the grid which is obturated.

Figure 52 presents the cartography of components V_Y of the dimensionless velocity at the 3 transects. The bar rack is viewed from upstream.

The transversal components are very different depending on the transects. For the transect at 10 m, the opening of the bottom gate generate a flow oriented to the right bank. The value of V_Y can reach up to -0.4 times V_0 near the gate. For the transect at 6 m, the component V_Y of the velocity is in general lightly negatiive (-0.1 times V_0) except locally along the left bank where there is a positive zone about 0.1 times V_0. For the transect at 2 m, the transversal velocities are more pronounced with significant changes of orientation showing the convergence of the flow to the outlets.

Figure 53 presents the cartography of tangentiel components V_t and normal V_n of the dimensionless velocity to the bar rack at the 3 transects.

At the 2 transects located at 10 m and 6 m upstream to top of bar rack, the tangentiel components V_t present values between 0.75 and 1.5 time V_0 in the middle of the channel and between 0.5 and 1.25 times V_0 along the banks.

At the transect located 2 m upstream the top of the grid (about 0.15 m upstream the entrance of the outlets), the components V_t decrease significantly between the outlets linked to the obturation of the

top of the grid with values about 0.25 to 0.75 V_0 in front of the outlets. To be note that for the velocity V_0 = 0.29 m/s, we obtain a maximum tangential velocity about 0.36 m/s.

The normal components of the velocity V_n to the bar rack vary acconrding the transects but are, in any case, lower than 50 cm/s. For the transect at 10 m, the opening of the bottom gate lead to a high normal velocity at the right bank (about 0.6 to 0.8 time V_0) while at the left bank the values vary between 0.3 and 0.6 times V_0. For the transect at 6 m, we note values between 0.5 and 0.7 times V_0 on the central part of the headrace channel and values about 0.3 to 0.5 times V_0 along the banks. For the transect at 2 m upstream the top of the bar rack where the flow is "plunging" under the top of the grid which is filled, we note values about 0.6 to 0.8 times V_0 in front of the outlets and lower values of 0.3 to 0.5 times V_0 between the outlets.

Figure 54 presents the cartography of the ratio between tangential and normal velocities V_t/V_n.

We note again the dissymmetry at the transect at 10 m for the ratio V_t/V_n with values about 1 to 1.75 m at the right bank and values about 2 to 3 m at the left bank. For the transect at 6 m, the ratio V_t/V_n is more homogeneous with values between 2 to 3. Finally for the transect at 2 m, the values of the ratio are lower. In front of the outlets the values of the ratio reach 1.5 to 2 but stay between 1 and 1.5 between the outlets.

Figure 56 presents a aerial view of the velocity vectors (V_X ; V_Y) of the flow moving towards from the left to the right and the outlets, at the 3 transects located at 10 m, 6 m, and 2 m. The orientation and the length of the vectors enquire on the direction and the intensity of the flow upstream the bar rack. At the transects at 10 m and 6 m, the vectors have the same orientation and are globaly very close to the output velocity. At the transect at 2 m, the vectors change of direction, moving towards the outlets with an almost null velocity at the filled zones.

At the transect at 2 m upstream the top of the bar rack, Figure 55 presents the cartography of the transversal components V_Y of the dimensionless velocity and Figure 57 represents the outline of the velocity component V_Y (in m/s), averaged on the water level, depending on the width of the water intake (positive value drawn up to the left bank and negative values drawn up to the right bank). The components of the velocity V_Y present value between -0.5 and 0.5 times V_0, i.e. between -0.145 and 0.145 m/s. These different representations allow to assess the lateral attractiveness of the outlets, with multiple direction changes (change of signs) of V_Y on the width of the water intake:

- The outlet located along the left bank (between Y=12.95 and 14 m) attract the flow on a distance around 3 m (till Y=10 m);

- The central outlet (between Y=7.47 and 8.52 m) attract only few the flow from the left bank (value almost null of V_Y between Y=8.5 and 10 m), but attract the flow from the right bank over a distance of 2 m (till about Y=5.5 m);

- The right outlet (between Y=2.0 and 3.05 m) attract the flow from the left bank over a distance of about 2.5 m (till Y=5.5 m) and from the right bank over a distance about 0.5-1.0 m. There is a zone between this outlet and the right bank where the flow is not attracted by the outlet. The width of this recirculation zone is about 1.0-1.5 m.

Globaly the lateral attractiveness of the outlets seems good with only 2 zones of reduced size where the downstream migration fishes are not guided to an outlet by the currentology (a zone near the central outlet between Y=8.5 and 10 m, and a zone alon the right bank at Y=1.5-1.0 m).
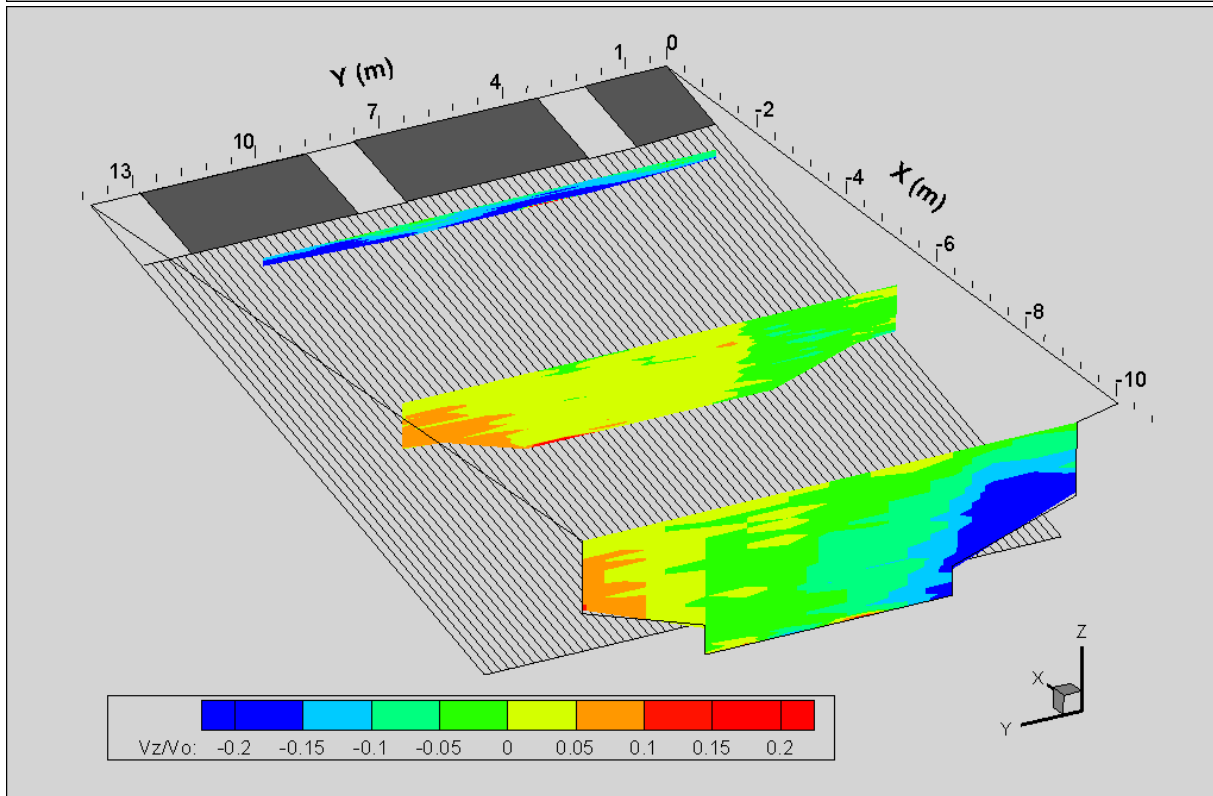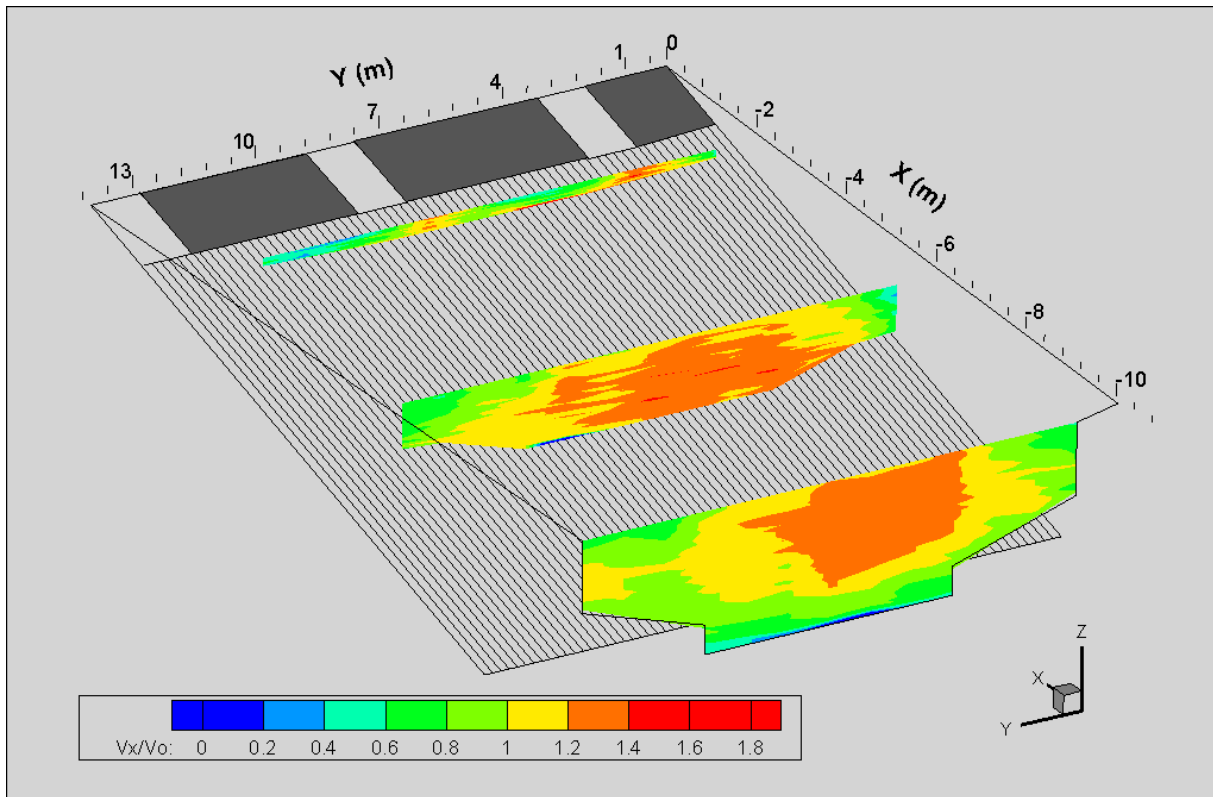
Figure 51: Cartographies of the dimensionless velocities V_x/V_0 (up) and V_z/V_0 (down) measures at Las Rives, V_0=0.29 m/s, 2017.
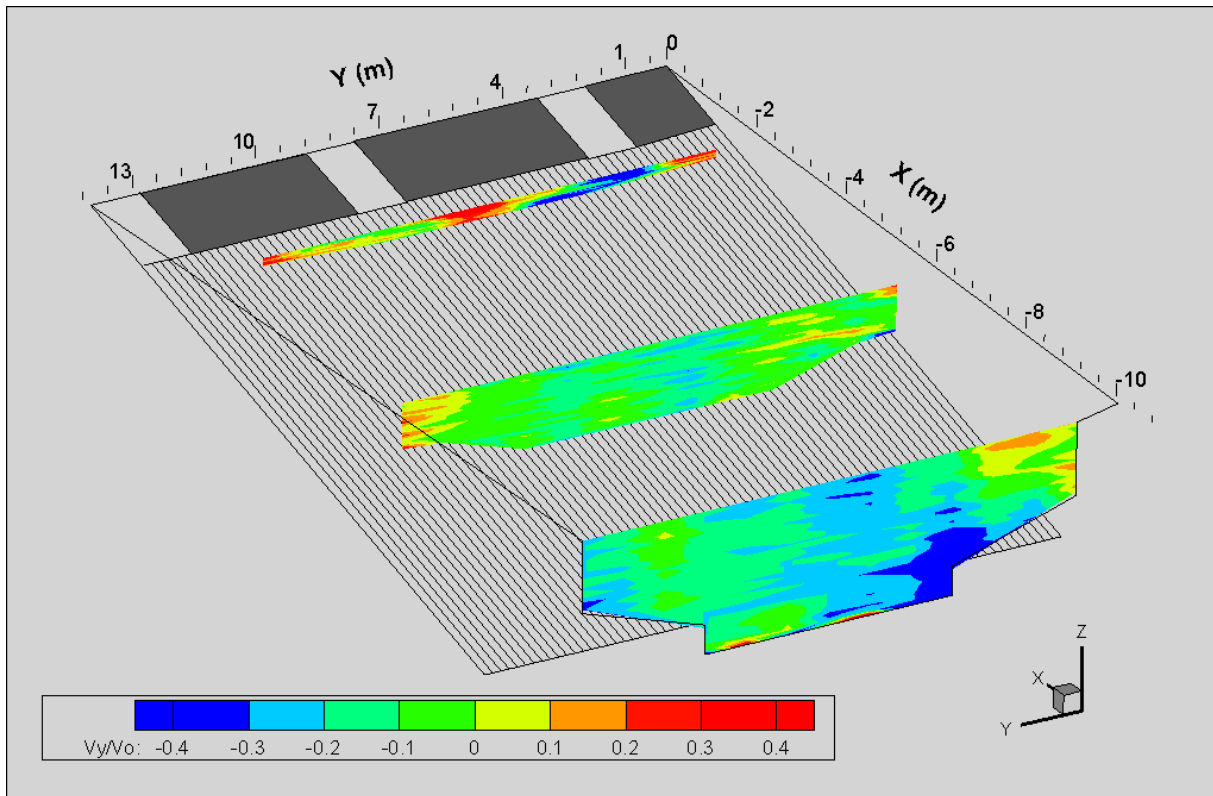
Figure 52: Cartographies of V_y/V_0 measured at Las Rives, V_0=0.29 m/s, 2017.
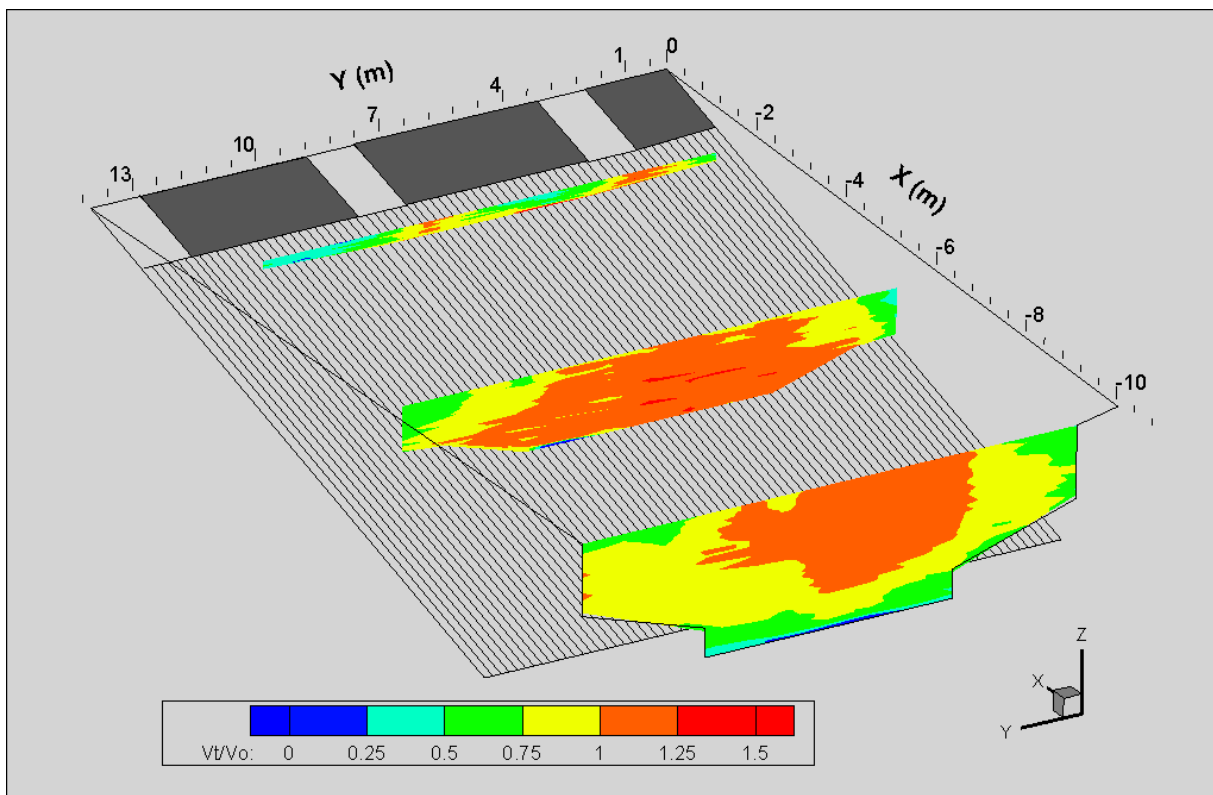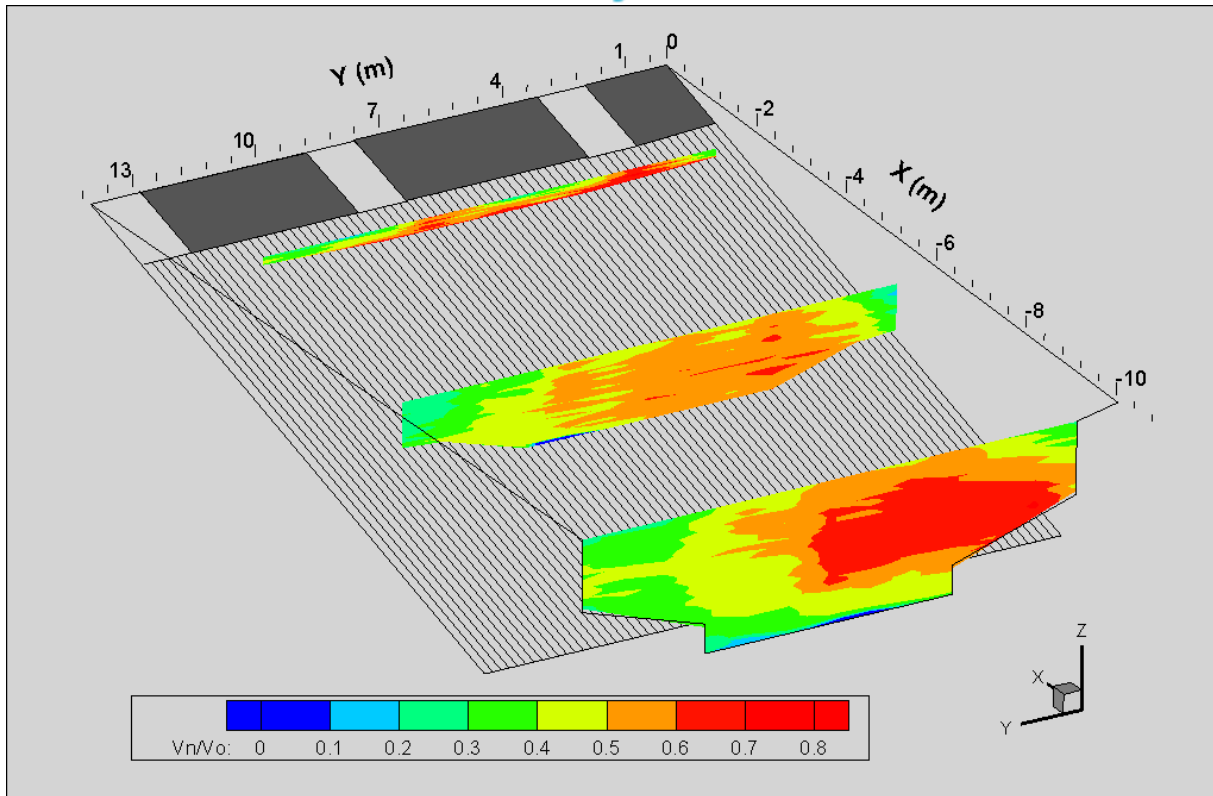
Figure 53: Cartographies of V_t/V_0 (up) and V_n/V_0 (down) measured at Las Rives, V_0=0.29 m/s, 2017.
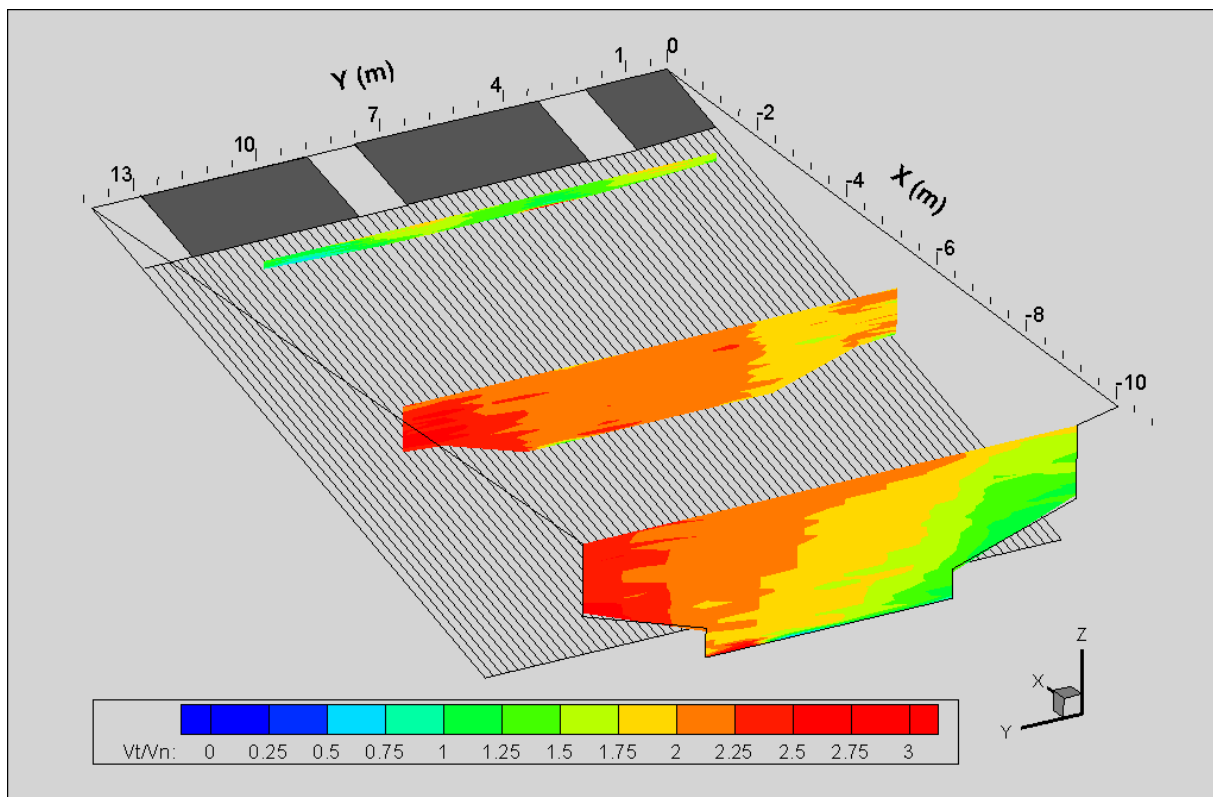
Figure 54: Cartography of the ratio V_t/V_n measured at Las Rives , V_0=0.29 m/s, 2017.
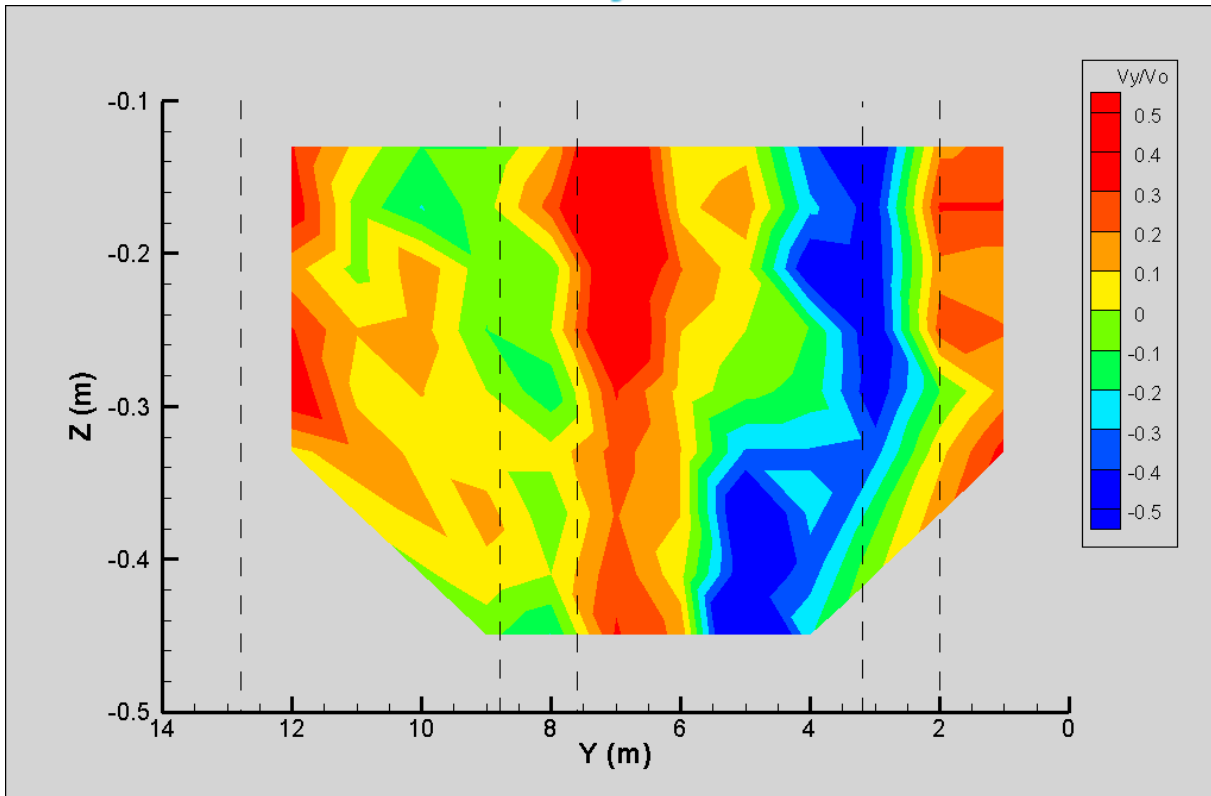
Figure 55: Cartography of V_y/V_0 of transect at 2 m upstream the top of the bar rack (about 0.15 m upstream the entrance of the outlets). The positive sense is oriented from the right to the left bank. The location of the outlets is defined by the dotted lines, V_0=0.29 m/s, 2017.
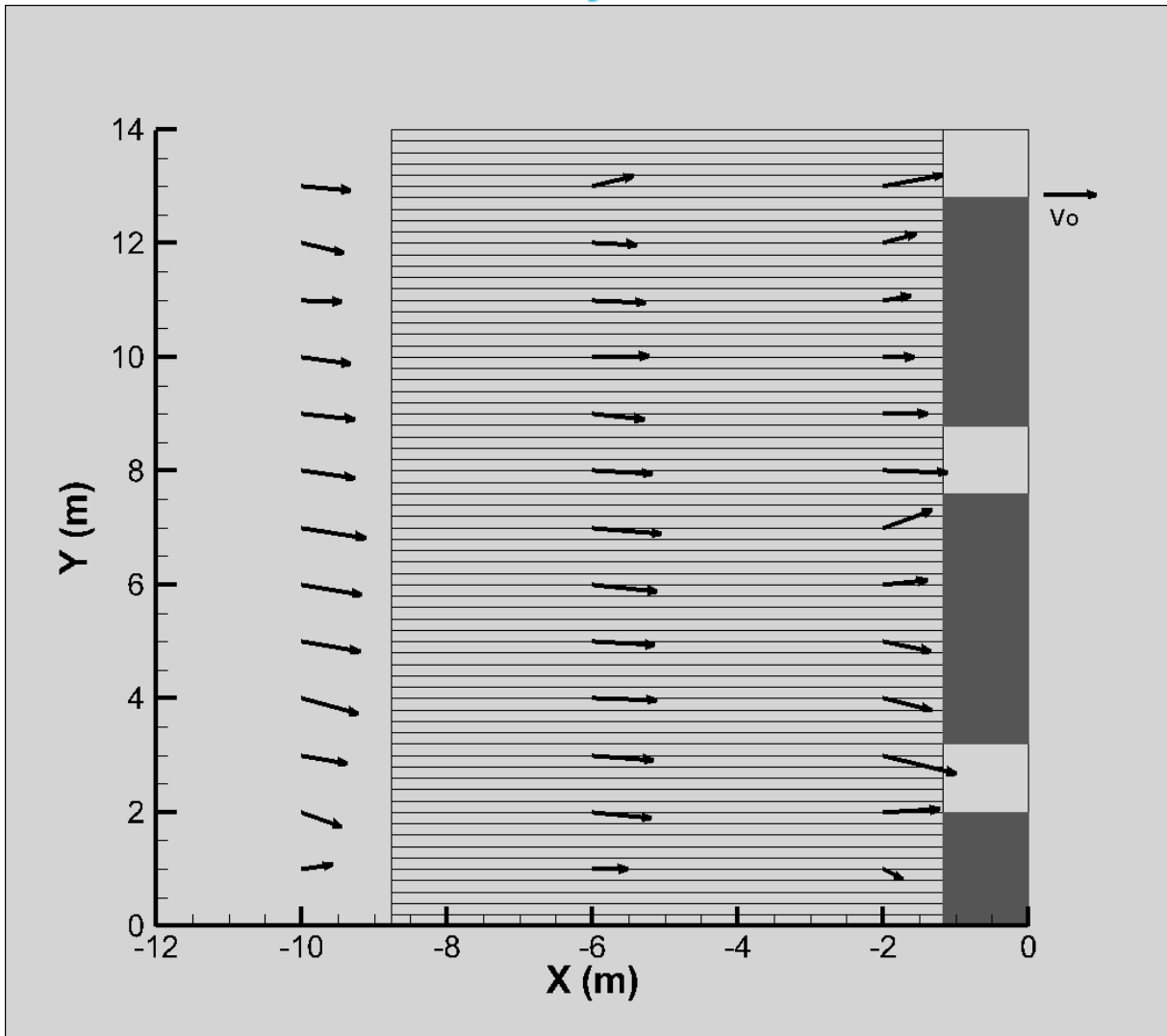
Figure 56: Aerial view of velocity vectors, averaged on water depth, at the 3 transects, at Las Rives, V_0=0.29 m/s, 2017.

Figure 57: The outline of the velocity component V_y, averaged on depth Z depending on Y, located at 2 m upstream the top of the bar rack, at Las Rives, 2017.

3.3.6.2. Measurements of July 2018

Figure 58 presents the cartography of components V_x and V_z of the dimensionless velocity at the 4 transects. The bar rack is viewed from upstream.

At the 3 transects located at 10 m, 6 m and 4 m upstream the top of the bar rack the components V_x vary between $0.6V_0$ and $1.2V_0$. Half of the water intake near the right bank presents velocities higher than the half at the left bank. This heterogeneity existing from the foot of the bar rack is probably linked to the general configuration of the water intake, and not to the bar rack itself. Between these 3 transects no significant acceleration or deceleration of component V_x appears.

At the transect located 2 m upstream to top of the bar rack (about 0.15 m upstream the entrance of the outlets), the components V_x decrease significantly: between 0 and $0.4V_0$ beside the outlets and between $0.4V_0$ to $0.8V_0$ in front of the outlets. It is linked to the obturation of the top of the grid on the same depth of the outlets. The components V_x are lower than the calculated velocities thanks to the assessment of the discharges in the outlets, however the transect is not at the immediate entrance of the outlets but 15 cm upstream.

The vertical components of V_z seem low at the first 3 transects (value between -0.05V_0 and +0.1V_0) and lightly positive in average (oriented to the surface). At the transect at 2 m upstream the top of the bar rack, the components V_z are noticeably negative (oriented to the floor), with values between -0.2V_0 and -0.3V_0 between the outlets and about -0.1V_0 near the outlets. This evolution is due to the fact that the flow has du "plunge" under the top of the grid which is clogged.
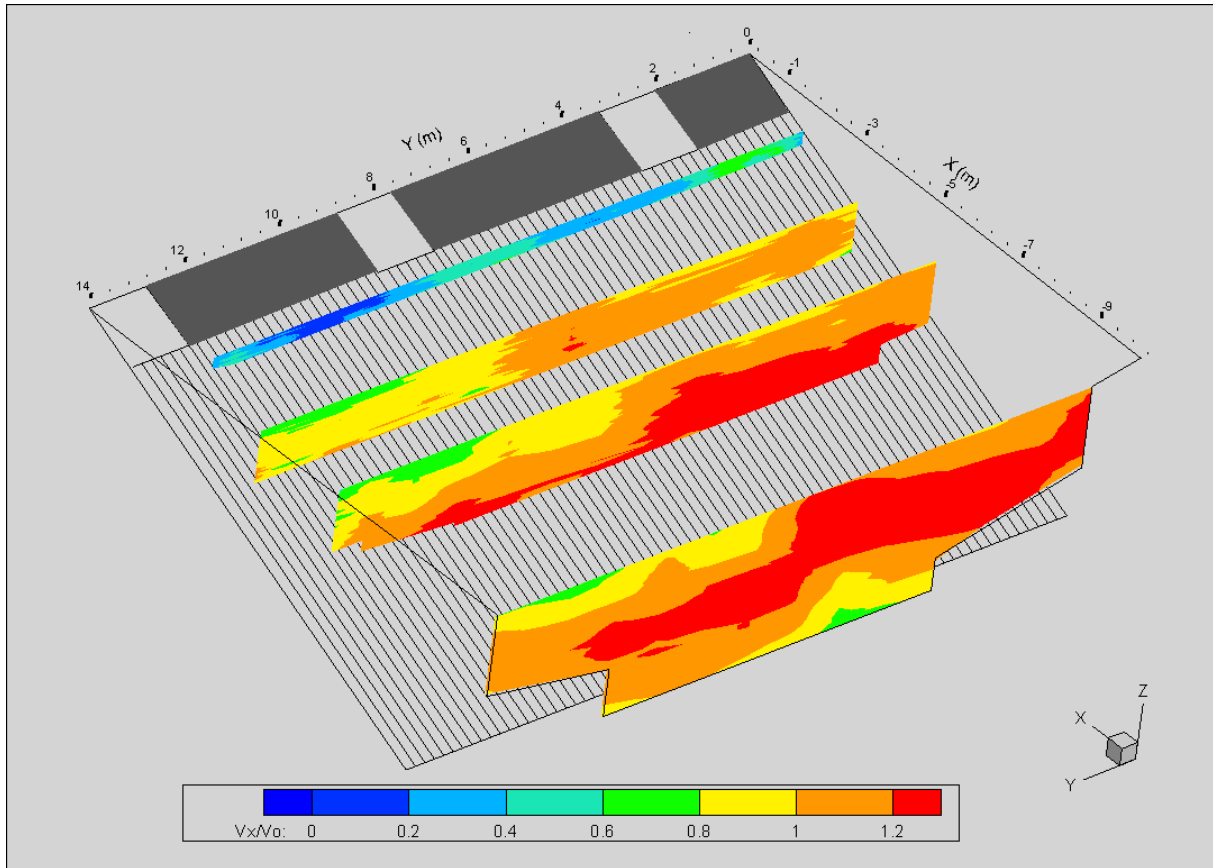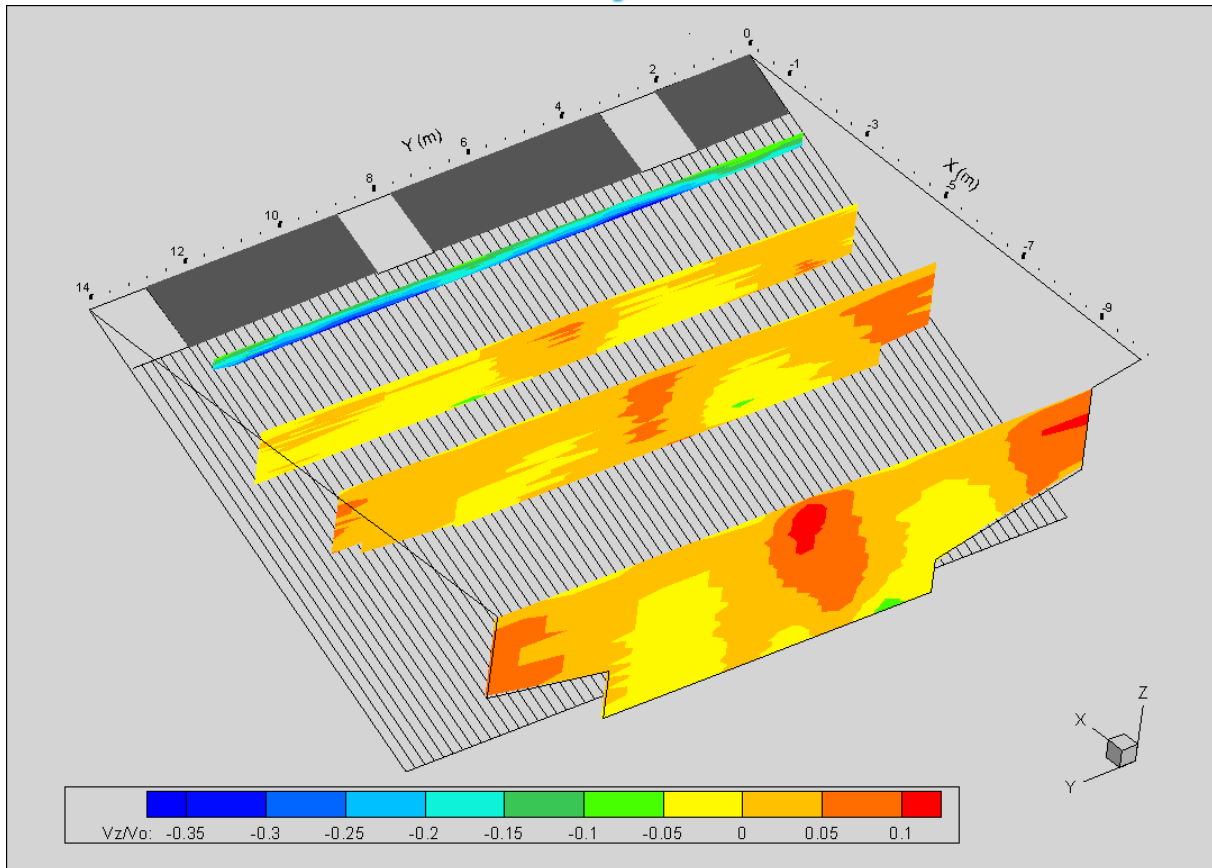
Figure 58: cartographies of the dimensionless velocities V_x/V_0 (up) and V_z/V_0 (down) measured at Las Rives, 2018

Figure 59 presents the cartography of the components of the transversal velocity V_Y. The transversal components are close to null at the more upstream transects. We can note that at the transect at 10 m, a general movement oriented to the right bank. For the other transects, the flow is rather oriented from the right bank to the left bank.

Figure 60 presents an aerial view of the velocity vectors (V_X ; V_Y) of the flow. The orientation and the length of the vectors indicate the direction and the intensity of the flow upstream the bar rack. The vectors are drawn up to the axis of the water intake at the 3 transects located at 10 m, 6 m and 4 m with values close to the output velocity V_0. At the transect at 2 m, the orientation of the velocity vectors are changing, due to the attraction of the 3 outlets, with reduced values between the outlets (filled areas) and between 0.5 to 0.7 times V_0 in front of the outlets.
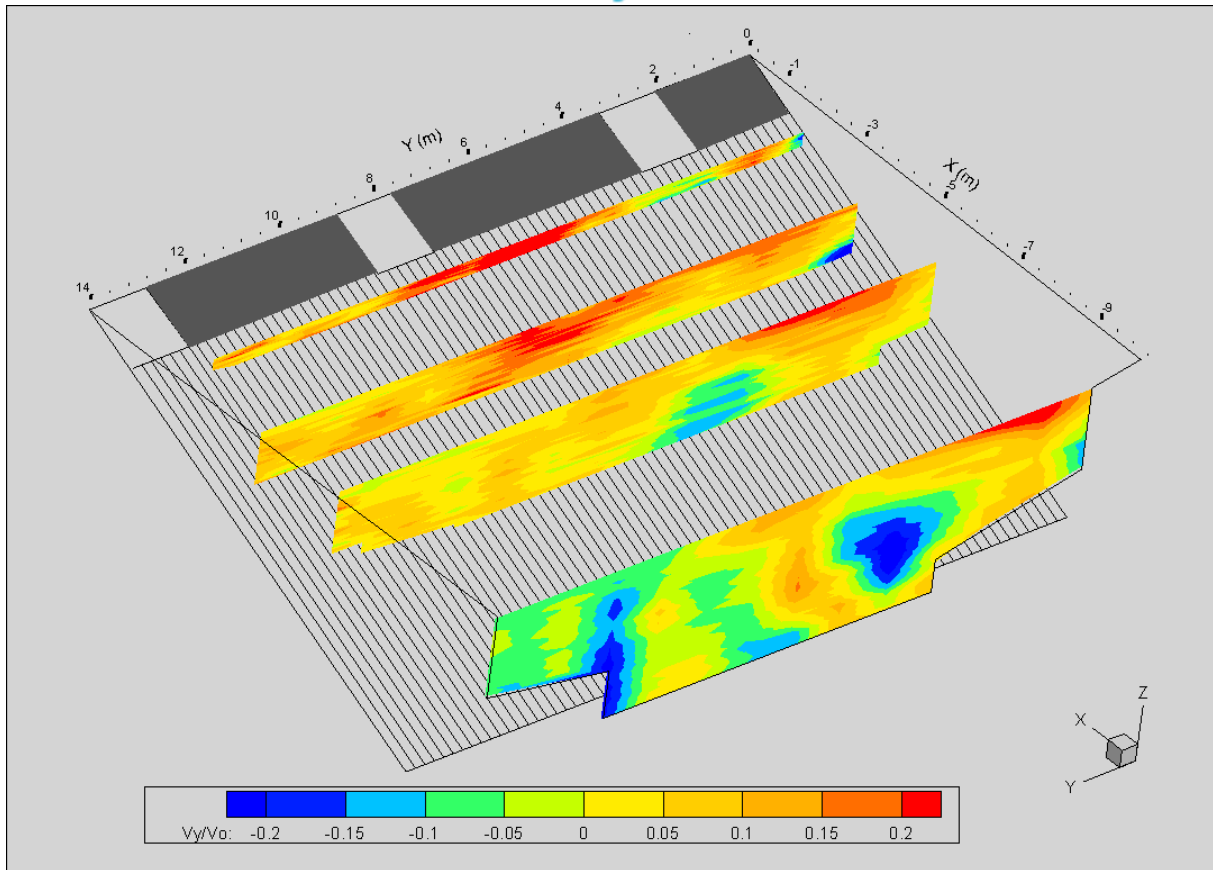
Figure 59: Cartography of the dimensionless velocities V_y/V_0 Las Rives, V_0= 0.8 m/s, 2018.
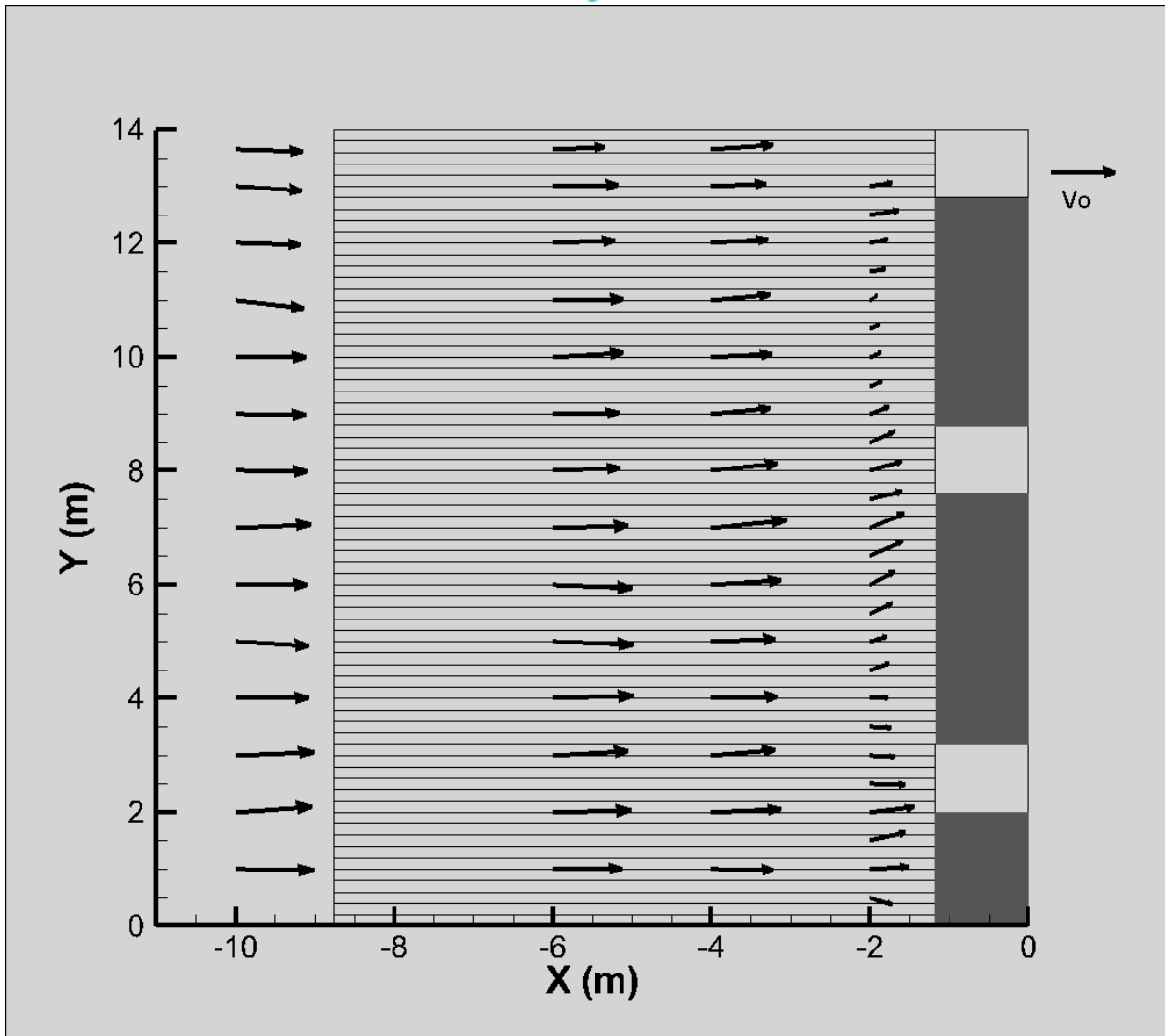
Figure 60: Aerial view of the velocity vectors averaged on the depth, at the 4 transects at Las Rives, V_0= 0.8 m/s, 2018.
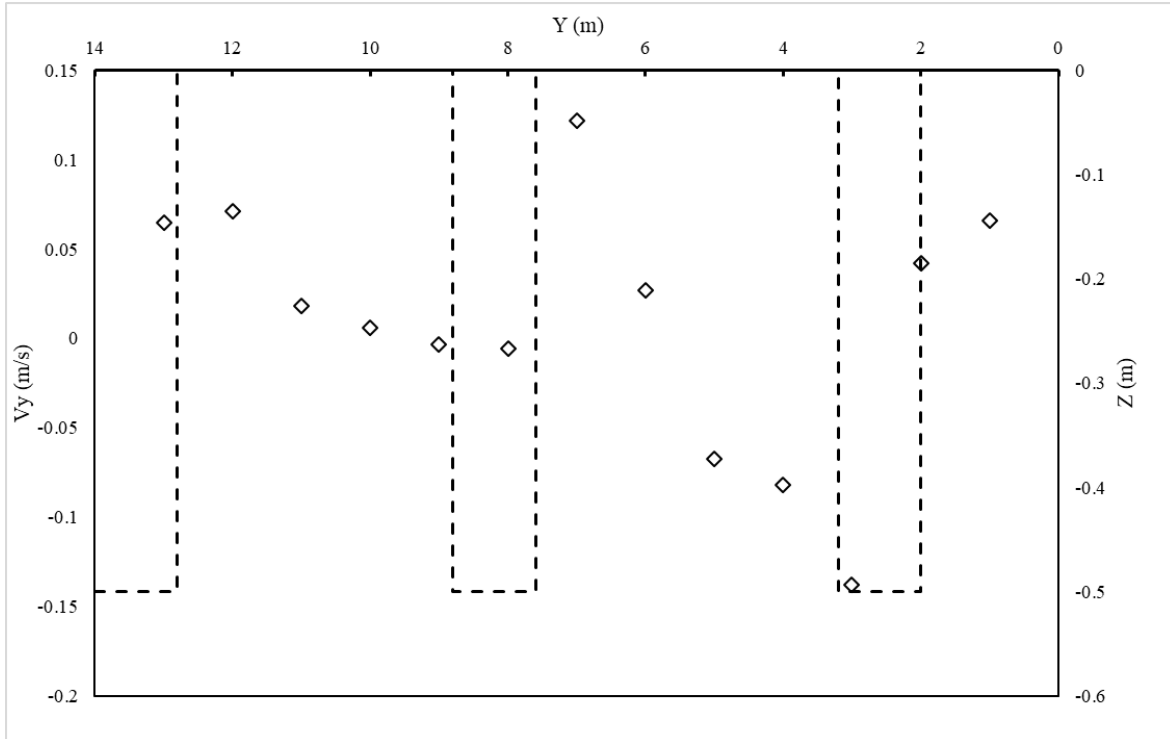
Figure 61 presents the cartography of the dimensionless tangential and normal components V_t and V_n of the velocity at the 4 transects.

At the 3 transects located at 10 m, 6 m and 4 m upstream the top of the bar rack the tangential components V_t are mainly between $0.6V_0$ and $1.2 V_0$. As for V_x, the values are higher in the right half part of the water intake.

At the transect at 2 m upstream the top of the grid (about 0.15 m upstream the entrance of the outlets), the components V_t decrease significantly linked to the clogging of the top of the grid: value nearly zero between the outlets and between 0.2 to $0.6V_0$ in front of the outlets.

The normal components of V_n velocity vary between 0.2 to $0.6V_0$ on the 4 transects, i.e. between 0.16 and 0.48 m/s, including the transect at 2m where the flow is plunging under the clogged top of the grid. The criteria aimed, normal velocity<0.5 m/s, is respected at Las Rives, even if the HPP works with its maximum turbined flow.

Figure 62 presents the cartography of the ratio between the tangential and normal velocities V_t/V_n.

At the 3 transects located at 10 m, 6 m and 4 m upstream the top of the bar rack, this ratio varies between, 1.5 and 2.5, with mean values of 2. This is compliant with the theoretical value.

At the transect at 2 m upstream the top of the grid (about 0.15 m upstream the entrance of the outlets), the ration is close to 0 between the outlets and close to 1.0-1.5 in front of the outlets. This is consistent with the evolution of the tangential components seen above.

At the transect at 2 m upstream the top of the bar rack, Figure 63 presents the cartography of the transversal components V_Y of the dimensionless velocity and Figure 64 represents the outline of the velocity component V_Y (in m/s), averaged on the water level, depending on the width of the water intake (positive value drawn up to the left bank and negative values drawn up to the right bank). The components of the velocity V_Y present value between -0.1 and 0.3 times V_0, i.e. between -0.08 and 0.24 m/s. These different representations allow to assess the lateral attractiveness of the outlets, with multiple direction changes (change of signs) of V_Y on the width of the water intake:

- The outlet located along the left bank (between Y=12.95 and 14 m) attract the flow till the central outlet (Y=8.52 m). The values of V_Y are quite low, about 0.05 to 0.08 m/s, this is probably linked to the low discharge value going through this outlet (0.184 m/s);

- The central outlet (between Y=7.47 and 8.52 m) doesn't attract the flow from the left bank by from the right bank over a distance of 3.5 m (till about Y=4 m);

- The right outlet (between Y=2.0 and 3.05 m) attract the flow from the left bank over a distance of about 1 m (till Y=4 m) but with low values (V_Y <0.05 m/s) and from the right bank over a distance about 1.0 m. There is a zone between this outlet and the right bank where the flow is not attracted by the outlet. The width of this recirculation zone is about 1.0-1.5 m.

Globaly the lateral attractiveness of the outlets seems good with only 1 zone of reduced size where the downstream migration fishes are not guided to an outlet by the currentology (along the right bank between the bank and Y=0.5-1.0 m). The transversal velocities V_Y are oriented from the right bank to the left bank, it is linked with the massive arrival of flow in the right half of the channel.
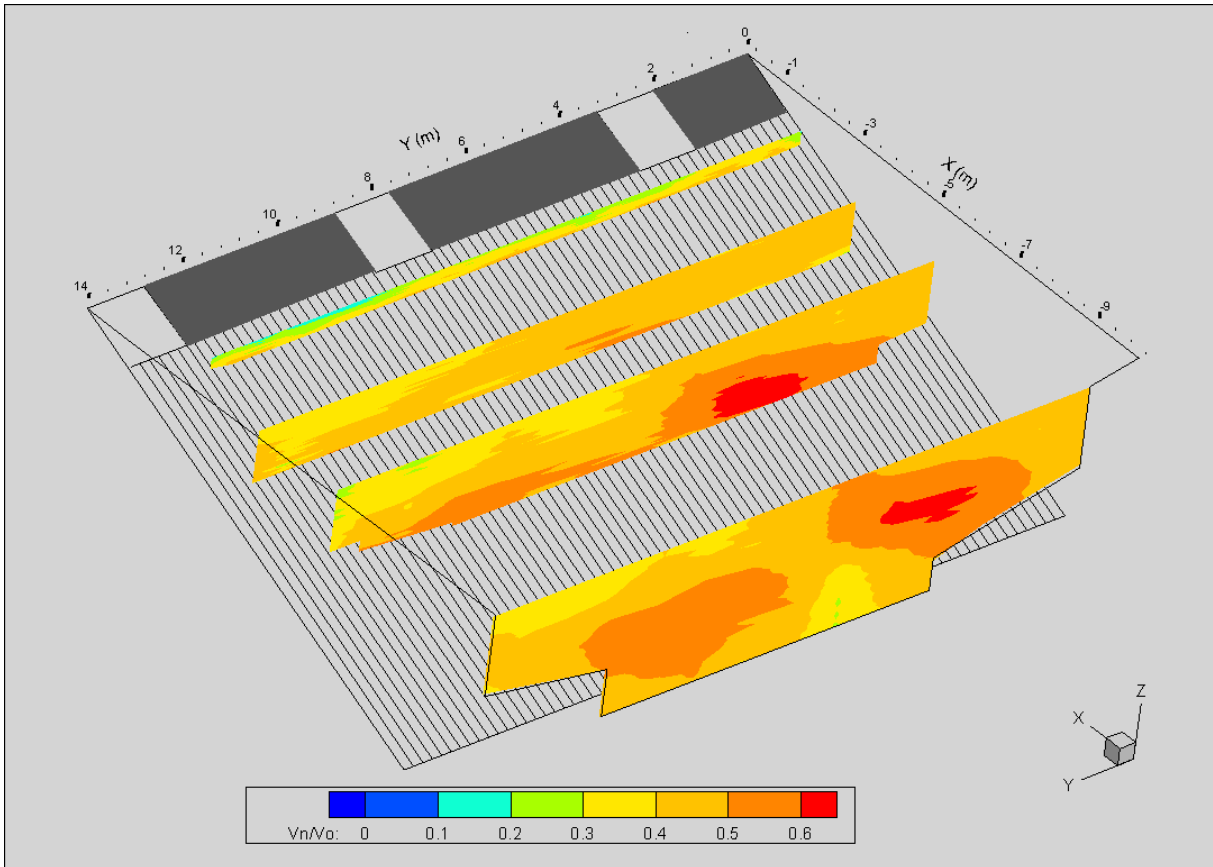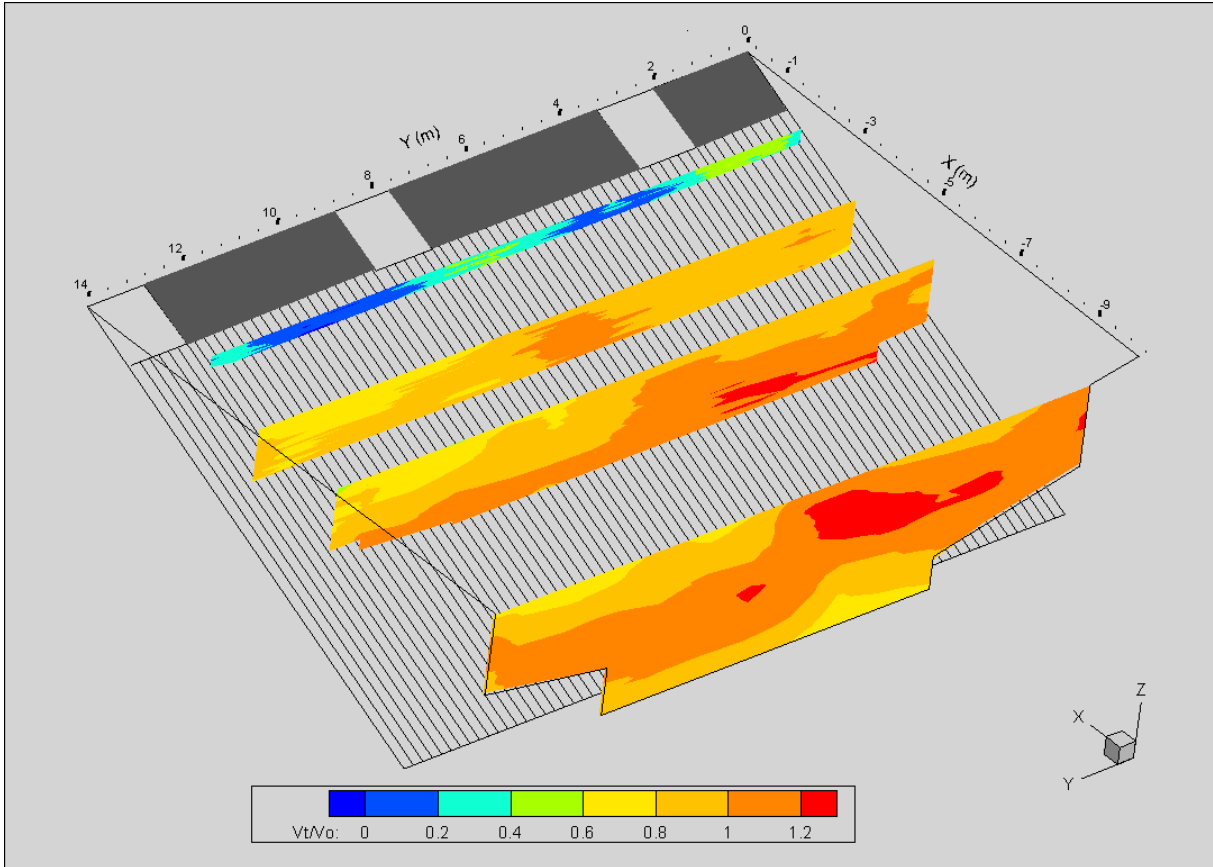
Figure 61: Cartographies of V_t/V_0 (top) et V_n/V_0 (bottom) measured at Las Rives, 2018
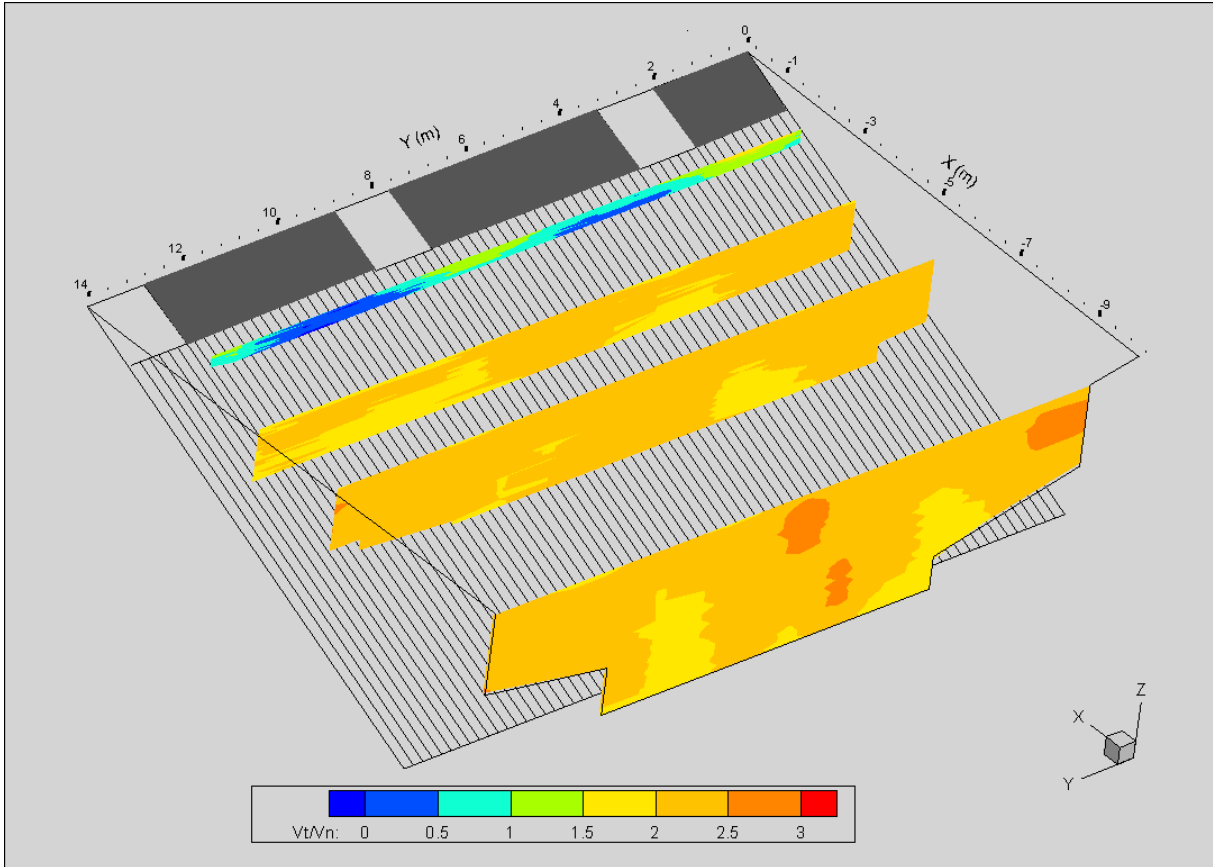
Figure 62: Cartography of ratio V_t/V_n measured at Las Rives, 2018
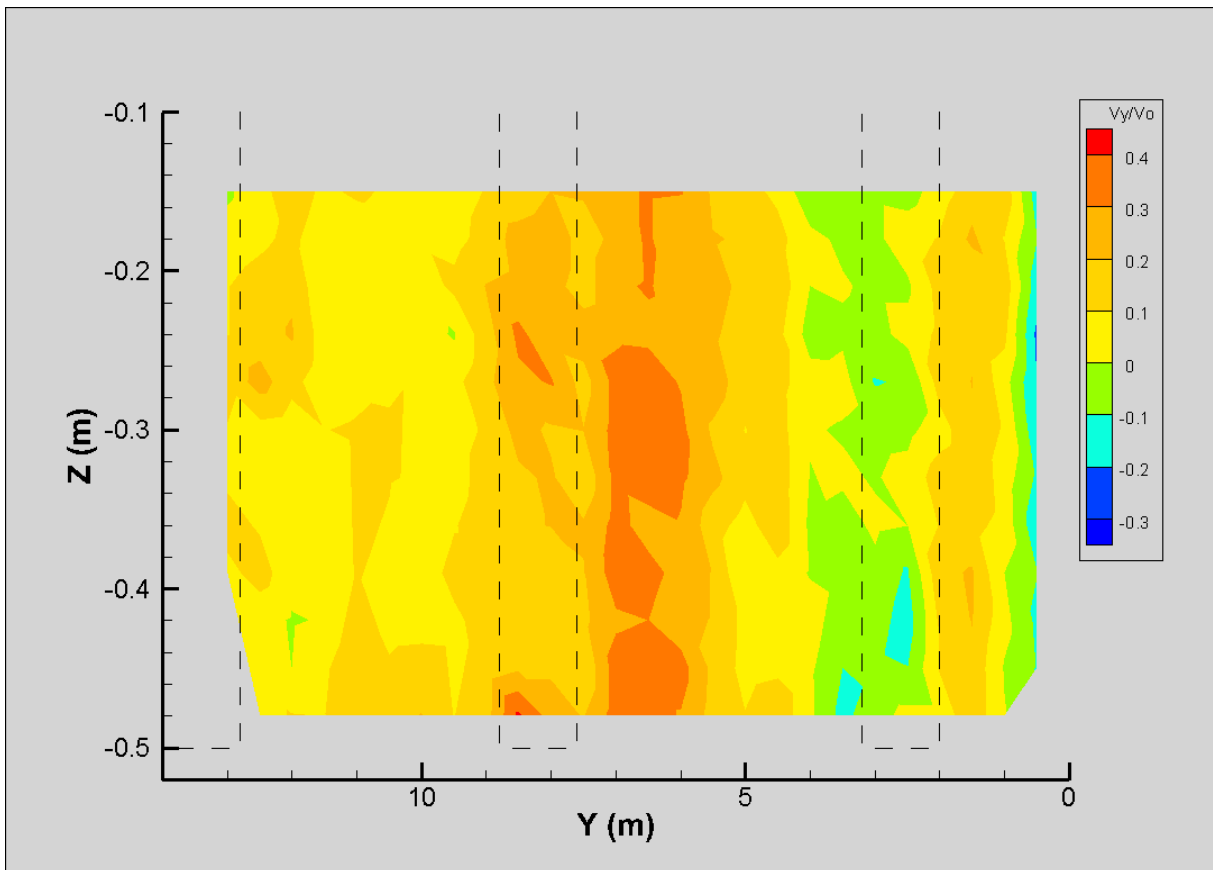
Figure 63: Cartography of V_y/V_0 of transect at 2 m upstream the top of the bar rack (about 0.15 m upstream the entrance of the outlets). The positive sense is oriented from the right to the left bank. The location of the outlets is defined by the dotted lines, V_0= 0.8 m/s, 2018.
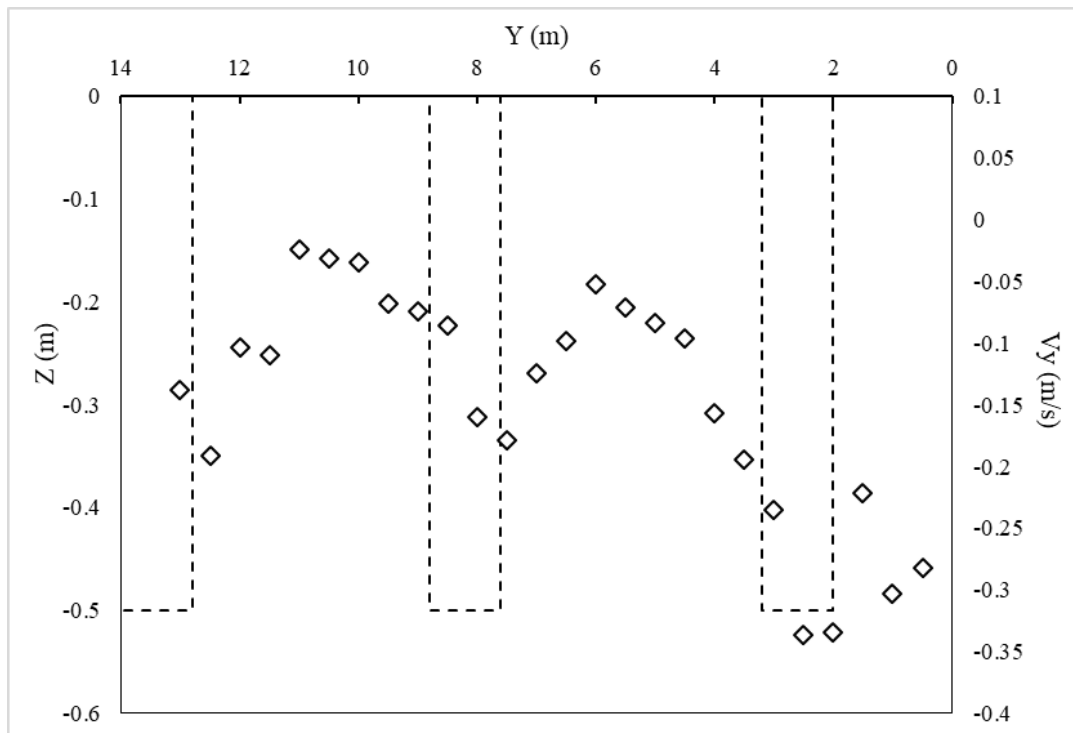
Figure 64: The outline of the velocity component V_y, averaged on depth Z depending on Y, located at 2 m upstream the top of the bar rack, Las Rives, 2018.

3.3.7. 3D Flow modelling and comparison with the field measurements

Methodology:

Numerical simulations have been performed using the multi-physics open-source library OpenFOAM (OpenField Operation And Manipulation), which provides solvers, meshing utilities and post-processing tools for various physics and mathematics problems. The code is written in C++ and solves partial differential equations (PDE) problems using the finite volume method. OpenFOAM is fully customizable and can address a number of fluid mechanics problems such as compressible and incompressible flows, multiphase flows, heat transfer, combustion, etc.

Free surface flow simulations of the laboratory bar-racks have been carried out using the interFOAM unsteady incompressible multiphase solver which solves the Navier-Stokes Equations (NSE) using the merged PISO-SIMPLE (PIMPLE) algorithm, and the phase concentrations using the VOF (Volume Of Fluid) method. The VOF method can be used to track free surfaces and fluid interfaces by considering the volume fractions of multiple fluids that are advected in the computational domain.

The full-scale simulations of the test-case HPP intakes have been conducted using the steady incompressible single phase simpleFoam solver, which solves the NSE using the SIMPLE algorithm.

Turbulence can be modelled using various approaches, and in particular the steady and Unsteady Reynolds-Averaged NSE (RANS and URANS) used in this study with the k-epsilon turbulence model.

Meshing

For all simulations, channels have initially been defined as cartesian blocks with base cell size set to 1 cm. Bar racks and bypass structures have been modelled as CAD elements which have then been subtracted for the initial blocks using mesh castellation and local surface adaptation. The openFOAM utilities blockMesh and snappyHexMesh have been used to perform these pre-processing operations.

Results

Single-phase numerical simulations have been carried out at full scale for the test-case HPP of Las Rives. The intake channel is 14 m wide with a water depth of 4.18 m. The 14 m wide bar rack is vertically inclined at 26° with respect to the river bed, comprising 10 mm thick bars with hydrodynamic profile, 20 mm free spacing between bars, and 7 horizontal spacer lines of width 12 mm. The total inflow is nominally set at 46.35 m³/s, from which 1.35 m³/s discharges trough the bypass on the right bank of the intake channel. The bar rack and progressive width bypass are shown in Figure 65. Preliminary field measurements were conducted at 4 stations above the bar rack using an ADCP, while flowmeter gauging was used downstream of the first and second entrances of the bypass, as schematized in Figure 65. The total flow rate across the bypass is regulated by a broad-crested weir and estimated using its discharge law.

Figure 65: Inclined bar rack and bypass entrances of the Las Rives HPP, with 1st and 2nd gauging sections.

For the numerical simulations the free surface is represented as a fixed horizontal boundary with the slip condition at the nominal water height. Figures 66 to 68 show the bar rack with its supporting elements, terminated by the 3-entrance bypass channel of progressive width.

The resulting average approach velocities at 4 stations along the rack are represented in Figures 66 (longitudinal and vertical velocity components) and 67 (tangential and normal velocities). The tangential-to-normal velocity ratio is presented in Figure 68.
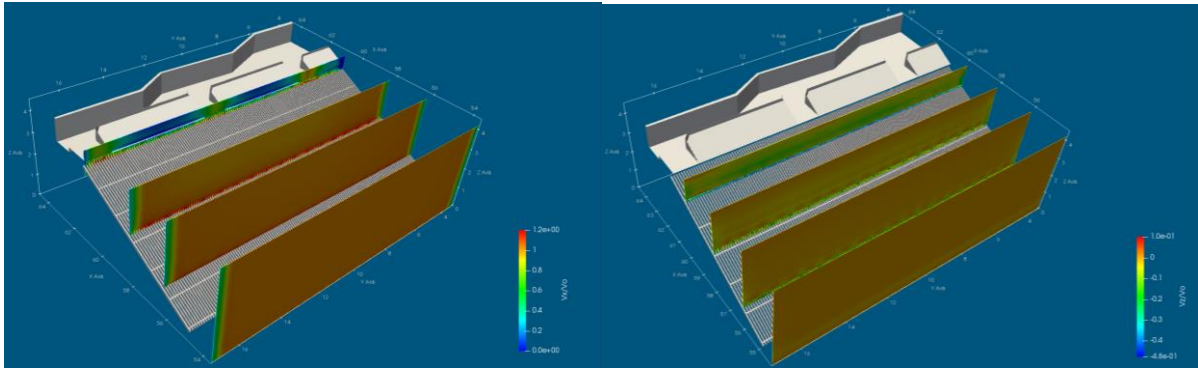
Figure 66: Cartography of the non-dimensional numerical velocity upstream of the Las Rives bar rack. Left: longitudinal velocity V_x, right: vertical velocity V_z.
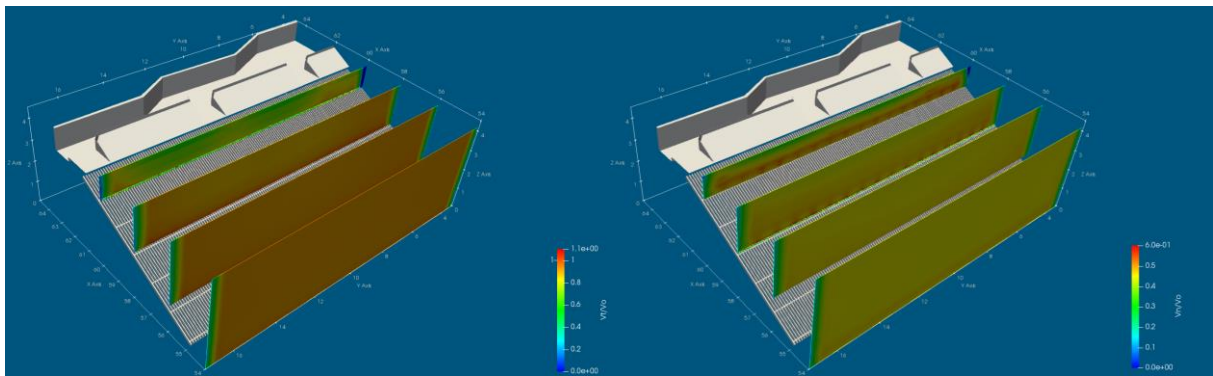
Figure 67: Cartography of the non-dimensional tangential (left) and normal (right) numerical velocities upstream of the Las Rives bar rack.
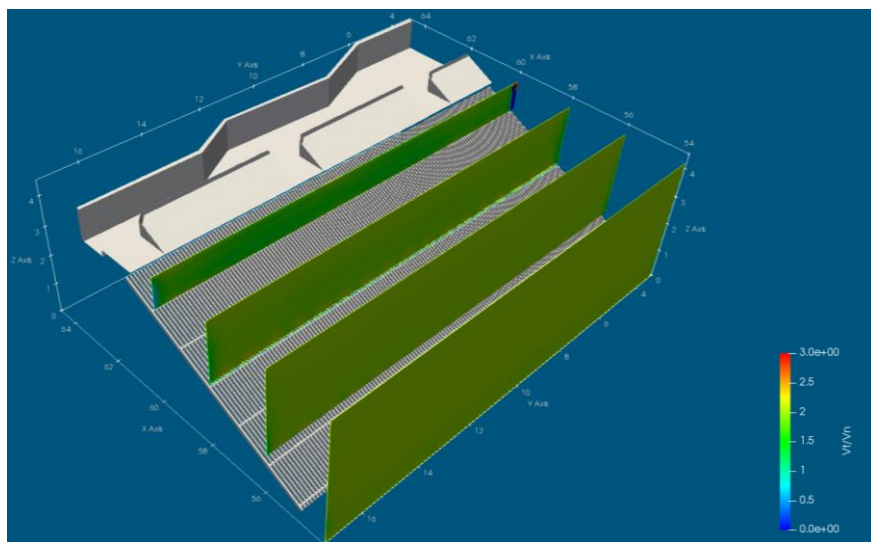
Figure 68: Cartography of the tangential-to-normal velocity ratio between upstream of Las Rives bar rack.

Figure 69 shows the velocity distribution and streamlines at free-surface level upstream of and across the bypass channel. The curvature of the streamlines evidences both the attractiveness of each of the bypass entrances and the homogenization effect of the progressive enlargements along the bypass channel. Compared to field measurements (Table 15), the numerical results tend to under-estimate the flow rate across the left bank entrance by 37% and to over-estimate the flow rate across the right

bank entrance by 18%. The distribution of flow rates is however acceptably reproduced in terms of flow deficit across the left bank entrance.
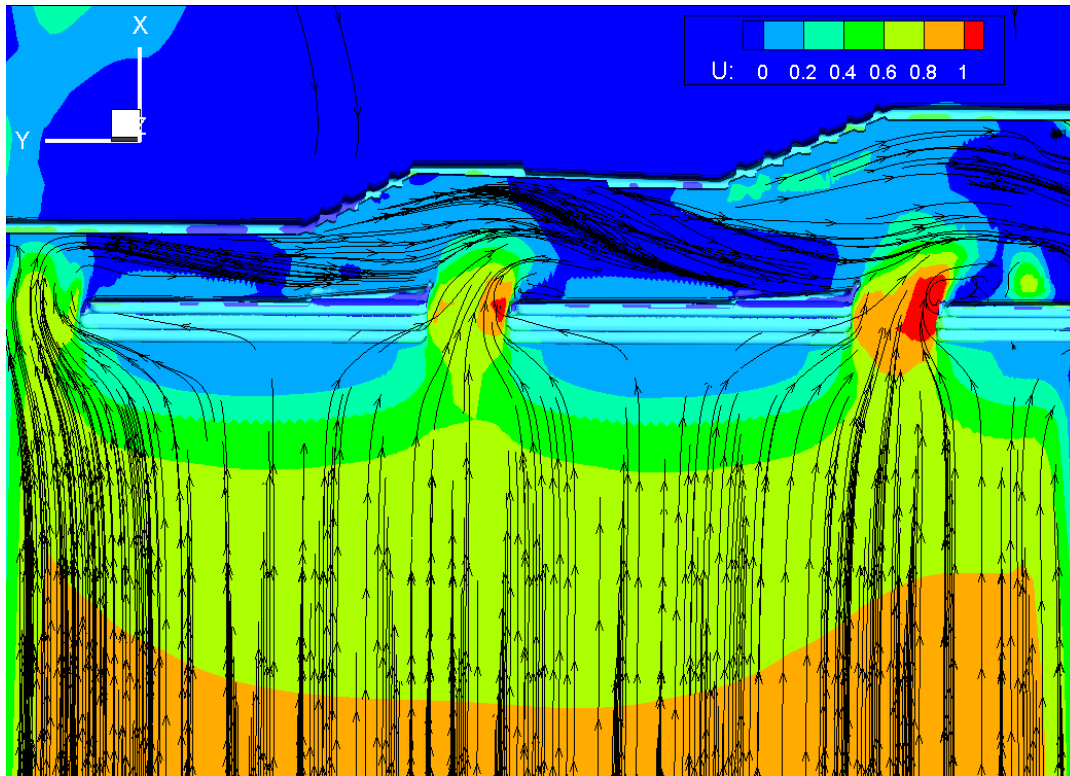
Figure 69: Non-dimensional numerical velocity distribution and streamlines across the bypass channel of Las Rives at free-surface level.

Table 15: Comparison between simulated and measured flow rates and velocities.

Bypass	1	2	3
In-situ velocity (m/s)	0.36	0.98	0.93
Numerical velocity (m/s)	0.6	0.79	1.19
Cumulated in-situ flow rate (m³/s)	0.184	0.671	1.134
Percentage of flow rate by bypass (%)	16.22	42.85	40.82
Cumulated numerical flow rate (m³/s)	0.143	0.7	1.349
Percentage of flow rate by bypass (%)	10.6	41.28	48.1
Theoretical flow rate (m³/s) fixed for the downstream migration	-	-	1.349

3.4. Scenario modelling

Seven scenarios were analysed, they correspond to different combination of mitigation measures (inclined bar rack or shutting down of the turbines) and the variation of their location. The calculation of the efficiency of the mitigation measures and the production allowed to compare the scenarios.

Then the Bayesian Networks (BN) method was applied to assess the cost-effectiveness. Both analyses show that scenario (c) combining an inclined bar rack (20mm bar spacing and inclined at 26° to the horizontal) is the most cost-effective. It is the combination that has been implemented on site.

Scenario modelling allow to compare and to choose between scenarios and to know which solutions is the more reasonable to implement regarding fish continuity and production.

Paper of the journal Sustainability to include when it will be accepted.

4. Conclusion

The Las Rives test case is a medium HPP with a fish friendly water intake in which is tested an inclined bar rack with several technical solutions. The efficiency of the inclined low bar spacing trashrack has been validated by radio telemetry for smolts (81% of efficiency) and eels (100% of efficiency). No cumulative effect on different successive HPPs has been shown during these tests. Depending on the river discharge, the fishes use bypasses as well as the overspill weir. ADCP measurements have been conducted at four cross-sections for different flow discharges, that show well-predicted normal and tangential components of the upstream velocity. This has also been validated by 3D modelling highlighting the attractiveness of the three bypasses, and confirmed by bypass discharge measurements. The landing conditions of the fishes at the foot of the control weir ending the downstream migration duct has also been studied and showed some fish damages (about 30%) which should bring on some modification of the landing zone. Finally, scenario modeling is proposed to see the cost effective solutions for the downstream migration on this site and promote the retained solution. Seven scenario have been compared for the downstream migration and were first analyzed and compared regarding monitoring and production calculation and then implement in a probabilistic network to assess the trade-off between downstream migration efficiency, productivity, and costs of the infrastructures for each scenario.

5. References

Bosc, S. and Larinier, M. 2000. *Définition d'une stratégie de réouverture de la Garonne et de l'Ariège à la dévalaison des salmonidés grands migrateurs - Simulation des mortalités induites par les aménagements hydroélectriques lors de la migration de dévalaison.* s.l. : Rapport GHAAPPE RA 00.01 / MIGADO G17-00-RT 53p., 2000.

Courret, D. and Larinier, M. 2008. *Guide pour la conception de prises d'eau "ichtyocompatibles" pour les petites centrales hydroélectriques.* 2008.

Croze, et al. 2001. *Etude de l'efficacité de trois dispositifs de dévalaison pour smolts de saumon atlantique (Salmo salar L.) - Usines hydroélectriques de Guilhot, Las Rives et Crampagna (Ariège - 09).* s.l. : Rapport GHAAPPE RA01.07, 2001. Rapport GHAAPE RA01.07.

Ecogea. 2011. *Etude pour l'amélioration du franchissement piscicole sur le cours de l'Ariège.* s.l. : Rapport Ecogea n° E 09 03 01, 2011.

Hydrec. 2014. *Centrale hydrauélectrique de Las Rives - Rivière Ariège - Commune de Varilhes et Saint Jean de Verges - Dimensionnement du plan de grille ichtyocompatible et des dispositifs de dévalaison des poissons.* 2014.

Larinier, M. and Dartiguelongue, J. 1989. La circulation des poissons migrateurs: le transit à travers les turbines des installations hydroélectriques. *Bull. Fr. Pêche Pisci.* 1989, 312-313, pp. 1-90.

Larinier, M. and Travade, F. 1999. La dévalaison des migrateurs: problèmes et dispositifs. *Bull. Fr. Pêche Pisci.* 1999, 353/354, pp. 181-210.

Le Coz, J., et al. 2011. *Contrôle des débits réglementaires - Application de l'article L 214-18 du Code de l'Environnement.* 2011.

Tetard S, Roy R, Tomanova S, Courret D, Mercier O, Richard S, Mataix V, Lagarrigue T, Frey A, De-Oliveira E. 2019. Effectiveness of fine-spaced low-sloping racks to protect Atlantic salmon smolts at four hydro powerplants in south-western France. American Fisheries Society & The Wildlife Society 2019 Joint Annual Conference, 2019, Septembre 30th, Reno, 2019.

Tomanova S, Courret D, Mercier O, Richard S, De-Oliveira E, Mataix V, Lagarrigue T, Frey A, Tetard S. 2019. Efficiency of downstream passage devices to protect migrating silver eels assessed with radiotelemetry. 5th International Conference on Fish Telemetry, Arendal, Norway, 2019, June 24th-28th., 2019.

Annex 1: Gauging of the discharge in the downstream migration duct and assessment of the total discharge

Table 17 and Table 18 present the results of the gaugings in the downstream migration duct at Las Rives. For the first gauging, corresponding to the discharge in the first outlet, the discharge is **0.184 m³/s**. For the second gauging, corresponding to the discharge of the two first outlets, the discharge is equal to **0.671 m³/s**.

The topography measurement were postpone to the gauging with the flow meter. The water levels varied during this period of time (Table 16). This will be taken into account during the exploitation of the results.

Table 16: Variation of water levels during the measures

	Gauging 1	Gauging 2	Upstream gates
Water level during the gauging (m)	0.73	0.77	-
Water level during topography measurements (m)	0.76	0.75	0.69

Table 17: Exploitation of measured velocities at Las Rives at the first point of gauging

Verticale	Mesure de vitesse à différentes hauteurs (m/s)						Vitesse moyenne (m/s)	Vitesse moyenne (m/s)
	Fond	0.2	0.4	0.6	0.8	Surface		
Berge RD								
1	0.19	0.14	0.33	0.33	0.28	0.32	0.267	0.301
	0.18	0.31	0.40	0.38	0.31	0.36	0.334	
2	0.18	0.31	0.31	0.33	0.32	0.37	0.309	0.294
	0.16	0.27	0.28	0.27	0.32	0.34	0.278	
3	0.36	0.29	0.26	0.33	0.33	0.34	0.312	0.314
	0.25	0.25	0.35	0.30	0.39	0.32	0.315	
4	0.37	0.40	0.37	0.38	0.39	0.40	0.385	0.375
	0.32	0.36	0.40	0.36	0.37	0.34	0.364	
Berge RG								

Verticale	Hauteur d'eau (m)	Distance depuis la rive gauche (m)	Section	Vitesse moyenne (m/s)	Largeur d'écoulement (m)	Hauteur d'eau moyenne (m)	Débit par section (m³/s)
Berge RD	0.75	0.80	RD - 1	0.27	0.10	0.75	0.020
1	0.75	0.70	1 - 2	0.30	0.20	0.74	0.044
2	0.73	0.50	2 - 3	0.30	0.20	0.73	0.044
3	0.73	0.30	3 - 4	0.34	0.20	0.73	0.050
4	0.73	0.10	4 - RG	0.34	0.10	0.73	0.025
Berge RG	0.73	0.00					

Table 18: Exploitation of measured velocities at Las Rives at the second point of gauging

Verticale	Mesure de vitesse à différentes hauteurs (m/s)						Vitesse moyenne (m/s)	Vitesse moyenne (m/s)
	Fond	0.2	0.4	0.6	0.8	Surface		
Berge RD								
1	0.17	0.20	0.14	0.20	0.14	0.10	0.163	0.1655
	0.23	0.16	0.19	0.20	0.16	0.03	0.168	
2	0.24	0.38	0.16	0.20	0.10	0.17	0.209	0.211
	0.24	0.41	0.23	0.17	0.13	0.01	0.213	
3	0.38	0.44	0.32	0.32	0.33	0.36	0.356	0.353
	0.34	0.46	0.31	0.31	0.34	0.32	0.35	
4	0.62	0.75	0.71	0.73	0.74	0.68	0.716	0.7035
	0.58	0.70	0.75	0.65	0.68	0.77	0.691	
5	0.72	0.87	0.95	0.96	0.90	0.74	0.882	0.876
	0.66	0.93	0.91	0.95	0.85	0.76	0.87	
6	0.83	0.90	0.89	0.96	0.91	0.85	0.9	0.8735
		0.92	0.99	0.98	0.94	0.81	0.847	
Berge RG								

Verticale	Hauteur d'eau (m)	Distance depuis la rive gauche (m)	Section	Vitesse moyenne (m/s)	Largeur d'écoulement (m)	Hauteur d'eau moyenne (m)	Débit par section (m³/s)
Berge RD	0.76	1.58	RD - 1	0.15	0.10	0.760	0.011
1	0.76	1.48	1 - 2	0.19	0.23	0.760	0.033
2	0.76	1.25	2 - 3	0.28	0.25	0.760	0.054
3	0.76	1.00	3 - 4	0.53	0.30	0.770	0.122
4	0.78	0.70	4 - 5	0.79	0.30	0.780	0.185
5	0.78	0.40	5 - 6	0.87	0.30	0.780	0.205
6	0.78	0.10	6 - RG	0.79	0.10	0.780	0.062
Berge RG	0.78	0.00					

Table 19 presents the measured data pour le calculation of the total discharge on the downstream migration duct by the discharge formula. It is necessary to determine the discharge coefficient of the weir from its characteristics. According the hydrometric guide of the ONEMA (Le Coz, et al., 2011), 2 approaches are possible:

- Considering that the weir is thick (Figure 70) as planed in the initial sizing (Hydrec, 2014). In a thorough manner, the head **h** on the weir should be lower or equal to the thickness **e** of the weir. At Las Rives, the measured head is 0.38 m; the condition is respected only if the thickness of the weir is equal or greater than 0.24 m (which has not been checked). Table 20 allows determining the coefficient **A1** according to the ratios **h/e** and **h/p** (p is the height of the weir from the floor of the duct). The discharge coefficient is then deduced:

$$C = 0.385A_1 = 0.385 \times 1.195 = 0.46$$

- Considering that the weir is thin (Figure 71). The weir don't have a reduction of the width compared to the duct (ratio **b/B** =1), so the coefficient **Cr** is equal to 0.05. The ratio h/p is equal to 1.16. The discharge coefficient is deduced:

$$C = 0.40 + C_r * \frac{h}{p} = 0.40 + 0.05 * 1.16 = 0.458$$

The two values of discharge coefficient are very close. The value of 0.46 is chosen.

Table 19: Measured data for the calculation of the total discharge thanks to the discharge formula

Water level upstream the bar rack	333.970	m
Water level upstream the weir	333.877	m
head losses between the upstream level and the weir	0.093	m
Level of the floor upstream the weir	333.184	m
Width of the duct	2.410	m
Width of the weir	2.410	m
Water level upstream the weir	0.693	m
Flow section upstream the weir	1.670	m²
Measured level of the weir	333.522	m
Level of the weir in the project	333.450	m
Head on the weir	0.355	m

Crête plane à arêtes vives
Profil longitudinal rectangulaire

$$Q = C \sqrt{2g}\, b\, h^{1,5}$$
$$C = 0,385\, A_1$$
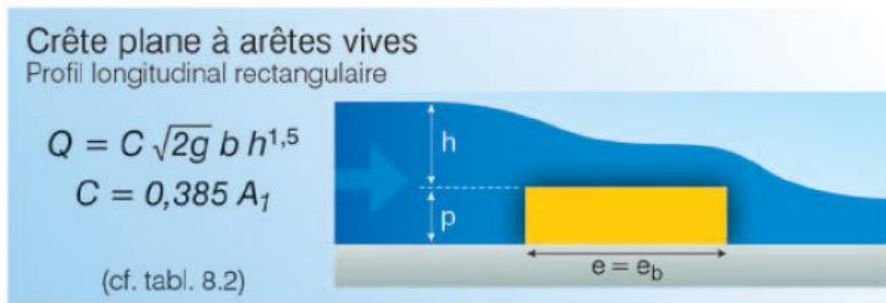
(cf. tabl. 8.2)

$e = e_b$

Figure 70: Expression of the discharge coefficient for a thick weir with a plane crest and sharp edges (source: (Le Coz, et al., 2011)).

Table 20: Determination table of A1 coefficient (source (Le Coz, et al., 2011))

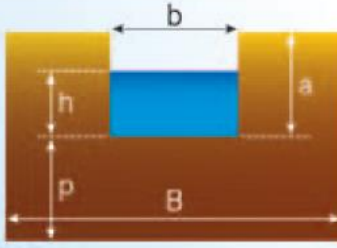| h/p	h/e																	
	0,1	0,2	0,3	0,4	0,5	0,6	0,7	0,8	0,9	1,0	1,1	1,2	1,3	1,4	1,5	1,6	1,7	1,8
0,1	0,850	0,850	0,850	0,861	0,870	0,885	0,893	0,925	0,948	0,971	0,993	1,016	1,039	1,062	1,085	1,106	1,130	1,148
0,2	0,855	0,855	0,855	0,864	0,874	0,888	0,907	0,930	0,954	0,977	1,001	1,026	1,050	1,074	1,096	1,120	1,142	1,159
0,3	0,864	0,864	0,864	0,868	0,879	0,894	0,913	0,936	0,961	0,986	1,011	1,037	1,061	1,085	1,110	1,132	1,152	1,169
0,4	0,873	0,873	0,873	0,874	0,885	0,901	0,920	0,945	0,969	0,995	1,021	1,047	1,072	1,097	1,122	1,144	1,163	1,180
0,5	0,882	0,882	0,882	0,883	0,894	0,909	0,929	0,954	0,978	1,005	1,032	1,057	1,083	1,109	1,133	1,154	1,173	1,188
0,6	0,892	0,892	0,892	0,894	0,904	0,920	0,941	0,964	0,990	1,016	1,043	1,067	1,094	1,120	1,143	1,164	1,182	1,196
0,7	0,901	0,901	0,901	0,906	0,916	0,932	0,952	0,975	1,000	1,026	1,052	1,077	1,104	1,129	1,152	1,171	1,188	1,203
0,8	0,911	0,911	0,912	0,916	0,926	0,942	0,962	0,985	1,010	1,036	1,062	1,086	1,112	1,136	1,158	1,176	1,194	1,209
0,9	0,921	0,921	0,922	0,926	0,936	0,952	0,972	0,996	1,021	1,046	1,072	1,096	1,120	1,143	1,163	1,181	1,199	1,214
1,0	0,929	0,929	0,931	0,936	0,946	0,962	0,982	1,006	1,031	1,056	1,081	1,106	1,128	1,150	1,169	1,187	1,204	1,220
1,1	0,935	0,937	0,940	0,946	0,956	0,972	0,993	1,017	1,042	1,066	1,092	1,115	1,138	1,159	1,177	1,195	1,212	1,228
1,2	0,941	0,944	0,949	0,956	0,966	0,982	1,004	1,028	1,053	1,077	1,103	1,126	1,148	1,168	1,186	1,204	1,222	1,237
1,3	0,946	0,951	0,957	0,966	0,977	0,993	1,016	1,040	1,063	1,089	1,114	1,136	1,158	1,178	1,196	1,214	1,232	1,250
1,4	0,953	0,959	0,967	0,975	0,986	1,005	1,028	1,050	1,075	1,101	1,124	1,147	1,168	1,187	1,206	1,224	1,244	1,266
1,5	0,961	0,968	0,975	0,984	0,997	1,018	1,040	1,061	1,088	1,111	1,134	1,156	1,176	1,196	1,215	1,235	1,258	1,277
1,6	0,972	0,978	0,985	0,994	1,010	1,030	1,050	1,073	1,096	1,119	1,142	1,164	1,184	1,204	1,224	1,245	1,268	1,289

Figure 71: Expression of discharge coefficient for a weir with thin wall and rectangular section (Le Coz, et al., 2011)
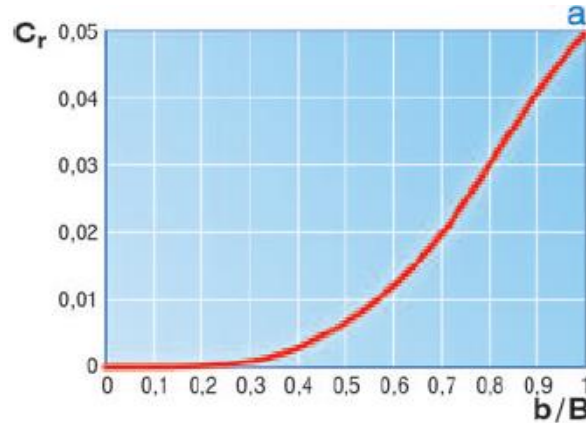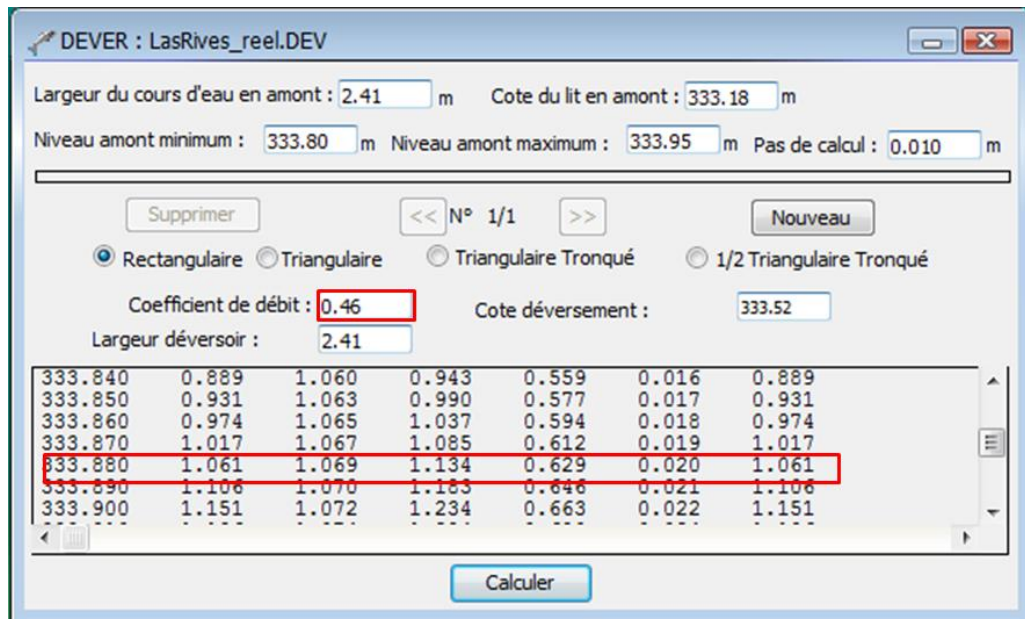

Figure 72: Abacus for the determination of Cr for a weir with thin wall and rectangular section (Le Coz, et al., 2011)

Figure 73 presents the results of the discharge calculation made with the Devers tool from Cassiopée software. A discharge of 1.13 m³/s is obtained; it is a few lower than the theoretical value of 1.35 m³/s (84%).

Figure 73: calculated discharge by Devers tool (C=0.46).